VOL. 107 NO. HY3. MARCH 1981

JOURNAL OF THE HYDRAULICS DIVISION

PROCEEDINGS OF
THE AMERICAN SOCIETY
OF CIVIL ENGINEERS

VOL.107 NO.HY3. MARCH 1981

JOURNAL OF THE HYDRAULICS DIVISION

PROCEEDINGS OF
THE AMERICAN SOCIETY
OF CIVIL ENGINEERS

ISSN 0044-796X

AMERICAN SOCIETY OF CIVIL ENGINEERS

CONTENTS

This Journal is published monthly by the American Society of Civil Engineers. Publications office is at 345 East 47th Street, New York, N.Y. 10017. Address all ASCE correspondence to the Editorial and General Offices at 345 East 47th Street, New York, N.Y. 10017. Allow six weeks for change of address to become effective. Subscription price to members is $16.50. Nonmember subscriptions available; prices obtainable on request. Second-class postage paid at New York, N.Y. and at additional mailing offices. HY.

TECHNICAL NOTES

Proc. Paper 16074

DISCUSSION

Proc. Paper 16067

*Discussion period closed for this paper. Any other discussion received during this discussion period will be published in subsequent Journals.

INFORMATION RETRIEVAL

The key words, abstract, and reference "cards" for each article in this Journal represent part of the ASCE participation in the EJC information retrieval plan. The retrieval data are placed herein so that each can be cut out, placed on a 3 × 5 card and given an accession number for the user's file. The accession number is then entered on key word cards so that the user can subsequently match key words to choose the articles he wishes. Details of this program were given in an August, 1962 article in CIVIL ENGINEERING, reprints of which are available on request to ASCE headquarters.

*Discussion period closed for this paper. Any other discussion received during this discussion period will be published in subsequent Journals.

16094 LOCAL DESTRATIFICATION OF LAKES

KEY WORDS: Computerized simulation; **Dispersion; Hydraulics; Hydrodynamics; Lakes;** Mixing; **Models; Reservoirs;** Stratification; **Water resources**

ABSTRACT: A numerical simulation of the flow field of the jet induced by an axial-flow propeller pump is performed by solving the governing equations of the flow field. The two-dimensional Los Alamos SOLA prediction technique has been expanded to include diffusion as well as buoyancy forces in an axisymmetric stratified flow field. Comparison with hydraulic models shows that this numerical simulation of the local destratification phenomenon is useful for the prediction of jet penetration depth or of the dilution factor (released water quality). The main dynamic effects are modeled adequately to show the same trends as the available physical data. The prediction procedure represents a low-cost basic tool to show the influence of design parameters on the flow field. An empirical expresssion for prediction of the penetration depth is suggested on the basis of experimental and computational results.

REFERENCE: Busnaina, Ahmed A., Lilley, David G., and Moretti, Peter M., "Prediction of Local Destratification of Lakes," *Journal of the Hydraulics Division,* ASCE, Vol. 107, No. HY3, **Proc. Paper 16094**, March, 1981, pp. 259-272

16099 EROSION IN RECTANGULAR LONG CONTRACTION

KEY WORDS: Bed load; Channel design; **Channel erosion;** Channels (waterways); **Contraction; Erosion;** Friction; **River engineering;** Scour

ABSTRACT: An experimental investigation into the general erosion within a long contraction problem is reported. The experimental results are used to verify Straub's theoretical one-dimensional model for general erosion. Local scour near the side walls in the inlet region was also measured and the results are reported. Two different sizes of sand were used in the experiments.

REFERENCE: Gill, Mohammad Akram, "Bed Erosion in Rectangular Long Contraction," *Journal of the Hydraulics Division,* ASCE, Vol. 107, No. HY3, **Proc. Paper 16099**, March, 1981, pp. 273-284

16110 MODEL FOR WIND INDUCED FLOW

KEY WORDS: **Channel flow;** Depth; Eddy currents; **Models; Numerical analysis; Surface waters;** Three dimensional flow; **Wind;** Wind forces

ABSTRACT: Based on a compilation of current data at the surface, the classical Ekman theory is inappropriate for calculating wind generated currents near the surface. The cause is found to be the assumption by Ekman of a vertical eddy viscosity, N_v, which is constant over a depth. A numerical model is described briefly, which allows for a variation of N_v over depth, z, as well as in the x and y directions. The model was developed using a Galerkin technique. The model can include a sharp, wind driven profile near the surface. The method is computationally reasonable, requiring about the same number of computations as a vertically averaged formulation. A relationship for choosing N_v versus depth is presented. Experimental data are compared to the numerical model results.

REFERENCE: Pearce, Bryan R., and Cooper, Cortis K., "Numerical Circulation Model for Wind Induced Flow," *Journal of the Hydraulics Division,* ASCE, Vol. 107, No. HY3, **Proc. Paper 16110**, March, 1981, pp. 285-302

16103 CELEBRATION OF KARAJI'S HYDROLOGY

KEY WORDS: **Ground water; Groundwater hydrology; History;** Hydrologic cycle; Underground conduits; Underground structures

ABSTRACT: A brief account of Mohammed Karaji, a Persian scholar of the tenth century, and his contributions to science, especially ground-water hydrology, is presented. Karaji wrote the first algebra text presented with symbolism. In engineering, he invented instruments that proved useful in the surveying and in the tunneling of underground chanels for conveying water. Most importantly, he expounded the basic principles of hydrology, understanding the proportionality law between the force of gravity and the mass of a body. Karaji noted that ground-waters, like surface waters, can be stagnant, and that still waters can be located under vast deserts and lowlands. A recently discovered text by Karaji on "hidden water" is the oldest known text on ground-water hydrology.

REFERENCE: Pazwash, Hormoz, and Mavrigian, Gus, "Millenial Celebration of Karaji's Hydrology," *Journal of the Hydraulics Division,* ASCE, Vol. 107, No. HY3, **Proc. Paper 16103**, March, 1981, pp. 303-309

16102 TURBULENCE MEASUREMENT STUDY

KEY WORDS: Electromagnetism; **Flow measurement; Hydraulics; Hydromechanics;** Instrumentation; Instrument sensitivity; **Meters;** Turbulence; **Turbulent flow;** Water current; Water metering

ABSTRACT: The capability of a modified commercially available electromagnetic water current meter was evaluated for measurement of parameters necessary to quantify turbulent flow. Values of turbulence intensity were measured, and Fourier analyses of their oscillograph recordings were performed to obtain the spectral distribution of the energy. Field tests were then conducted at three locations selected on the basis of their differences in flow regime. The results showed that values of turbulent intensity for flows between very high to light turbulence levels ranged from 0.71 to 0.06, respectively, and the Fourier analysis of the data shows the energy to be concentrated generally below 5 Hz. This instrument can be used to obtain relative values of turbulent intensity and spectral information from field measurement.

REFERENCE: Griffith, O. Franklyn, III, and Grimwood, Charles, "Turbulence Measurement Study," *Journal of the Hydraulics Division,* ASCE, Vol. 107, No. HY3, **Proc. Paper 16102**, March, 1981, pp. 311-326

16144 ULTIMATE DIMENSIONS OF LOCAL SCOUR

KEY WORDS: **Analysis (mathematics);** Comparative studies; **Erosion; Hyperbolic functions;** Linear functions; Logarithms; **Scour;** Time measurement; **Urban highways**

ABSTRACT: A mathematical method is presented for determining the ultimate dimensions of local scour from relatively short term measurement of the progression of scour with time. The method involves plotting the logarithm of the rate of change of the scour dimension against the logarithm of time. A hyperbolic curve is fitted to the plotted data, and the asymptote of the hyperbola is used to determine the ultimate scour dimension. A example is used to compare the hyperbolic logarithmic method with the linear logarithmic and linear semilogarithmic methods (in which the scour depth increases without limit) which require an estimate of the time required to reach a practical equilibrium. The hyperbolic logarithmic method predicts both the time progression of scour and the ultimate scour dimensions.

REFERENCE: Blaisdell, Fred W., Anderson, Clayton L., and Hebaus, George G., "Ultimate Dimensions of Local Scour," *Journal of the Hydraulics Division,* ASCE, Vol. 107, No. HY3, **Proc. Paper 16144**, March, 1981, pp. 327-337

16124 THREE-PARAMETER PROBABILITY DISTRIBUTIONS

KEY WORDS: **Flood frequency;** Floods; **Frequency distribution; Hydrology;** Low flow; Probability density functions; **Probability distribution functions; Probability theory;** Statistical analysis; Weibull density functions

ABSTRACT: The lognormal, Weibull, Pearson type 3, and log Pearson type 3, each a three-parameter distribution, were evaluated in a generalized fashion in terms of the dimensionless variate K ($K=X/\upsilon_X$, in which X equals randon variable, and υ_n equals its mean) which has a population mean of unity. The bounds of the distributions, areas of the portions of distributions in the negative region of variate when they enter such regions, and the differences in some important quantiles among the four distributions, are presented. The four distributions become less applicable for hydrologic frequency analysis as they deviate more and more from their two-parameter counterparts (lognormal in the case of log Pearson). When they have well-applicable properties, their quantile values differ little for some or all distributions indicating that choice of a distribution makes little difference. Some guidelines are provided for selecting the best applicable distribution for a given hydrologic sample.

REFERENCE: Rao, Donthamsetti Veerabhadra, "Three-Parameter Probability Distributions," *Journal of the Hydraulics Division,* ASCE, Vol. 107, No. HY3, **Proc. Paper 16124**, March, 1981, pp. 339-358

U.S. Customary-SI Conversion Factors

In accordance with the October, 1970 action of the ASCE Board of Direction, which stated that all publications of the Society should list all measurements in both U.S. Customary and SI (International System) units, the following list contains conversion factors to enable readers to compute the SI unit values of measurements. A complete guide to the SI system and its use has been published by the American Society for Testing and Materials. Copies of this publication (ASTM E-380) can be purchased from ASCE at a price of $3.00 each; orders must be prepaid.

All authors of *Journal* papers are being asked to prepare their papers in this dual-unit format. To provide preliminary assistance to authors, the following list of conversion factors and guides are recommended by the ASCE Committee on Metrication.

To convert	To	Multiply by
inches (in.)	millimeters (mm)	25.4
feet (ft)	meters (m)	0.305
yards (yd)	meters (m)	0.914
miles (miles)	kilometers (km)	1.61
square inches (sq in.)	square millimeters (mm^2)	645
square feet (sq ft)	square meters (m^2)	0.093
square yards (sq yd)	square meters (m^2)	0.836
square miles (sq miles)	square kilometers (km^2)	2.59
acres (acre)	hectares (ha)	0.405
cubic inches (cu in.)	cubic millimeters (mm^3)	16,400
cubic feet (cu ft)	cubic meters (m^3)	0.028
cubic yards (cu yd)	cubic meters (m^3)	0.765
pounds (lb) mass	kilograms (kg)	0.453
tons (ton) mass	kilograms (kg)	907
pound force (lbf)	newtons (N)	4.45
kilogram force (kgf)	newtons (N)	9.81
pounds per square foot (psf)	pascals (Pa)	47.9
pounds per square inch (psi)	kilopascals (kPa)	6.89
U.S. gallons (gal)	liters (L)	3.79
acre-feet (acre-ft)	cubic meters (m^3)	1,233

JOURNAL OF THE HYDRAULICS DIVISION

PREDICTION OF LOCAL DESTRATIFICATION OF LAKES

By Ahmed A. Busnaina,[1] David G. Lilley,[2] and Peter M. Moretti[3]

INTRODUCTION

Thermal stratification may occur in water reservoirs during the hot months of summer, and then three main layers of water with different characteristics may be observed. The epilimnion, the top layer, contains warm low-density water (usually rich in oxygen because of atmosphere reaeration and photosynthesis, and thus considered high-quality water). The hypolimnion, the bottom layer, consists of cold high-density water (often poor in oxygen and thus considered low-quality water). The region of rapid temperature change (between the other two layers) is called the thermocline or metalimnion. This stratification presents a serious problem for reservoirs with low-level release structures in that the quality of water released, as characterized by its oxygen content, may be poor, since most of the exit flow comes from the bottom layer of water in the reservoir. Since many old reservoirs have release structures located near the bottom, there is indeed a problem of finding suitable and economically feasible alleviation techniques.

Artificial destratification, structural modification, and localized mixing are three possible alleviation techniques that can be used to improve the release water quality. Artificial destratification can be either mechanical pumping (with assorted piping) or diffused-air pumping. These mixing devices, however, require a substantial amount of energy to destratify a large body of water, (see Ref. 13). Structural modification of the dam involves elevating the release gate position in order to allow some of the water to be drawn from the epilimnion. This method, although effective, is extremely costly. On the other hand, localized mixing of epilimnion water into the hypolimnion has been found to be effective

[1]Grad. Student, School of Mech. and Aerospace Engrg., Oklahoma State Univ., Stillwater, Okla. 74074.

[2]Assoc. Prof., School of Mech. and Aerospace Engrg., Oklahoma State Univ., Stillwater, Okla. 74074.

[3]Prof., School of Mech. and Aerospace Engrg., Oklahoma State Univ., Stillwater, Okla. 74074.

Note.—Discussion open until August 1, 1981. To extend the closing date one month, a written request must be filed with the Manager of Technical and Professional Publications, ASCE. Manuscript was submitted for review for possible publication on July 23, 1980. This paper is part of the Journal of the Hydraulics Division, Proceedings of the American Society of Civil Engineers, ©ASCE, Vol. 107, No. HY3, March, 1981. ISSN 0044-796X/81/0003-0259/$01.00.

and economical in enhancing the quality of water release from low-level release gates. There has been a continued interest in local mechanical destratification of reservoirs to improve water quality. A low-energy axial flow propeller may be positioned just below the water surface to provide a downward-directed jet of water and thereby locally mix the reservoir in the vicinity of the release structure of the dam. The high-quality epilimnion water is transported downwards, and the effectiveness of a pump of this type has been illustrated in field experiments at Pine Creek Reservoir, Okla. (8), and Lake Okatibbe, Miss. (6,7). Fig. 1 shows a schematic of the mixing produced when there is no exit beneath the propeller. The jet or plume penetrates some distance below the level of the thermocline. There is mixing of epilimnetic and hypolimnetic water in the shear layers of the plume, and the resulting intermediate-density water spreads out in a lens-like gravity flow at the level of the thermocline.

Fig. 2(*a*) shows the practical application of localized mixing in the proximity of the release structure of a dam with a low-level release gate. The flow field produced is fully three-dimensional. However, an axisymmetric two-dimensional

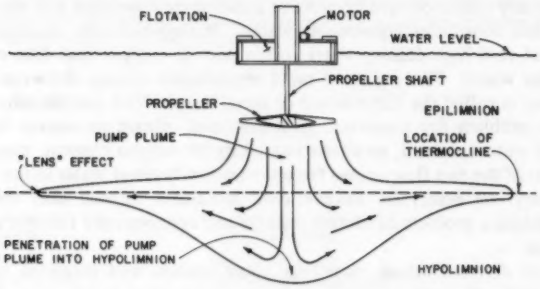

FIG. 1.—Schematic of Typical Propeller Pump and Flow Field Produced without Exit Flow

simulation of this phenomenon is shown in Fig. 2(*b*). In this, the release flow is represented by a circular opening at the bottom of the flow field, directly beneath the propeller. This does not represent correctly the position of the exit, since in practice it is in an off-axis position, but it provides a useful simplification of the true problem. In either case, the release flow can entrain some or all of the jet or plume of water from the surface. If the arrangement is successful, the release flow will consist mostly of epilimnetic water, along with some hypolimnetic water that enters the plume through mixing, and the dilution factor (as defined later) will be near one. If the velocity of the downward jet is insufficient for penetrating deeply into the stratification, only hypolimnetic water will be withdrawn, and the dilution factor will be zero. If the jet velocity is adequate, but the propeller flow rate small compared to the release flow rate, or the plume located too far from the release gate, then the dilution factor will have some intermediate value.

Hydraulic model experiments have enabled considerable success to be achieved in understanding the phenomena (11). Recent numerical simulations (3 and 4)

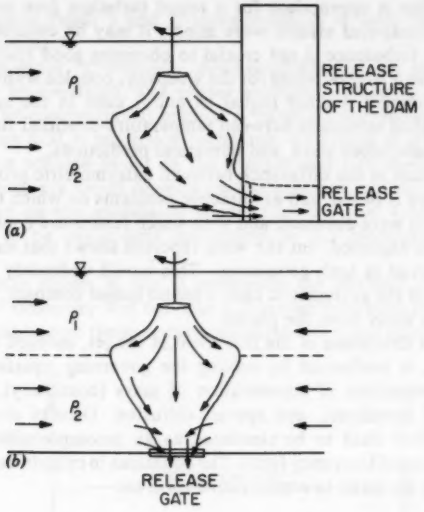

FIG. 2.—Schematic of Typical Propeller Pump and Flow Field Produced with Exit Flow via Low-Level Release Gate: (*a*) In Release Structure of Dam; (*b*) Directly Beneath Propeller

of local mixing supplement the experimental program, and demonstrate substantial promise for improvement in modeling the transient mixing behavior during destratification. Advantages of being able to calculate (rather than experiment in the laboratory or in the field) are enormous in terms of their cost/benefit ratio. Such procedures confirm and extend the available experimental data to a larger set of cases, and supplement the rather limited theoretical treatment of associated problems (see, e.g., 1, 2, and 5).

Mathematical Model

Several fundamental questions arise in the correct modeling of the physical phenomena. First, consider the question of modeling turbulence. Over the range of parameters studied, flow visualizations in the laboratory suggest that the controlling factor for the dilution of the release water will epilimnetic water is the entrainment of the downward plume into the release flow, rather than the mixing process in the vicinity of the plume (which is the governing mechanism for whole-lake mixing). Thus, the modeling of jet penetration depth on the one hand, and critical release flow rates on the other, are key items in the representation of the physical phenomena. The viscous or turbulent mixing processes in the shear layers are less important, and do not greatly affect the jet velocity at which the dilution factor increases from a low to a high value. In the numerical model, this has been confirmed by varying the viscosity from a laminar value to a *constant large viscosity* with minor effect on the results.

That such a value is appropriate for a round turbulent free jet is well-known (12). Since the computed effects were minor, it may be concluded that precise modeling of the turbulence is not crucial to obtaining good results. The present work incorporates a laminar value for the viscosity, coupled with a turbulent-flow value for the Schmidt number (equal to unity) used in the species equation. The result is a good similitude between temperature-stratified field tests, chemically-stratified laboratory tests, and numerical predictions.

Another question is the difference between axisymmetric problems on which the present theory is based, and asymmetric problems on which the experimental data of Moon (10) were obtained, and with which results are compared. Identical results cannot be expected, but the work reported shows that similar parametric trends are observed in both geometries. This would undoubtly not be the case if the geometry of the asymmetric case were no longer compact, with the release gate laterally far away from the plume.

The numerical simulation of the flow field of the jet, induced by an axial-flow propeller pump, is performed by solving the governing equations of the flow field, i.e., the equations of conservation of mass (continuity), momentum (in axial and radial directions), and species diffusion. Density changes are slight and allow the flow field to be simulated as an incompressible flow with the addition of an upward buoyancy force. The equations in cylindrical (axisymmetric) coordinates may be taken in conservative form as:

$$\frac{\partial U}{\partial x} + \frac{\partial V}{\partial y} + \frac{U}{x} = 0 \quad \ldots\ldots (1)$$

$$\frac{\partial U}{\partial t} + \frac{\partial}{\partial x}(U^2) + \frac{\partial}{\partial y}(UV) + \frac{U^2}{x} = -\frac{1}{\rho_1}\frac{\partial P}{\partial x} + \frac{\mu}{\rho_1}\left(\frac{\partial^2 U}{\partial x^2} + \frac{\partial^2 U}{\partial y^2} + \frac{1}{x}\frac{\partial U}{\partial x} - \frac{U}{x^2}\right) \quad \ldots\ldots (2)$$

$$\frac{\partial V}{\partial t} + \frac{\partial}{\partial x}(UV) + \frac{\partial}{\partial y}(V^2) + \frac{UV}{x} = -\frac{1}{\rho_1}\frac{\partial P}{\partial y} - g\left(\frac{\rho - \rho_1}{\rho_1}\right) + \frac{\mu}{\rho_1}\left(\frac{\partial^2 V}{\partial x^2} + \frac{\partial^2 V}{\partial y^2} + \frac{1}{x}\frac{\partial V}{\partial x}\right) \quad \ldots\ldots (3)$$

$$\frac{\partial m_1}{\partial t} + \frac{\partial}{\partial x}(m_1 U) + \frac{\partial}{\partial y}(m_1 V) + \frac{m_1 U}{x} = \frac{\mu}{\rho_1 \sigma_{sc}}\left(\frac{\partial^2 m_1}{\partial x^2} + \frac{\partial^2 m_1}{\partial y^2} + \frac{1}{x}\frac{\partial m_1}{\partial x}\right) \quad \ldots\ldots (4)$$

$$m_1 + m_2 = 1 \quad \ldots\ldots (5)$$

$$\rho = m_1 \rho_1 + m_2 \rho_2 \quad \ldots\ldots (6)$$

in which x, y = the coordinates in the radial and axial directions, respectively; U, V = velocity components in x, y directions, respectively; P = the static pressure deviation from hydrostatic pressure; μ = dynamic viscosity; g = gravitational acceleration; m_1, m_2 = mass fractions of fluids 1 and 2, respectively;

ρ_1, ρ_2 = densities of fluids 1 and 2, respectively; ρ = local density; and σ_{sc} = the Schmidt number.

With these equations, a vertically downward-directed jet in the stratified environment can be simulated, and proper account is taken of species mixing and buoyancy. The computational method is based on the transient two-dimensional Los Alamos SOLA prediction technique, described in Ref. 9, which is a finite difference scheme based on the Marker and Cell method. The finite difference equations are based directly on the primitive pressure-velocity variables, rather than on the associated stream function and vorticity variables, and this proves to be particularly convenient in the imposition of boundary conditions.

The flow domain shown in Fig. 3 represents the physical problem. It has a vertical axis of symmetry and contains a downward-flowing jet of fluid from the propeller. Initially, two fluids occupy positions above and below the interface,

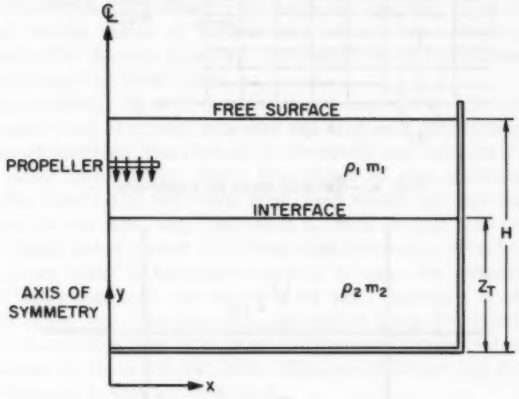

FIG. 3.—Axisymmetric Flow Domain

as shown, so that their mass fractions are $m_1 = 1$; and $m_2 = 0$ (for $y > Z_T$, the height of the interface), and vice versa. Fig. 4 shows how the cylindrical region is divided into equal-sized rectangular cell divisions. This solution domain is complemented by a layer of cells on all sides, so as to allow easy simulation of the required boundary conditions. A single cell of this mesh is enlarged in Fig. 5 which shows the location of each field variables, P, u, v, and other variables in this cell. The pressure, P, and mass fraction of fluid 1, m_1, are located at the center of each cell and the radial and axial velocities lie directly on the physical boundaries of the solution domain, while the pressure and mass fractions are displaced half a cell interval inside the flow field. In this way, the exterior fictitious cells are particularly convenient when applying the boundary conditions.

Fig. 4 also shows how inlet and exit flows are handled. The exit release flow is via a circular opening directly beneath the propeller, with the flow

rate specified a priori. The available volume of the flow domain is very limited. To allow the outlet of release water without dramatically decreasing the fluid

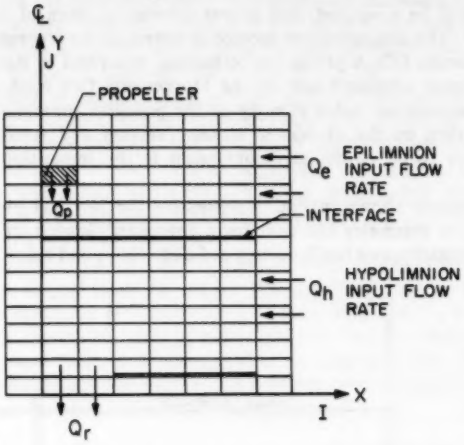

FIG. 4.—General Mesh Arrangement

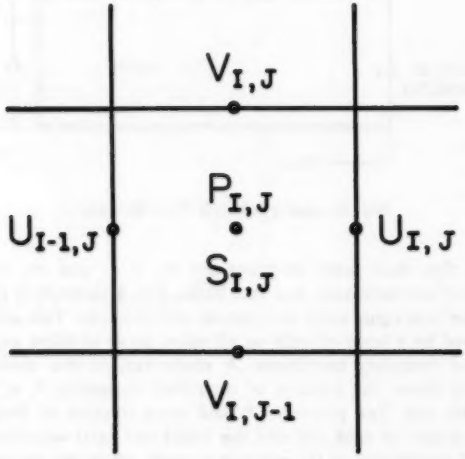

FIG. 5.—Arrangement of Finite Difference Variables in Typical Cell

level, there is a compensating incoming flow which is distributed among the top and bottom layers in amounts equal to the epilimnetic and hypolimnetic

water released. The peripheral inflow is at two different elevations in such a way that epilimnetic water enters through a circumferential opening into the upper layer and does not disturb the density profile. The large circumferential opening allows the inflow to be at a low velocity in order to avoid any disturbance to the flow field. Similarly, hypolimnetic water is fed into the bottom layer.

The solution algorithm consists of a time-march procedure. At each step of the march, velocity guesses are calculated explicitly from their respective conservation of momentum equations. Application of the diffusion equation (conservation of chemical species) to the low-density fluid 1 (initially the top layer of fluid in the solution domain), enables the respective proportions of fluid 1 and fluid 2 (the high-density fluid initially forming the bottom layer of fluid in the solution domain), to be calculated, and thus, the density at all locations. The newly-calculated velocities are considered to be first approximations at the new time level, since the continuity requirement has not yet been imposed. The approximations are improved in an iterative fashion, adjusting cell pressures and velocities to satisfy the continuity equation. When convergence is achieved, current values of pressure and velocity are accepted and taken as initial values for the next time step. Associated useful calculations may now be deduced in terms of these values.

Boundary conditions on solid boundaries are imposed on the velocities and species concentration after each time step and after each pass through the mesh during pressure iterations. Convergence to the steady-state solution is established by taking many forward time steps. The choice of time increment must be restricted (for stability) in two ways. First, fluid should not pass through more than one cell in one time step. Therefore Δt must be less than (usually 0.25 times–0.33 times) the minimum cell transit time taken over all cells. Secondly, when a nonzero value of kinematic viscosity is used, the momentum should not diffuse more than one cell in one time step. Accuracy is enhanced by using small space and time intervals, the choice being determined in an ad hoc manner as a suitable trade-off between accuracy and economy of computation. A full examination of the general finite difference technique and its application to this problem are readily available (3,9).

Results and Analysis

Comparison of results with hydraulic laboratory model data of Moon (10) shows that the numerical simulation of local destratification phenomena is a useful predictive tool. The dilution factor (release water quality) is as follows:

$$DF = \frac{\rho_r - \rho_2}{\rho_1 - \rho_2} \quad \text{(7)}$$

in which ρ = the density; and subscripts r, 2, and 1 refer to release, hypolimnion (bottom), and epilimnion (top) locations, respectively. The dilution factor is found to be a strong function of the following.

1. The densimetric Froude number:

$$F = \frac{V_o}{\left[g \frac{\Delta\rho}{\rho_1} H\right]^{1/2}} \quad \text{(8)}$$

in which V_o = the initial jet velocity from the propeller; g = the gravitational acceleration; and $\Delta\rho/\rho_1$ = the stratification.

2. The nondimensional metalimnion (interface) location:

$$Z_T^* = \frac{Z_T}{H} \quad (9)$$

in which Z_T = the metalimnion location measured from the bottom.

3. The nondimensional flow rate:

$$Q^* = \frac{Q_p}{Q_r} \quad (10)$$

in which Q represents the flow rate; and subscripts p and r refer to the propeller and release locations, respectively.

4. The nondimensional propeller diameter:

$$D^* = \frac{D}{H} \quad (11)$$

in which D = the propeller diameter.

5. The nondimensional propeller depth:

$$L^* = \frac{L}{H} \quad (12)$$

in which L = propeller depth below the surface.

A standard base case is taken with the following parameters (typical of experimental data): $\mathsf{F} = 2$; $Z_T^* = 0.6$; $Q^* = 0.44$; $D^* = 0.211$; and $L^* = 0.211$, from which certain changes are made and individually assessed in the subsequent analysis. Figs. 6–10 show the computed effect of variation of each of these parameters on the dilution factor, DF, while the other parameters are maintained at their respective base values. Appropriate experimental results are also shown where available, and it is to be observed that the main dynamic effects are modeled adequately and show the same trends as the available physical data.

In Fig. 6, the dilution factor, DF, is shown to be a strong function of the densimetric Froude number, F, in both predictive and laboratory data. The general result is that release water quality (the fraction of epilimnetic or top water in the exit stream) increases with higher values of the Froude number, such conditions being achieved with higher jet velocities from the propeller, or a lower degree of stratification in the lake, or both. The favorable comparison of experiment and theory is clearly seen. From the designer's view, the important result is the Froude number at which the dilution factor rises sharply, since that determines the velocity required at the propeller for the given conditions. This Froude number is predicted very well by the computer program. A second point of interest is the maximal dilution factor achievable, which is predicted within the scatter of the experiments.

The relation between the dilution factor, DF, and the normalized metalimnion location, Z_T^*, is presented in Fig. 7. The computation is carried out for the base case of $\mathsf{F} = 2$, which is on the relatively flat part of the dilution factor

versus the Froude number curve (see Fig. 6), and results in dilution factors having nearly maximal values. The location of the metalimnion is seen in Fig. 7 to have a strong effect on the penetration depth of the jet of water from the propeller, and thus has an effect also on the ultimate dilution factor. As the metalimnion (interface) height (above the base) increases, buoyancy forces

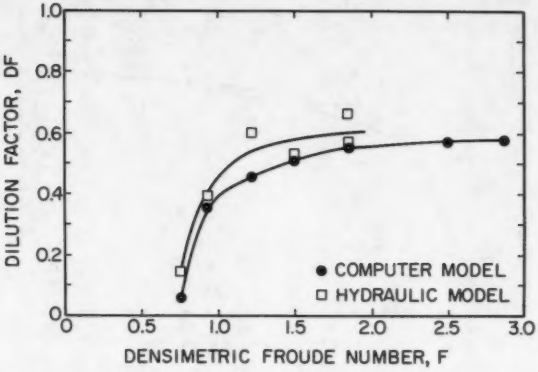

FIG. 6.—Dilution Factor, DF, as Function of Densimetric Froude Number, F ($Z_T^* = 0.6$; $Q^* = 0.44$; $D^* = 0.211$; $L^* = 0.211$)

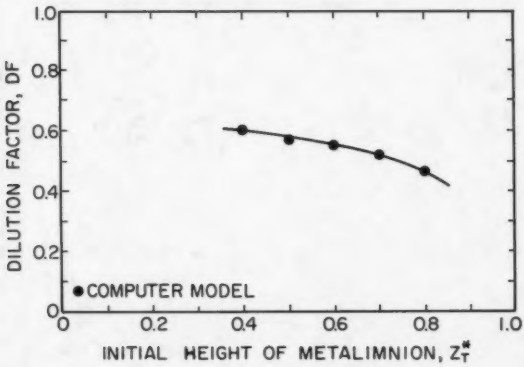

FIG. 7.—Dilution Factor, DF, as Function of Nondimensional Metalimnion Location Z_T^* ($F = 2$; $Q^* = 0.44$; $D^* = 0.211$; $L^* = 0.211$)

increase, and this will hinder the jet penetration, increase the dispersion of the plume, and thus reduce the dilution factor. No experimental data are currently available to directly substantiate this predicted result.

Fig. 8 shows that the dilution factor, DF, is a strong function of the flow-rate

ratio Q^*. Generally, release water quality improves with an increase in the value of Q^*, a condition achieved with low release rates and high propeller flow rates. The figure shows the relationship found in both the hydraulic laboratory model and computer simulation, and the agreement is extremely good. Contrary to first intuition, the dilution factor can exceed the flow-rate ratio. This illustrates

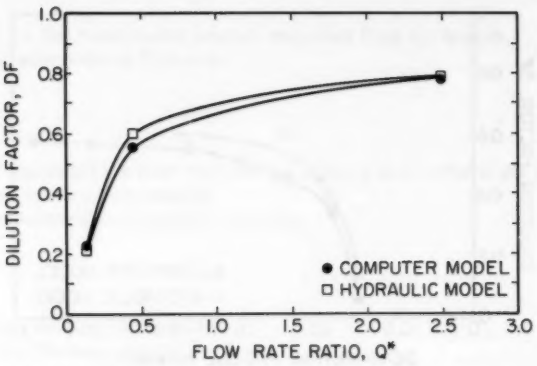

FIG. 8.—Dilution Factor, DF, as Function of Nondimensional Flow Rate, Q^* ($F = 2$; $Z_T^* = 0.6$; $D^* = 0.211$; $L^* = 0.211$)

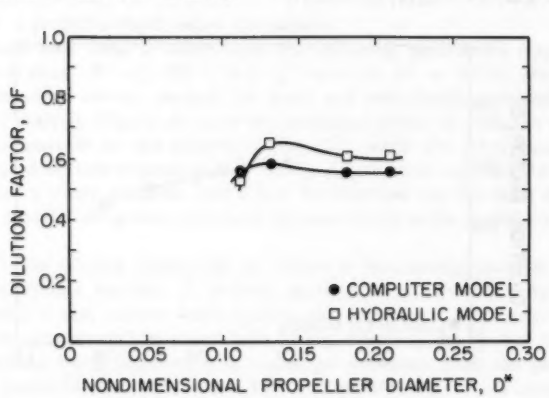

FIG. 9.—Dilution Factor, DF, as Function of Nondimensional Propeller Diameter, D^* ($F = 2$; $Z_T^* = 0.6$; $Q^* = 0.44$; $L^* = 0.211$)

the complex interaction between the propeller flow field and the release flow field, and shows the need for the application of numerical computations.

The effect of changing the propeller diameter, but retaining the propeller flow rate, Q^*, the same, is shown in Fig. 9. Again, there is good agreement between predicted and experimental evidence of the effect of normalized diameter,

D^*, on dilution factor, DF. These and other results show that values of D^* less than 0.1 are ineffective, and that a value of about 0.13 gives the best results. In view of the differences in geometry, the discrepancies between hydraulic and numerical models are surprisingly small.

The final parameter influence considered is that of depth of the propeller below the surface. Fig. 10 shows a predicted, almost linear slight decrease of dilution factor, DF, as the nondimensional propeller depth, L^*, increases, illustrating that as the propeller is lowered toward the metalimnion, less epilimnetic water is driven to the exit. Predicted results with values of L^* less than D^* are unrealistic, since in the numerical model a constant surface location is specified. In practice, surface effects would occur when the propeller is too high in the water, with entrained vortex air bubbles being pumped downward, thus decreasing the water flow rate, jet penetration, and dilution factor. Experi-

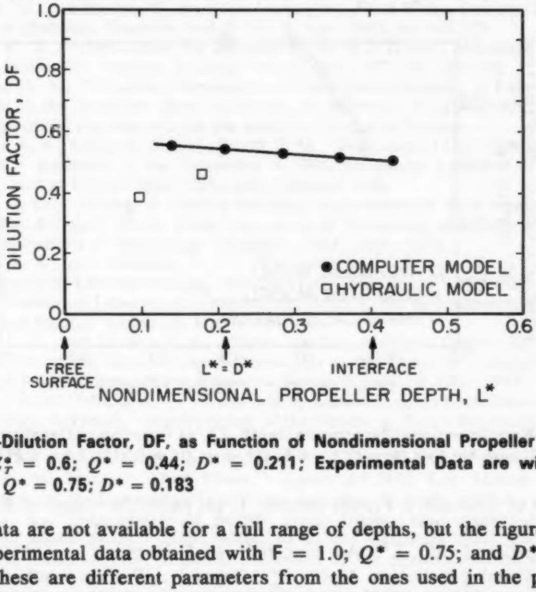

FIG. 10.—Dilution Factor, DF, as Function of Nondimensional Propeller Depth L^* (F = 2; Z_T^* = 0.6; Q^* = 0.44; D^* = 0.211; Experimental Data are with F = 1; Z_T^* = 0.6; Q^* = 0.75; D^* = 0.183

mental data are not available for a full range of depths, but the figure includes some experimental data obtained with F = 1.0; Q^* = 0.75; and D^* = 0.183. Though these are different parameters from the ones used in the prediction, effects of the proximity of a free surface are evident, and the predictions in these cases are clearly not representative of the physical situation.

When there is no exit flow, ($Q^* = \infty$), the nondimensionalized jet penetration depth

$$Z_p^* = \frac{Z_p}{H} \quad \ldots\ldots\ldots\ldots\ldots\ldots\ldots\ldots\ldots\ldots \quad (13)$$

in which Z_p = the jet penetration depth measured from the surface; and H = the total depth, is of special interest. For example, if Z_p^* = 1, then one is assured that epilimnion water is transported to the lowest level, and a release

gate placed there will enhance the epilimnion water transportation. It is interesting to investigate the value of Z_p^* as a function of densimetric Froude number, F.

An empirical expression for prediction of the penetration depth is suggested on the basis of experimental and computation results (3), and deduced as

$$V^2 = V_o^2\left(\frac{CD}{h}\right)^2 - 2g\int_0^h \frac{\rho_h - \rho_1}{\rho_1}\,dh; \quad (\text{for } h \geq CD) \quad \ldots\ldots\ldots\ldots (14)$$

in which V_o = the jet downward velocity; V = the local jet center line downward velocity at a distance, h, below the propeller of diameter, D; ρ = the local density; and C = an empirical constant evaluated as 3.5 from the experimental data of Moon (10). That this equation exhibits good qualitative predictions when compared with available data is seen in Fig. 11, which shows normalized penetration depth (whose corresponding depth, h, below the propeller, may be obtained by setting V equal to zero in the aforementioned expression) as

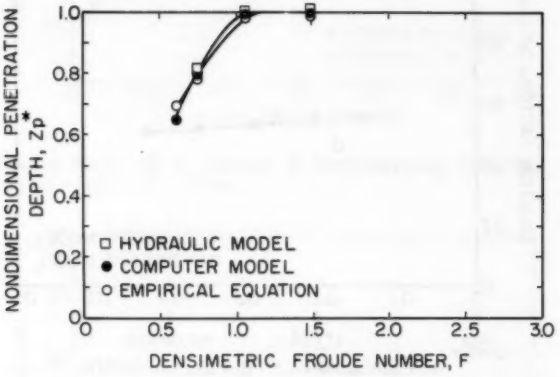

FIG. 11.—Nondimensional Penetration Depth, Z_p^*, as Function of Densimetric Froude Number, F, with No Exit Flow ($Z_T^* = 0.6$; $Q^* = \infty$; $D^* = 0.211$; $L^* = 0.211$)

a function of densimetric Froude number, F, for particular values of dimensional propeller diameter, D^*, initial metalimnion (interface) location, Z_I^*, and normalized propeller depth, L^*. As expected, as F increases, so also does the nondimensional penetration depth, Z_p^*. Beyond a Froude number of unity, penetration of the jet to the floor of the lake is predicted. Similar results are also obtained with different values of the parameters.

Conclusions

The prediction procedure represents a low-cost basic tool to show the influence of design parameters on the flow field. Comparison with hydraulic models shows that this numerical simulation of the local destratification phenomenon is useful for the prediction of the dilution factor (released water quality) and jet penetration depth. The main dynamic effects are modeled adequately to show the same

trends as the available physical data. The dilution factor and the nondimensional depth are functions of the densimetric Froude number, metalimnion location, propeller flow rate relative to the release flow rate, propeller diameter, and propeller depth below the surface. An empirical expression for prediction of the penetration depth is suggested on the basis of experimental and computational results, and it correlates well the available data within its range of applicability.

Acknowledgment

The writers wish to express their appreciation to the United States Army Corps of Engineers, Waterways Experimental Station, at Vicksburg, Miss., for their financial support.

Appendix I.—References

1. Abraham, G., and Eysink, W. D., "Jets Issuing Into Fluid With a Density Gradient," *Journal of Hydraulic Research*, Vol. 7, No. 2, Apr., 1969, pp. 145–175.
2. Baines, W. D., "Entrainment by a Plume or Jet at a Density Interface," *Journal of Fluid Mechanics*, London, England, Vol. 68, Apr., 1976, pp. 309–320.
3. Busnaina, A. A., "Numerical Simulation of Local Destratification of Lakes," thesis presented to the Oklahoma State University, at Stillwater, Okla., in 1979, in partial fulfillment of the requirements for the degree of Master of Science.
4. Busnaina, A. A., Lilley, D. G., and Moretti, P. M., "Prediction of Local Destratification of Lakes," presented at the November 9, 1979, Oklahoma Academy of Sciences Meeting, held at Central State University, Edmond, Okla.
5. Ditmars, J. D., "Mixing of Density Stratified Impoundments With Buoyant Jets," *Report No. KH-R-22*, W. M. Keck Laboratory of Hydraulics and Water Resources, California Institute of Technology, Pasadena, Calif., Sept., 1970.
6. Dortch, M. S., and Wilhelms, S. C., "Enhancement of Releases from a Stratified Impoundment by Localized Mixing, Okattibee Lake, Mississippi," *Miscellaneous Paper H-78-1*, Hydraulics Laboratory, United States Army Corps of Engineers, Waterways Experiment Station, Vicksburg, Miss., Jan., 1978.
7. Garton, J. E., and Jarrell, H. R., "Demonstration of Water Quality Enhancement Through Use of the Garton Pump," *Supplement to the Technical Completion Report No. C-5228-A*, Oklahoma Water Resources Research Institute, Okla., 1976.
8. Garton, J. E., and Peralta, R. C., "Water Quality Enhancement by Point Destratification, Gillham lake, Arkansas," special report of the Oklahoma Water Resources Research Institute, Okla., Feb., 1978.
9. Hirt, C. W., Nichols, B. D., and Romero, N. C., "SOLA: A Numerical Solution Algorithm for Transient Fluid Flows," *Report LA-5882*, Los Alamos Scientific Laboratory and the University of California, Los Alamos, N.M., 1975.
10. Moon, J. J., "Enhancement of Release Water Quality by Localized Mixing—A Hydraulic Model Study," thesis presented to the Oklahoma State University at Stillwater, Okla., in 1978, in partial fulfillment of the requirements for the degree of Master of Science.
11. Moretti, P. M., and McLaughlin, D. K., "Hydraulics Modeling of Mixing in Stratified Lakes," *Journal of the Hydraulics Division*, ASCE, Vol. 103, No. HY4, Proc. Paper 12868, Apr., 1977, pp. 367–380.
12. Schlichting, H., *Boundary Layer Theory*, 6th ed., McGraw-Hill Publishing Co., Inc., New York, N.Y., 1968, p. 699.
13. Symons, J. M., Irwin, W. H., Robinson, E. L., and Robeck, G. G., "Impoundment Destratification for Raw Water Quality Control Using Either Mechanical or Diffused-Air-Pumping," *Journal of the American Water Works Association*, Vol. 59, No. 10, Oct., 1967, pp. 1268–1291.

Appendix II.—Notation

The following symbols are used in this paper:

C = constant, with the deduced value 3.5;
D_p = propeller diameter;
D^* = D_p/H = nondimensional propeller diameter;
DF = $(\rho_r - \rho_2)/(\rho_1 - \rho_2)$ = dilution factor;
F = $V_o/[g(\Delta\rho/\rho_1)H]$ = densimetric Froude number;
g = gravitational acceleration;
H = total depth of model;
h = depth below propeller;
L = propeller depth below the surface;
L^* = L/H = nondimensional propeller depth;
m_1 = mass fraction of fluid of density, ρ_1 (epilimnion);
m_2 = mass fraction of fluid of density, ρ_2 (hypolimnion);
P = pressure deviation from hydrostatic pressure;
Q_p = propeller flow rate;
Q_r = release flow rate;
Q^* = Q_p/Q_r = nondimensional flow rate;
U = velocity in radial direction;
V = velocity in axial direction;
V_o = initial jet velocity;
x = radial direction;
y = axial direction;
Z_p = penetration depth (measured from the surface);
Z_p^* = Z_p/H = nondimensional penetration depth;
Z_T = metalimnion location (measured from the bottom);
Z_T^* = Z_T/H = nondimensional metalimnion location;
μ = dynamic viscosity;
ρ_h = initial density profile as a function of h;
ρ_1 = epilimnion or top water density;
ρ_2 = hypolimnion or bottom water density; and
σ_{sc} = Schmidt number.

JOURNAL OF THE HYDRAULICS DIVISION

BED EROSION IN RECTANGULAR LONG CONTRACTION

By Mohammad Akram Gill,[1] M. ASCE

INTRODUCTION

When the width of a rectangular channel is reduced by building long side walls so that the width within the side walls remains constant, the contracted channel may be called a rectangular long contraction. A river channel within the parallel guide banks, built on diversion works such as weirs and barrages, is a practical example of rectangular long contraction. The width of river channels is greatly reduced within the guide banks in order to economize the cost of constructing diversion works. For example, at the site of the Mailsi Siphon, Pakistan (see Fig. 1), the natural width of the Sutlej river is reduced from 12 km to merely 432.0 m (6).

The effect of reducing the channel width is to increase the bed shear stress of the flow, which is responsible for causing considerable erosion within the contracted reach. In order to guard against the destructive effects of excessive erosion within the reach, it is important to be able to estimate the depth of maximum erosion. The results of a laboratory study are presented here, which may hopefully be used for the purpose of practical design.

One of the earliest works which presented a simplified one-dimensional theory of the equilibrium depth of erosion for a rectangular long contraction is due to Straub (5). His work was later followed by Ashida (1) and Komura (3). In the Indo-Pakistani river engineering practice, suitable scaling factors (>1.0) are used together with the regime flow depth for estimating the depth of maximum erosion in long contractions. Essentials of Straub's one-dimensional theory are presented here and the final result will be used to fit the experimental data.

[1]Prof., Dept. of Civ. Engrg., Ahmadu Bello Univ., Zaria, Nigeria.

Note.—Discussion open until August 1, 1981. To extend the closing date one month, a written request must be filed with the Manager of Technical and Professional Publications, ASCE. Manuscript was submitted for review for possible publication on July 8, 1980. This paper is part of the Journal of the Hydraulics Division, Proceedings of the American Society of Civil Engineers, ©ASCE, Vol. 107, No. HY3, March, 1981. ISSN 0044-796X/81/0003-0273/$01.00.

One-Dimensional Erosion Theory

With reference to Fig. 2, the equation of continuity for water flow is written as

$$Q = B_1 V_1 d_1 = B_2 V_2 d_2 \quad (1)$$

in which Q = total discharge; B = channel width; V = average cross-sectional velocity; d = average flow depth; and superscripts 1 and 2 refer to the upstream uncontracted and contracted channel reaches, respectively. It is assumed that the hydraulic resistance, both in the upstream uncontracted and contracted

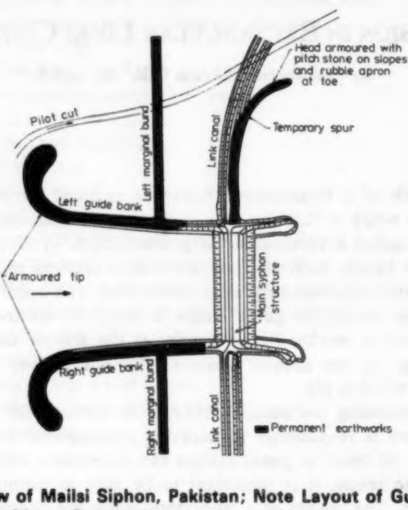

FIG. 1.—Plan View of Mailsi Siphon, Pakistan; Note Layout of Guide Banks Which Is Similar to That of Long Contraction

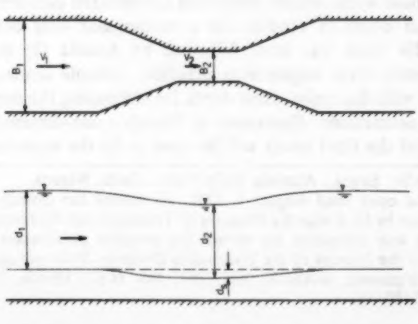

FIG. 2.—Schematic Diagram of Flow Through Long Contraction

reaches, is described by the Manning formula, written as follows

$$V = \frac{1}{n} d^{2/3} S_e^{1/2} \quad \ldots\ldots (2)$$

in which n = Manning's coefficient of bed friction; and S_e = energy gradient. The equation of continuity of sediment discharge is written as

$$B_1 q_{s1} = B_2 q_{s2} \quad \ldots\ldots (3)$$

in which q_s = unit sediment discharge. The rate of sediment transport is assumed to be given by

$$q_s = q_{so} \left[\frac{\tau}{\tau_c} - 1 \right]^m \quad \ldots\ldots (4)$$

in which q_{so} = constant $[g(S_s - 1)D^3]^{1/2}$; m = constant; g = gravitational acceleration; S_s = specific gravity of the bed material; D = average size of bed material; τ = bed shear stress; and τ_c = critical shear stress of the bed material. Assuming that any depression of water level within the contraction is negligible, and also ignoring the effect of sorting, Eqs. 1–4 can be solved to give

$$\frac{d_2}{d_1} = \left(\frac{B_1}{B_2}\right)^{6/7} \left[\left(\frac{B_1}{B_2}\right)^{1/m} \left(1 - \frac{\tau_c}{\tau_1}\right) + \frac{\tau_c}{\tau_1} \right]^{-3/7} \quad \ldots\ldots (5)$$

Eq. 5 holds for flows in which the sand bed in the upstream uncontracted channel is moving. For flows in which the upstream uncontracted sand bed is stationary, i.e., when $\tau_1/\tau_c < 1.0$, $\tau_c/\tau_1 - 1 = 0$, and Eq. 5 gives

$$\frac{d_2}{d_1} = \left(\frac{B_1}{B_2}\right)^{6/7} \left(\frac{\tau_1}{\tau_c}\right)^{3/7} \quad \ldots\ldots (6)$$

The maximum depth of erosion is predicted at the threshold of movement of the upstream bed, i.e., when $\tau_c/\tau_1 = 1.0$, and is given by

$$\frac{d_2}{d_1} = \left(\frac{B_1}{B_2}\right)^{6/7} \quad \ldots\ldots (7)$$

At high rates of sediment transport, $\tau_c/\tau_1 \to 0$, so that Eq. 5 gives

$$\frac{d_2}{d_1} = \left(\frac{B_1}{B_2}\right)^{(6/7 - 3/7m)} \quad \ldots\ldots (8)$$

The highest value of m in the known empirical formulas is 3, as in the Einstein-Brown formula; the lowest value of m is 1.5, as in the Meyer-Peter formula. For these values, Eq. 8 gives the following equations, respectively

$$\frac{d_2}{d_1} = \left(\frac{B_1}{B_2}\right)^{0.714} \quad \ldots\ldots (9)$$

and

$$\frac{d_2}{d_1} = \left(\frac{B_1}{B_2}\right)^{0.571} \quad \ldots\ldots (10)$$

For a typical contraction ratio of $B_2/B_1 = 1/2$, Eq. 9 gives $d_2/d_1 = 1.64$, and Eq. 10 gives $d_2/d_1 = 1.49$. The difference in these values is between 9%–10%, which in view of the choice of the extreme types of sediment transport formulas, is not very great. For $B_2/B_1 = 1/4$, the difference is between 18%–22%. Even this difference is not much compared with the scatter that is common in the data of erosion and sediment transport problems. For the purpose of constructing a theoretical model, the choice of a sediment transport formula will not usually affect the validity and applicability of the model seriously,

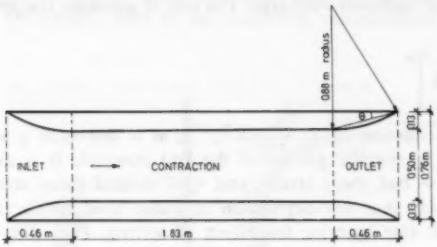

FIG. 3.—Plan of 1.83-m Long Contraction with Details of Transitional Sections

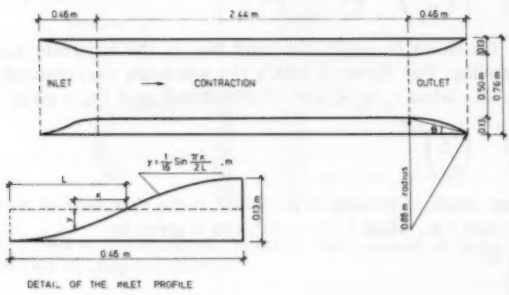

FIG. 4.—Plan of 2.44-m Long Contraction with Details of Transitional Inlet Section

although it is advisable to adopt the highest maximum value of erosion depth, e.g., that obtained from Eq. 9, for design purposes.

Experimental Facility

Laboratory Channel.—The experiments were conducted in a rectangular steel channel which was 11.4 m long, excluding the inlet and outlet sections. The width and depth of the channel were 0.76 m and 0.46 m, respectively. The channel could be tilted using a hand-operated screw at the upstream end. A tainter gate was mounted in the channel at about 1.2 m upstream of the lower end of the channel in order to control water depths in the channel. Usual devices of reducing turbulence at the upstream end, e.g., honey combs, use of smooth

transition at the inlet, etc., were used. A venturimeter was provided in the 0.20-m diam pipeline for the measurement of discharge. The water and bed levels were measured using point gages. For the details of arrangements for measuring longitudinal slope, sand feed, and sand transport, see Ref. 2.

Bed Material.—Two sizes of sand were used in the experiments. The average size of the coarse sand, D_{50}, was 1.53 mm, while the average size of the fine sand was 0.92 mm. The sands were nearly uniform in size; the gradation curves are available in Ref. 2.

Long Contractions.—In a first series of experiments, the effective length of the contraction was 1.83 m, excluding the upstream (inlet) and downstream (outlet) transitions, each 0.46 m long (see Fig. 3). The overall length was thus 2.75 m. Later, the effective length was increased to 2.44 m, with transitions each 0.46 m long (see Fig. 4). In the 1.83-m long contraction, the upstream and downstream transitions were identical in shape. The transitional curve was a simple circular arc, as shown in Fig. 3. The width of the side wall was 0.127 m; the total contraction was thus 0.25 m in a channel 0.76 m in width. The angle of inclination, θ, was nearly 15°, slightly greater than 12.5° as proposed by Hinds and quoted by Smith (4), for smooth transitions. In view of some recent investigations on simplified flume inlets (4), a 15° inclination was considered satisfactory. In the very first few experiments, it was observed that deep holes were scoured near the transition walls at the inlet. In order to check if the deep scour could be avoided or sufficiently reduced by providing a better type of transition at the inlet, the simple circular transition was later changed to the sinusoidal transition, as shown in Fig. 4. However, the downstream transition was not changed. The local scour near the inlet region was not reduced, and continued to be appreciably deeper than that within the long contraction.

The contraction of the channel was achieved by placing wooden side walls, each 0.127 m wide, within the channel. The walls were placed symmetrically opposite each other. The transition pieces, also made of wood, were screwed to the main body of the contraction. The whole structure of the contraction was painted to a smooth finish.

Experimental Procedure

Before releasing the water in the channel, the sand bed was leveled, both in the contracted and the uncontracted sections, using wooden screeds of appropriate dimensions. The sand bed was 22.5 cm thick. The depth of flow was adjusted by the tainter gate. The water levels recorded at the end of the experiments were used in the calculations of the flow depths and the bed shear stresses, since these values were believed to correspond to the equilibrium conditions of bed scour. Each experiment was run for at least 6 h.

The determination of the correct rate of sand feed in the experiments with bed load movement was approximate. Although the rate of sediment transport was measured at the outlet end in several experiments, it however did not indicate the average rate of sediment movement in the upstream uncontracted channel. Visual judgment was used in controlling the feed rate during an experiment. At the end of an experiment, if the bed of the upstream channel was found to be substantially lowered below or raised above its initial flat position, then the experiment was repeated with an adjusted rate of sand feed.

The sole criterion of a steady flow of sand was thus the final condition of the bed in the upstream channel. Although a very accurate evaluation of the mean position of the bed level at the end of the experiments in cases where ripples were formed over the bed, was difficult, a fairly good idea about the condition of sand flow could be obtained by taking numerous readings on the bed. Since the sands were of uniform size and the ripples were two-dimensional and fairly long (0.61 m–1.22 m), the evaluation of the mean bed level could be satisfactorily done.

The scour depth, d_s, as shown in Fig. 2, was obtained by averaging several (generally four) depth readings taken along the longitudinal section passing through the midwidth of the channel, over a distance of 0.61 m. The section 0.61 m in length was nearly equidistant from the inlet and outlet of the long contraction.

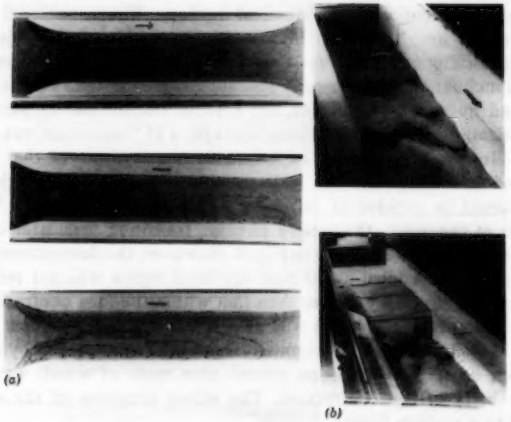

FIG. 5.—Contours of Eroded Sand Bed in Long Contraction

For the details of sand feed arrangement, measurement of feed rate, sand trap and measurement of sand transport, see Ref. 2.

Erosion Patterns

Patterns of erosion in a long contraction are influenced by the condition of flow in the upstream uncontracted channel. When the bed shear stress in the upstream channel was less than the critical shear stress, the bed in the long contraction was eroded, but did not have sand waves over the bed at the equilibrium condition of scour for the bed materials used in the experiments. In the beginning, when the flow was just released, some sand waves might appear in the long contraction, but their growth was progressively inhibited as the bed shear stress went on continuously decreasing with the development of scour in the long contraction. Finally, as the equilibrium condition was reached, the sand waves disappeared altogether.

In the case of bed load movement in the upstream channel, the sand waves

may or may not disappear in the long contraction, depending on the flow conditions and the bed material size.

Erosion Patterns with Stationary Bed in Upper Reach

Erosion in the long contraction was generally nonuniform, both in the longitudinal and transverse directions. A contour map of the eroded bed is shown in Fig. 5 for a typical experiment. Fig. 5(*a*) shows a 1.83-m long contraction; Fig. 5(*b*) shows a 2.44-m long contraction. In Fig. 5(*b*), deep local scour near the left side wall is clearly shown. Two-dimensional sand waves in the uncontracted upper channel and inside the contraction are clearly shown in the figures.

In the inlet region, deep holes were scoured on either side close to the walls. The reason for this was believed to be the generation of secondary currents. In most of the experiments, it was observed that there was a deeper scour

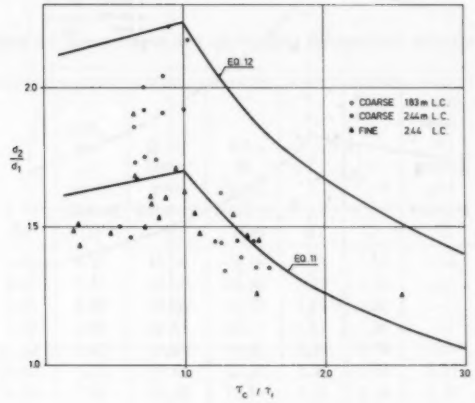

FIG. 6.—Plot of Experimental Data on d_2/d_1 and τ_c/τ_1 Coordinates for General Erosion Inside Contraction

in the region close to the right wall of the contraction than that in the corresponding region near the opposite wall. The difference in the maximum depth of scour on the two sides in some experiments was as much as 2.5 cm. This was believed to be mainly due to higher local velocity near the right wall. The wooden walls by which the channel was contracted were manufactured to an accuracy of 0.3 cm. Slight misalinement of the contraction walls could have been a source causing different scour depths on the two sides. However, great care was taken in alining the contraction walls. These walls were removed and replaced at least three times during the course of these experiments, and because the deeper scour always occurred near the right side wall, a higher velocity near the right side wall may have been caused by some very slight transverse slope which could, however, not be detected. Some velocity measurements were actually taken which supported the preceding premise.

Inside the contraction, the maximum scour generally occurred at the center of the channel or close to it, although in some experiments, the maximum erosion was close to the right wall.

Erosion Patterns with Moving Bed in Upper Channel

When there was bed load movement in the upper reach, sand was fed at an appropriate rate so that the material removed from the bed surface by the flow was replaced by sand feed. At relatively small rates of bed load transport, the eroded bed in the upper reach remained more or less flat. When the bed load transport was increased, sand waves started forming both in the upper reach and inside the long contraction. Erosion profiles inside the long contraction were similar to those when the upper channel sand bed was stable, the difference

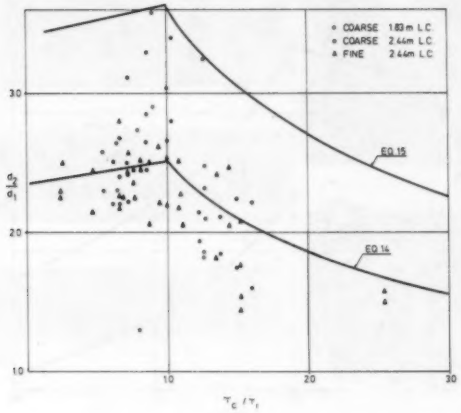

FIG. 7.—Plot of Experimental Data on d_2/d_1 and τ_c/τ_1 Coordinates for Local Scour Near Side Walls in Inlet Region

being that the bed was covered with sand waves at high rates of bed load movement.

Analysis of Results

Long Contraction.—The experimental data have been appropriately reduced in order to check Straub's formula for the equilibrium depth of scour. The results are plotted in a diagram with τ_c/τ_1 and d_2/d_1 as coordinates (see Fig. 6). The prediction from Straub's formula that the maximum value of d_2/d_1 occurs at $\tau_c/\tau_1 = 1.0$ is supported by the experimental results. Eq. 5, with $m = 3$, has been plotted on this diagram for the sake of comparing the predicted values with the experimental ones. Despite obvious scatter, the experimental data are well described by the calculated values scaled up by about 20%. Thus, the following equation appears to give the average value of d_2/d_1 in Fig. 6

$$\frac{d_2}{d_1} = 1.2\left(\frac{B_1}{B_2}\right)^{6/7}\left[\left(\frac{B_1}{B_2}\right)^{1/3}\left(1-\frac{\tau_c}{\tau_1}\right)+\frac{\tau_c}{\tau_1}\right]^{-3/7} \quad \ldots\ldots\ldots\ldots (11)$$

The experimental values are in fact the values of maximum depth of scour in the central plane within the long contraction as already mentioned, whereas Eq. 5 correlates the ratio of the average cross-sectional scour depth and the upstream depth with τ_c/τ_1. The experimental values of d_2/d_1 are thus expected to be somewhat higher than the theoretical values. In Fig. 6, the outer envelope curve is also plotted, which corresponds to the following equation

$$\frac{d_2}{d_1} = 1.58\left(\frac{B_1}{B_2}\right)^{6/7}\left[\left(\frac{B_1}{B_2}\right)^{1/3}\left(1-\frac{\tau_c}{\tau_1}\right)+\frac{\tau_c}{\tau_1}\right]^{-3/7} \quad \ldots\ldots\ldots\ldots (12)$$

Since the design is invariably done against the worst situation, it is suggested that Eq. 12 be used in design practice. There does not seem to be any great

TABLE 1.—Data on Scour Depth in 1.83-m Long Contraction with Coarse Sand Bed

Number (1)	$S \times 10^4$ (2)	d_1, in centimeters (3)	Q, in liters per second (4)	d_2, in centimeters (5)	d_2/d_1 (6)	τ_c/τ_1 (7)	Sand feed, in grams per second (8)	d_2/d_1, LH* (9)	d_2/d_1, RH* (10)
1	9.60	6.71	15.04	9.14	1.36	1.51	—	—	—
2	9.60	7.25	16.46	10.06	1.39	1.40	—	—	—
3	9.60	8.05	19.86	11.58	1.44	1.26	—	1.85	2.10
4	9.60	8.08	22.41	13.11	1.62	1.26	—	1.82	2.52
5	23.30	5.43	15.04	9.45	1.74	0.79	—	1.30	2.75
6	23.30	6.71	19.86	12.50	1.86	0.64	2.27	2.30	2.65
7	23.30	7.93	23.83	11.89	1.50	0.54	2.27	2.30	2.58
8	33.00	3.44	9.93	7.62	2.22	0.90	2.27	2.90	3.58
9	33.00	4.27	15.04	8.53	2.00	0.71	3.18	—	—
10	21.40	3.63	9.08	4.88	1.34	1.26	—	2.48	3.25
11	21.40	4.76	13.34	9.14	1.92	1.00	—	2.66	3.03

*LH and RH = left hole and right hole near the side walls in the inlet region, respectively.

influence of the bed material size on the scour depth as far as these experiments reveal. Attention must, however, be drawn to the fact that while the fine sand bed reached nearly a state of equilibrium in 6 h, the coarse bed might continue eroding beyond this time limit. Such additional erosion is, however, believed to be relatively small. Since the experiments were performed with only two grades of sediments, the statement that the sediment size is unimportant as far as the maximum relative scour depth is concerned, cannot be generalized unless supported with additional data with other different sizes of sediments.

The average value of bed shear stress, τ_1, for which no erosion would occur in the long contraction, can be obtained from Eq. 6 by making $d_2/d_1 = 1.0$.

This gives

$$\frac{\tau_1}{\tau_c} = \left(\frac{B_2}{B_1}\right)^2 \quad (13)$$

The value of B_2/B_1 in the present experiments was 2/3 so that $\tau_1/\tau_c = 4/9$, for which the bed within the long contraction should remain uneroded. This value should, however, be corrected in view of the present experimental results which indicated that the observed value of d_2/d_1 is about 1.2 times greater than the predicted. After making this correction, $\tau_1/\tau_c = 0.37$ is the maximum value at which no erosion should occur in the long contraction with $B_2/B_1 = 2/3$. In the experiments, a value of $\tau_1/\tau_c = 0.63$ was reached for which d_2/d_1 was nearly 1.38.

Inlet Region.—There were deep holes eroded in the sand bed near the upstream transition walls of the long contraction on either side, as already described.

TABLE 2.—Data on Scour Depth in 2.44-m Long Contraction with Coarse Sand Bed

Number (1)	$S \times 10^4$ (2)	d_1, in centimeters (3)	Q, in liters per second (4)	d_2, in centimeters (5)	d_2/d_1 (6)	τ_c/τ_1 (7)	Sand feed, in grams per second (8)	d_2/d_1, LH[a] (9)	d_2/d_1, RH[a] (10)
1	9.60	6.34	15.04	8.53	1.35	1.60	—	1.60	2.22
2	9.60	6.83	16.46	9.75	1.43	1.49	—	1.75	2.25
3	9.60	7.41	19.58	10.67	1.44	1.37	—	1.85	2.11
4	9.60	8.35	21.00	11.89	1.42	1.22	—	1.94	2.15
5	23.30	4.94	15.61	9.45	1.91	0.85	1.09	2.45	2.85
6	23.30	5.94	20.71	10.36	1.75	0.71	2.27	2.41	3.11
7	23.30	6.40	23.55	10.67	1.67	0.66	4.36	2.20	2.40
8	23.30	4.08	12.20	8.84	2.17	1.03	—	2.80	3.40
9	23.30	6.89	25.25	10.06	1.46	0.61	4.36	2.10	2.51
10	33.60	3.44	9.93	7.01	2.04	0.85	—	2.65	3.30
11	33.60	4.12	14.19	7.93	1.92	0.71	2.27	2.22	2.50
12	21.80	6.89	12.22	11.89	1.73	0.65	3.18	2.20	2.68

[a]LH and RH = left hole and right hole near the side walls in the inlet region, respectively.

The maximum depth of scour in these holes was nondimensionalized by dividing the local flow depth by d_1. In Fig. 7, all the data for the coarse, as well as the fine sand, and also the data for the right and left scour holes, are plotted on d_2/d_1 and τ_c/τ_1 coordinates. The following equation is also plotted in Fig. 7 and appears to pass through the mean position of the plotted points

$$\frac{d_2}{d_1} = 1.77\left(\frac{B_1}{B_2}\right)\left[\left(\frac{B_1}{B_2}\right)^{1/3}\left(1-\frac{\tau_c}{\tau_1}\right)+\frac{\tau_c}{\tau_1}\right]^{-3/7} \quad (14)$$

TABLE 3.—Data on Scour Depth in 2.44-m Long Contraction with Fine Sand Bed

Number (1)	$S \times 10^4$ (2)	d_1, in centimeters (3)	Q, in liters per second (4)	d_2, in centimeters (5)	d_2/d_1 (6)	τ_c/τ_1 (7)	Sand feed, in grams per second (8)	d_2/d_1, LH[a] (9)	d_2/d_1, RH[a] (10)
1	5.20	6.55	12.20	8.23	1.26	1.51	—	1.45	1.77
2	5.20	6.86	16.46	10.06	1.47	1.44	—	2.05	2.48
3	5.20	3.87	7.09	4.88	1.26	2.55	—	1.58	1.51
4	9.04	4.36	9.36	6.71	1.54	1.34	—	1.82	2.42
5	9.04	5.33	12.20	8.23	1.54	1.08	—	2.18	2.52
6	9.04	5.43	13.34	8.84	1.63	1.00	—	2.20	2.55
7	9.04	6.68	16.17	10.67	1.60	0.87	—	2.06	2.52
8	9.04	7.53	21.28	11.89	1.58	0.76	—	2.25	2.45
9	9.04	7.56	21.56	12.19	1.61	0.75	2.27	—	2.35
10	12.30	6.37	9.93	9.45	1.48	1.09	—	2.05	2.18
11	12.30	2.74	5.11	3.96	1.45	1.52	—	1.55	2.08
12	12.30	5.18	15.04	7.93	1.53	0.81	1.09	2.45	2.52
13	12.30	4.45	12.20	7.62	1.71	0.94	—	2.22	2.62
14	12.30	5.91	17.31	8.84	1.50	0.71	2.27	2.42	2.58
15	12.30	6.55	21.85	12.50	1.91	0.64	4.99	2.18	2.25
16	16.60	4.72	14.47	7.93	1.68	0.65	3.18	2.25	2.80
17	16.60	6.61	22.70	9.75	1.48	0.47	7.63	2.15	2.45
18	28.10	6.49	25.25	9.45	1.46	0.25	20.70	2.50	2.25
19	52.90	4.05	16.17	6.10	1.51	0.24	20.70	2.30	2.25
20	62.00	3.90	15.32	5.79	1.49	0.21	27.24	—	—

[a]LH and RH = left hole and right hole near the side walls in the inlet region, respectively.

In order to cover the extreme values of scour depth, the following outer envelope equation is also plotted in Fig. 7

$$\frac{d_2}{d_1} = 2.56 \left(\frac{B_1}{B_2}\right)^{6/7} \left[\left(\frac{B_1}{B_2}\right)^{1/3} \left(1 - \frac{\tau_c}{\tau_1}\right) + \frac{\tau_c}{\tau_1}\right]^{-3/7} \quad \ldots\ldots\ldots\ldots (15)$$

Thus, all the values of scour depth actually measured are less than or equal to the calculated values from Eq. 15. The data are given in Tables 1–3.

Conclusions

Straub's simple one-dimensional model can be used for predicting scour depth in a long contraction with reasonable accuracy. For design purposes, the predicted depths should, however, be scaled up by about 58% to get a maximum local value. The inlet region close to the walls is subjected to severe local erosion. In order to obtain an estimate of the extreme maximum depth of scour in this region, the theoretical values should be multiplied by 2.56.

Acknowledgment

The work presented herein is abstracted from the writer's doctoral thesis. The original work was conducted in the Hydraulics Laboratory of the Imperial College of Science and Technology, at London, England, under the direction of the late Professor J. R. D. Francis. Partial financial support from the Dr. Wali Mohammad Fellowship, the Covenantors Educational Trust, and the S. J. Perry Foundation is gratefully acknowledged. The diagrams in this paper were prepared by J. Brezezina, Department of Civil Engineering, Ahmadu Bello University, Zaria, Nigeria.

Appendix I.—References

1. Ashida, K., "On River Bed Variation and Stable Channels in Alluvial Streams," *Bulletin of the Disaster Prevention Research Institute,* Japan, Vol. 14, Part I, 1964.
2. Gill, M. A., "Bed Erosion Around Obstructions in Rivers," thesis presented to the University of London, at London, England, in 1970, in partial fulfillment of the requirements for the degree of Doctor of Philosophy; also "Erosion of Sand Beds Around Spur Dikes," *Journal of the Hydraulics Division,* ASCE, Vol. 98, No. HY9, Proc. Paper 9198, Sept., 1972, pp. 1587–1602.
3. Komura, S., "Equilibrium Depth of Scour in Long Contractions," *Journal of the Hydraulics Division,* ASCE, Vol. 92, No. HY5, Proc. Paper 4898, Sept., 1966, pp. 17–37.
4. Smith, C. D., "Simplified Design for Flume Inlets," *Journal of the Hydraulics Division,* ASCE, Vol. 93, No. HY6, Proc. Paper 5550, Nov., 1967, pp. 25–34.
5. Straub, L. G., "Effect of Channel Contraction Works upon Regimen of Movable Bed Streams," *Transactions,* American Geophysical Union, Part II, 1934.
6. Wilkinson, A. R., "The Design and Construction of the Mailsi Siphon," *Proceedings,* Institution of Civil Engineers, London, England, Vol. 32, 1965.

Appendix II.—Notation

The following symbols are used in this paper:

B_1, B_2 = widths of normal and contracted channels;
D = size of bed material;
d_1, d_2 = flow depths in the normal and contracted channels;
g = gravitational acceleration;
m = constant;
n = Manning's coefficient of bed friction;
Q = discharge;
q_s = rate of sediment transport per unit channel width;
q_{so} = $[g(S_s - 1)D^3]$;
S_e = energy gradient;
S_s = specific gravity;
V = flow velocity;
τ_1 = bed shear stress in the normal channel; and
τ_c = critical shear stress of the bed material.

JOURNAL OF THE HYDRAULICS DIVISION

NUMERICAL CIRCULATION MODEL FOR WIND INDUCED FLOW

By Bryan R. Pearce[1] and Cortis K. Cooper,[2] Associate Members, ASCE

INTRODUCTION

If the wind driven motion near the free surface is carefully examined, one often finds a sharp velocity gradient in that upper few meters of water. Van Dorn (32) suggests that the drift current at a depth of 2 cm may be as little as one half the surface value. Shulman and Bryson (24) measured a very sharp gradient and Teeson, et al. (28) concluded, based on field studies, that the velocity gradient near the surface is large enough so that the draft of an object used to determine surface drift will have an effect on the observation. A variety of laboratory experiments have been performed by Shemdin (23), Baines and Knapp (1), and Larnaes (14), among others, which indicate a large velocity gradient exists near the surface, similar to a logarithmic law of the wall type profile.

Fig. 1 is based on data from Stolzenbach, et al. (27) and shows results of surface drift experiments in terms of the "deflection angle" and the "wind factor." The deflection angle is the angle of the surface drift, measured to the right of the wind speed and the wind factor is the surface drift speed, normalized by the 10-m wind speed. It is of interest to note that 3% of the wind speed is a common rule of thumb for estimating surface oil slick movement. Also note that the wind factor in the data varies from 1% to about 6% indicating that the rule is an oversimplification.

As a first try at interpreting the data available on wind induced currents, the writers turned to the classical Ekman (9) theory. However, for deep water the Ekman (9) theory produces a surface current that is 45° to the right of the wind direction (in the northern hemisphere). It can be readily observed from Fig. 1 that the measured deflection angles consistently fall between 0° and 13° with none close to 45°. Several of these experiments were examined

[1]Assoc. Prof. of Civ. Engrg., Univ. of Maine, 351 Aubert Hall, Orono, Me. 04469.
[2]President, New England Coastal Engrs., Penobscot Plaza, Bangor, Me. 04401.

Note.—Discussion open until August 1, 1981. To extend the closing date one month, a written request must be filed with the Manager of Technical and Professional Publications, ASCE. Manuscript was submitted for review for possible publication on June 3, 1980. This paper is part of the Journal of the Hydraulics Division, Proceedings of the American Society of Civil Engineers, ©ASCE, Vol. 107, No. HY3, March, 1981. ISSN 0044-796X/81/0003-0285/$01.00.

in detail to determine if bottom or unsteady effects could explain the discrepancy between theory and observation but none of these were successful. Therefore, the most likely explanation would appear to be the assumption in the Ekman formulation that the vertical eddy viscosity is constant over the depth.

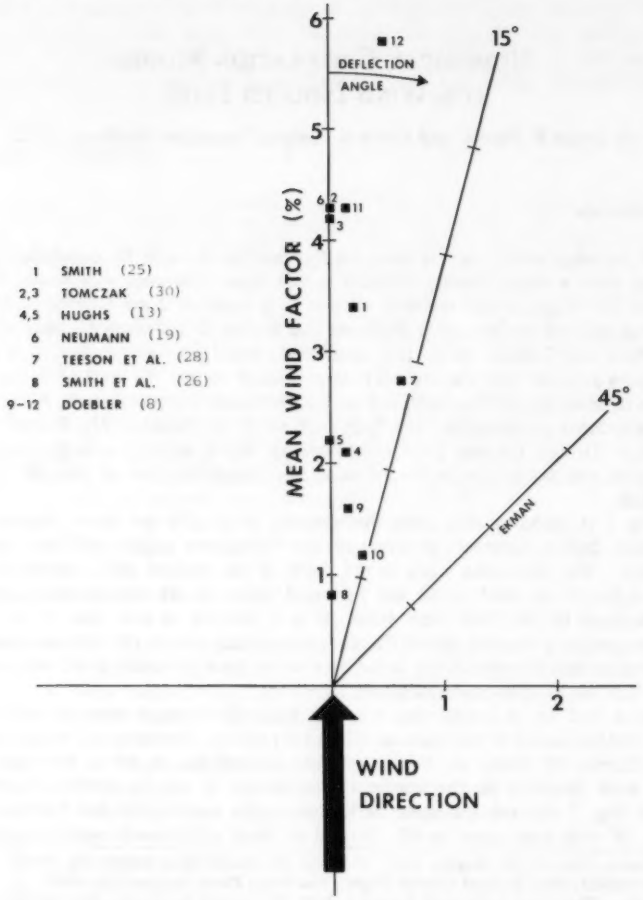

FIG. 1.—Comparison of Observed Surface Drift to Deep Water Ekman Solution

The vertical eddy viscosity arises from the turbulent frictional force between water layers, τ_{xz} and τ_{yz}. Ekman used the laminar analogy to write these stresses as a function of the turbulent vertical eddy viscosity coefficient, N_v, which

can also be written in terms of the turbulent shear stress components or:

$$\tau_{xz} = \overline{-\rho u' w'} = N_v \frac{\partial u}{\partial z}; \quad \tau_{yz} = \overline{-\rho v' w'} = N_v \frac{\partial v}{\partial z} \ldots\ldots\ldots\ldots\ldots (1)$$

in which u', v', w' = the turbulent components of the velocity in the x, y, and z directions, respectively; and ρ = the water density. Fig. 2 indicates the coordinate system used in this paper.

The component, w' will be zero near a solid boundary, and since $\partial u/\partial z$ (or $\partial v/\partial z$) will not, in general, be zero near the boundary, it follows that N_v must be zero in the vicinity of a solid boundary in order to satisfy the right side of Eq. 1. If waves are not breaking at the surface, then the foregoing argument implies that N_v must be near zero at the surface. Thus, based on a physical interpretation of N_v, it is concluded that a realistic variation would be a shape with N_v near zero at the surface and the bottom, and a maximum somewhere in between.

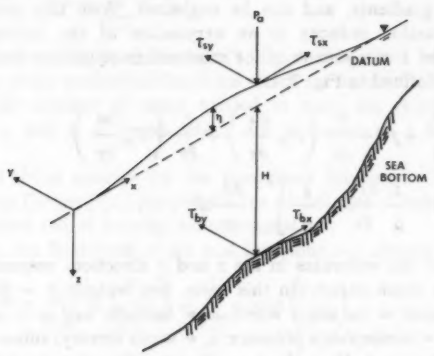

FIG. 2.—Definition of Variables

Arguments for a vertical variation in N_v have been advanced by many including Fjeldstad (10), Bowden, et al. (2), Murray (16), and Thomas (29). Madsen (15) assumed the vertical eddy viscosity to be zero at the surface and to increase linearly with depth. For steady state, his results indicate a deflection angle of approx 10° at the surface—a value more consistent with the field observations in Fig. 1. Other aspects of Madsen's model remain comparatively similar to Ekman's model, including the magnitude of the surface current and the total mass flux.

Another situation in which a vertical variation of the eddy viscosity results in a more realistic flow pattern, is for the case of flow in a long channel of finite depth with the wind blowing in the axial direction. For this situation, an analytic solution that assumes a constant vertical eddy viscosity, yields a linear velocity profile. If instead it is assumed that N_v varies parabolically (zero at the surface and at the bottom) then the solution for the velocity is a logarithmic profile near the surface and the bottom. This profile is substantiated in laboratory

experiments performed by Shemdin (23) and others.

The model to be presented here combines advantages of both analytical and numerical approaches. In particular, the model: (1) Makes relatively few simplifying assumptions; (2) has reasonable computation requirements; and (3) yields a continuous vertical variation for the velocities. The model is a logical extension of a model presented by Heaps (12) which uses the Galerkin weighted residual technique to simplify the Navier-Stokes equation. However, the model presented in this paper does not assume the vertical eddy viscosity to be constant in the vertical direction. In its present form, the model is being successfully applied in several estuarine and coastal areas for the calculation of wind and tidally generated currents.

Numerical Scheme

In many sea and lake circulation problems of practical importance, the vertical velocity component and its gradient are considerably smaller than the horizontal velocities and gradients, and can be neglected. With this assumption, the z momentum equation reduces to an expression of the hydrostatic pressure distribution. The x component of the momentum equations used in the model, with variables defined in Fig. 2, is:

$$\frac{du}{dt} = -g\frac{\rho_s}{\rho}\frac{\partial \eta}{\partial x} + fv + \frac{\partial}{\partial x}\left(N_H\frac{\partial u}{\partial x}\right) + \frac{\partial}{\partial y}\left(N_H\frac{\partial u}{\partial y}\right)$$

$$+ \frac{\partial}{\partial z}\left(N_v\frac{\partial u}{\partial z}\right) - \frac{1}{\rho}\frac{\partial P_a}{\partial x} - \frac{g}{\rho}\int_{-\eta}^{z}\frac{\partial \rho}{\partial x}\,d\zeta \quad \ldots\ldots\ldots\ldots\ldots\ldots (2)$$

in which u, v = the velocities in the x and y direction, respectively; η = the water depth to some datum (in this case, low water); g = gravity; f = the Coriolis parameter = $2\omega \sin \phi$ where ϕ = latitude; and ω = angular velocity of the earth; P_a = atmospheric pressure; ρ_s = water density; subscript s designates the surface value; and N_H = horizontal eddy viscosity. A similar expression is used for the y direction. The vertically integrated form of the continuity equation for an incompressible fluid is

$$\frac{\partial \bar{U}}{\partial x} + \frac{\partial \bar{V}}{\partial y} = \frac{\partial \eta}{\partial t} \quad \ldots\ldots\ldots\ldots\ldots\ldots\ldots\ldots\ldots\ldots (3)$$

in which $\bar{U} = \int_{-\eta}^{H} u\,dz$; and $\bar{V} = \int_{-\eta}^{H} v\,dz$.

The surface boundary condition is:

$$\tau_{sx} = -\rho_s N_v\frac{\partial u}{\partial z}\bigg|_{z=-\eta}; \quad \tau_{sy} = -\rho_s N_v\frac{\partial v}{\partial z}\bigg|_{z=-\eta} \quad \ldots\ldots\ldots\ldots\ldots (4)$$

in which τ_{sx} and τ_{sy} = the surface shear stresses induced by the wind in the x direction and y direction, respectively.

The shear stresses at the bottom boundary can be expressed as

$$\tau_{bx} = -\rho N_v\frac{\partial u}{\partial z}\bigg|_{z=H}; \quad \tau_{by} = -\rho N_v\frac{\partial v}{\partial z}\bigg|_{z=H} \quad \ldots\ldots\ldots\ldots\ldots (5)$$

in which τ_{bx} and τ_{by} denote the components of bottom friction in the x and y directions, respectively.

A linear bottom friction is assumed, or

$$\frac{\partial u}{\partial z} = \frac{-c_b u}{N_v}\bigg|_{z=H} ; \quad \frac{\partial v}{\partial z} = \frac{-c_b v}{N_v}\bigg|_{z=H} \quad \ldots\ldots\ldots\ldots\ldots\ldots (6)$$

in which c_b = the "slip coefficient."

The governing equations are simplified by using an expanded version of a Galerkin or weighted residual approach used by Heaps (11, 12). A detailed description of the development will not be included here but can be found in Cooper and Pearce (4) or Pearce, et al. (20). However, since the development is somewhat unusual, it is appropriate to include a brief outline.

The application of a weighted residual technique begins by assuming a functional relationship to approximate the true solution:

$$\hat{u} = u_o + \sum_{I=1}^{I'} c_I \Omega_I ; \quad \hat{v} = v_o \sum_{I=1}^{I'} d_I \Omega_I \quad \ldots\ldots\ldots\ldots\ldots\ldots (7)$$

in which $\hat{u}$ and $\hat{v}$ = the "trial functions"; Ω_I = prescribed function; c_I and d_I = coefficients of the prescribed functions which are determined in the solution process; I' = the number of terms needed to reach the required degree of accuracy; and u_o and v_o = terms which are functions of z but constant in time.

Heaps (11,12) chose cosines for the prescribed functions. Other functions have been tried by Davies (7). Cosines have the advantages of being well behaved when differentiated and of forming an orthogonal set.

Using cosines, the final form of the trial functions was chosen as

$$\hat{u} = \frac{\tau_{sx} z^2 (z - H)}{\rho_s H^2 N_b} + \frac{\tau_{sx}}{\rho_s \alpha} \ln\left(\frac{N_b}{N_v}\right) + \sum_{I=1}^{I'} c_I \cos\left(\frac{a_I z}{H}\right) \quad \ldots\ldots\ldots\ldots (8)$$

$$\hat{v} = \frac{\tau_{sy} z^2 (z - H)}{\rho_s H^2 N_b} + \frac{\tau_{sy}}{\rho_s \alpha} \ln\left(\frac{N_b}{N_v}\right) + \sum_{I=1}^{I'} d_I \cos\left(\frac{a_I z}{H}\right) \quad \ldots\ldots\ldots\ldots (9)$$

in which all symbols are specified constants or constant functions except for the undetermined parameters, c_I and d_I. The variable N_b has the value of N_v at the bottom. The values of a_I are determined by satisfying the bottom boundary conditions and can be found as the solution to:

$$a_I \tan a_I = \frac{c_b H}{N_b} \quad \ldots\ldots\ldots\ldots\ldots\ldots\ldots\ldots\ldots\ldots (10)$$

Eqs. 8 and 9 are the results of an evolutionary process by the writers. Originally, a simpler form (4) without the logarithmic term was chosen. It was discovered, however, that by using a variation of N_v which became small near a boundary, a convergence problem occurred in the model. It was reasoned that since the velocity profile in the upper several meters of water develops rapidly, then a form for u_o, v_o that contains a logarithmic term would aid convergence. The u_o and v_o shown in Eqs. 8 and 9 dramatically improved convergence so that, in general, only three cosine terms in the series are needed for the variety

of applications investigated so far. A no-slip boundary condition at the bottom was included in the initial formulation and caused a similar problem with convergence. However, the solution in this case could not be remedied as in the case of the surface and a slip bottom boundary was imposed, Eq. 6.

The trial functions, Eqs. 8 and 9, are substituted into the momentum equations, Eq. 2 and its y analogy. In general, there will be an error associated with this substitution, since the trial functions are not the exact solutions to the momentum equations. This error is sometimes referred to as the "residual," and is minimized by specifying that the integral of the residual over a region be zero. The Galerkin method consists of multiplying the residual by Ω_j and integrating over the water column. The integration yields:

$$\int_0^H R\Omega_j\,dz = \int_0^H \left\{ \frac{d\hat{u}}{dt} + g\frac{\rho_s}{\rho}\frac{\partial \eta}{\partial x} - \left[\frac{\partial}{\partial x}\left(N_H \frac{\partial \hat{u}}{\partial x} \right) + \frac{\partial}{\partial y}\left(N_H \frac{\partial \hat{u}}{\partial y} \right) \right] \right.$$
$$\left. - \left(\frac{\partial N_v}{\partial z}\frac{\partial \hat{u}}{\partial z} \right) - N_v \frac{\partial^2 \hat{u}}{\partial z^2} - f\hat{v} + \frac{1}{\rho}\frac{\partial P_a}{\partial x} + g\frac{1}{\rho}\int_0^z \left[\frac{\partial \rho}{\partial x}\,d\zeta \right] \right\} \Omega_j\,dz = 0 \qquad (11)$$

in which the N_v term has been differentiated and conveniently separated. There is an equivalent Galerkin expression for the y direction.

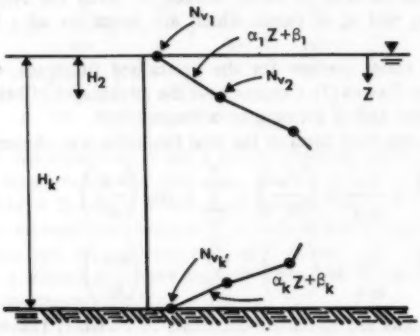

FIG. 3.—Functional Form for Vertical Variation of N_v

Observe that the lower limit of the integration in Eq. 11 has been moved from $z = -\eta$ to $z = 0$. For η other than zero, the integrations in Eq. 11 would become a function of time, thus, complicating the solution and increasing computation time.

In order to evaluate the integrals, the vertical variation of N_v must be specified. This is done by approximating N_v with a series of linear segments as shown in Fig. 3. The slope α_k, the intercept β_k, and the number of segments k' are assumed given. [When more than one linear segment is used (i.e., $k' \geq 3$) then N_b in Eqs. 8, 9, and 10 should be replaced by $N_b = \alpha_1 H + \beta_1$.]

Carrying out the integrations implied in Eq. 11, transforms the x component of Eq. 3 into I' equations in terms of the undetermined parameters c_j and d_j or:

$$0 = \left(\frac{\partial}{\partial t} - \epsilon\right) c_J - f d_J + \left(B_J \frac{\partial \eta}{\partial x} + A_J\right) - \sum_{I=1}^{I'} c_I E_{IJ}; \quad \text{for} \quad J = 1, 2, \ldots, I' \quad (12)$$

in which A_J, B_J, and E_{IJ} = constants which arise from the integration; and ϵ = a parameter such the $\epsilon u = \partial/\partial x (N_H \partial u/\partial x) + \partial/\partial y (N_H \partial u/\partial y)$. Linearization of the N_H terms is considered by Neumann (17) and Neumann and Pierson (18). An equation similar to Eq. 12 exists for the y direction. In the present formulation, the convective terms (those of the form $u\ \partial u/\partial x$ and $u\ \partial u/\partial y$), density gradient and atmospheric pressure gradient terms have been neglected.

Note that the constants B_J, A_J, and E_{IJ}, need to be evaluated only once or when N_v changes in time. The time scale for significant changes of N_v is of the order of hours, whereas the time step is of the order of minutes. Thus, the computational cost of the evaluation of the constants is relatively small. Addition of the vertical eddy viscosity variation adds the E_{IJ} term. Without this term, the number of calculations per time step per grid element would increase linearly with I' (recall I' is the number of cosine terms in the series expansion, see Eq. 7). With the E_{IJ} term, the number of calculations will increase approximately as I' squared.

Eq. 12 and its equivalent in the y direction represent a set of $2I'$ equations with $2I' + 1$ unknowns (c_J,d_J,η). To solve for the unknowns, one more equation linking c_J, d_J, and η must be specified. This is accomplished using the continuity equation, Eq. 3. Expressions for $\bar{U}$ and $\bar{V}$ in Eq. 3 can be obtained by integrating the trial functions over the depth. The variables, $\bar{U}$ and $\bar{V}$, are then substituted into Eq. 3, which will be discretized along with Eq. 12 and its y counterpart. Thus a set of $2I' + 1$ equations is now available to deal with the set of $2I' + 1$ unknowns.

The method chosen for the horizontal discretization is the "split-time," finite difference scheme used by many modelers such as Platzman (21) and Reid and Bodine (22). Originally selected for simplicity and as a vehicle for examining the suitability of using the Galerkin method, the split-time method has performed well but should not be considered limiting.

Numerical three-dimensional (3-D) models can be limited in scope because their computer time and storage requirements are too large for problems of practical interest. One of the major objectives of this research was to develop a three-dimensional model which could be applied inexpensively. The number of multiply-divides carried out by the program per time step per grid element is $[2(I')^2 + 11(I') + 7]$ which for $I' \leq 7$ is about the same as an efficiently programmed, explicit, vertically-averaged circulation model. Weare (33), estimates about 200 multiplications per grid point per time step for one vertically-averaged, explicit, finite difference scheme.

The split-time finite difference scheme is conditionally stable. An expression indicating the stability criteria for the full model described here has not yet been derived. Two conditions serve to provide a reasonably good choice for the time step, Δt. The condition [Courant, et al. (5); Platzman (21)]:

$$\Delta t < \frac{\Delta L}{\sqrt{2gH}} \quad \ldots\ldots\ldots\ldots\ldots\ldots\ldots\ldots\ldots\ldots\ldots\ldots\ldots\ldots\ldots\ldots\ldots\ldots \quad (13)$$

in which ΔL = the horizontal grid spacing, must be satisfied. In general, Eq.

13 is the only condition needed for vertically-averaged explicit models. It has been found, however, that Eq. 13 alone is not sufficient for this model; an additional condition is needed. An approximate form can be obtained by examining the Galerkin statement, Eq. 11. Ignoring the horizontal eddy viscosity terms and the Coriolis term, assuming N_v is constant, and carrying out the indicated integration produces:

$$0 = \frac{\partial c_J}{\partial t} + \frac{N_v a_J^2}{H^2} c_J \quad (14)$$

Performing a forward difference in time, with time step Δt yields:

$$\frac{c_J(t) - c_J(t + \Delta t)}{\Delta t} = \frac{N_v a_J^2}{H^2} c_J(t) \quad (15)$$

The method of von Neuman [Carnahan, et al. (3)] introduces $c_J(t) = \lambda(t)\, e^{i\alpha x}$, the harmonic component of a perturbation. That substitution yields upon rearrangement:

$$A = \frac{\lambda(t + \Delta t)}{\lambda(t)} = 1 - \Delta t \frac{N_v a_J^2}{H^2} \quad (16)$$

in which A = the amplification factor, which must obey the criterion, $|A| \le 1$, to yield a stable scheme. Since the second term in the right side of Eq. 16 is always positive, the limiting condition for Δt is:

$$\Delta t < \frac{2H^2}{N_v a_J^2} \quad (17)$$

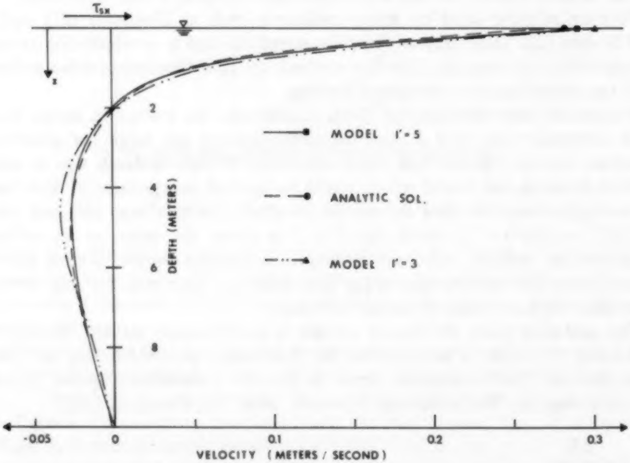

FIG. 4.—Comparison Between Model and Analytic Solution for Case of Finite Channel ($c_b = \infty$, α = 0.014 m/s, β = 0.00093 m²/s, Wind = 20 m/s)

Experience operating the model so far indicates that Eq. 17 is too lax a criterion and that

$$\Delta t < \frac{H^2}{N_v a_J^2} \quad \ldots \quad (18)$$

gives a better estimate of the time step. The discrepancy is undoubtedly due to the many simplifying assumptions made during Eq. 17. While Eq. 18 provides a working criteria, it is hoped that a more complete analysis can be developed in the future.

Analytic Test Cases

To address questions concerning convergence, stability, and verification of computer coding, comparisons were made to analytical solutions. The problems for which closed form solutions can be found tend to be for simplified geometry and flow situations. Nevertheless, this aspect of the process is valuable since it provides the only situation where nearly perfect agreement can be expected.

In the case of wind over a closed-ended channel with linearly varying eddy

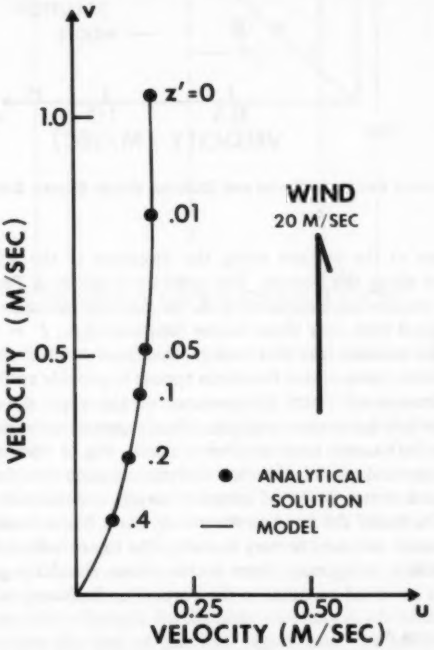

FIG. 5.—Comparison Between Model and Analytic Solution for Case of Linearly Varying N_v (α = 0.0061 m/s, β = 0.00093 m^2/s, $c_b = \infty$)

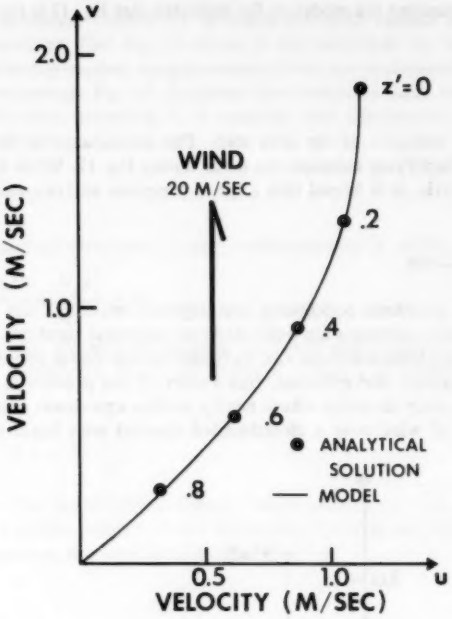

FIG. 6.—Comparison Between Model and Shallow Water Ekman Solution ($\beta = 0.094$, $c_b = \infty$)

viscosity, a flow at the surface along the direction of the wind is expected with return flow along the bottom. The solution is given in Pearce, et al. (20) and the model results are compared with the analytic solution in Fig. 4. The comparison is good with only three cosine functions (i.e., $I' = 3$). To illustrate convergence, the solution for five cosine functions is also shown in Fig. 4. Here and elsewhere, three cosine functions appear to provide sufficient accuracy.

Many one-dimensional (1-D) comparisons of the type shown above have been carried out and have shown similar characteristics of rapid convergence. Comparisons to 3-D cases have also been made. Fig. 5 shows a comparison between the numerical model and the analytic solution for the case of wind induced flow in a water body of constant depth and infinite lateral extent. The problem is basically the same as the steady-state Ekman solution (9) except that N_v in this case is assumed to vary linearly. The figure indicates an essentially identical comparison using only three cosine terms. Similarly good results are obtained if N_v is assumed constant in the vertical as indicated in Fig. 6.

Estimation of c_b and N_v

The comparisons described in the previous section confirms the model formulation and coding for simple cases, but to further investigate the charac-

teristics of the model and to gain insight into the functional form of the vertical eddy viscosity parameter, a series of comparisons to laboratory data was undertaken. Experiments suitable for comparison have been carried out by Shemdin (23) and Baines and Knapp (1). Before making comparisons to this data, however, some variation for N_v must be decided upon. Furthermore, if the model is to be successful in a predictive sense, then it is necessary to select a method or algorithm for choosing values for N_v and c_b.

Distribution of N_v.—The distribution of N_v with depth is, of course, a matter of considerable interest and has been addressed in a variety of ways. Based on Refs. 2, 6, and others, a reasonable distribution for N_v would appear to be as shown in Fig. 7. The justification for that distribution is described in the following paragraphs.

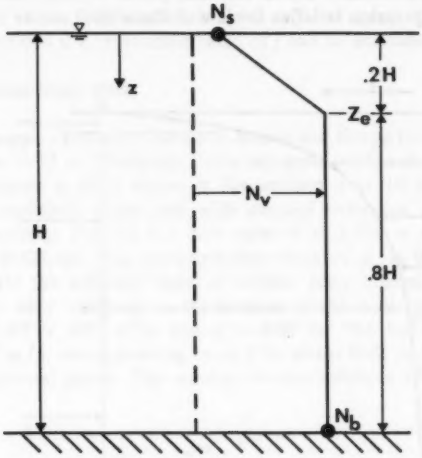

FIG. 7.—Distribution of N_v Used in Model Simulations

Bowden, et al. (2) inferred the variation of N_v from tidal current observations. Although the data showed considerable scatter, he concluded that the N_v values tended to be highest in the middle of the water column and lowest at top and bottom. This result is consistent with the earlier argument in the Introduction. Bowden's recommendation is to use a model based on a constant eddy viscosity in the bulk of the fluid above a friction layer near the bottom. In cases where wind generated currents are important, a boundary layer near the surface is also important and thus, from Bowden's recommendation, a friction layer near the surface is also justified.

Csanady (6) provides a formula for the eddy viscosity at a boundary or turbulent interface and covers the law of the wall region near the interface where the velocity distribution is logarithmic. The eddy viscosity is constant in the "core" region very near the interface. The core region is equivalent to the laminar sublayer near a solid boundary except that "viscous wavelets" may be present

which increase the effective eddy viscosity to a value greater than the molecular value, ν. Fig. 8 indicates the various regimes. Csanady found the depth of the core layer to be generally small, on the order of 10^{-2} cm for one experiment, and he gives values for N_v in the core region as a function of a Reynolds number, $u_* H/\nu$, in which $u_* = \sqrt{\tau/\rho}$ at the surface.

The problem remains to find N_v outside the core region. Townsend (31) has compiled data on the subject, including turbulent flow in pipes and channels, and he notes that the simple assumption that the eddy viscosity is constant outside the wall layer describes the velocity distribution for various flows. From similarity arguments, Townsend concluded that in the wall layer

$$N_v = \kappa u_* z \quad (19)$$

in which z = the distance above the bed; and κ = von Karman's constant, $\kappa \simeq 0.4$. This expression satisfies the law of the wall.

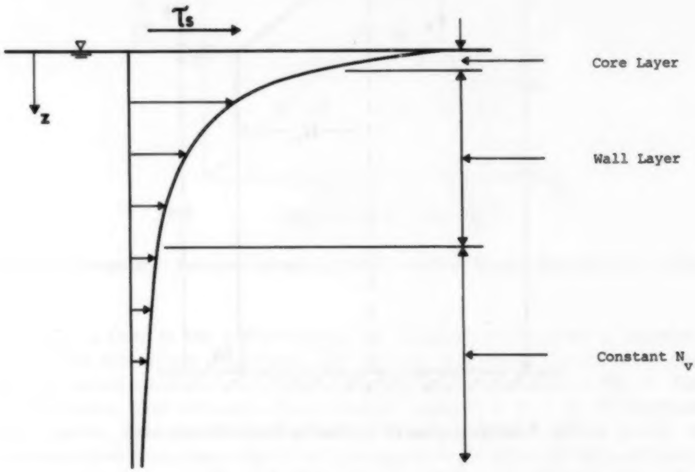

FIG. 8.—Various Regimes of N_v

For the case of open channel flow, Townsend indicates that the limit of the wall layer occurs at the position where:

$$R = \frac{u_* H}{N_v} \simeq 13 \quad (20)$$

in which H = the channel depth; and R = the flow Reynolds number = $u_* H/N_v$. Other sources indicate values of about the same magnitude. The flow Reynolds number, R = 12, is chosen here for convenience. If it is assumed that N_v at $z = 0$ is much smaller than in the constant region, then Eqs. 19 and 20

can be used to evaluate the distance, z_e, from the surface at which N_v becomes constant or:

$$z_e = \frac{H}{\kappa R} \qquad (21)$$

Taking $\kappa = 0.4$ and the flow Reynolds number, $R = 12$ implies that $z_e \simeq 0.2H$. Thus, for an open channel, the wall layer comprises about 20% of the water column. Following this analogy for the surface, provides a distribution of N_v as shown in Fig. 7.

Choice of c_b.—The boundary layer at the bottom is simulated by the use of a slip coefficient, c_b, at the bottom. The bottom stress is given in the numerical model by $\tau = \rho c_b u_b$, in which u_b = the velocity at the bottom. If this is equated to the shear stress derived from a quadratic formula such as the Darcy equation $\tau = \rho f u_b^2/8$, then values for f can be obtained as $f = 8c_b/u_b$. Thus an estimate for c_b can be obtained if a reasonable value of f can be estimated.

Comparisons to Laboratory Data

Baines and Knapp.—The experiments of Baines and Knapp (1) were performed in a 1 m × 1 m × 13 m laboratory flume equipped with a fan. The resulting air motion produced a shear stress at the surface over 10 m of the flume. Two air flow conditions were used with average velocities of 6.1 m/s and 3.9 m/s, respectively. For the 6.1 m/s case: $R = 2{,}870 = u_*H/\nu$ in which H = depth (= 0.328 m). The corresponding value of u_* is 0.00875 m/s and from Csanady (6) the effective core or surface eddy viscosity, $N_s \simeq 2.5 \times 10^{-6}$ m²/s. The eddy viscosity at the bottom of the wall region is then $N_v \simeq u_*H/12 = 1.87 \times 10^{-4}$ m²/s and $z_e = 0.06$ m. The bottom friction was set at 4×10^{-5} m/s, corresponding to an f of about 0.02, a reasonable value for that experimental setup. The solution is not sensitive to c_b. Fig. 9 is a

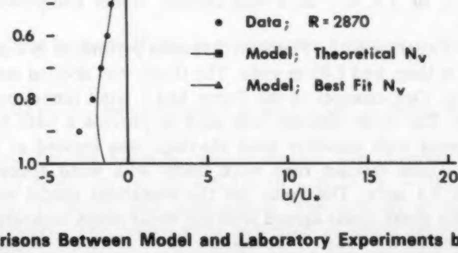

FIG. 9.—Comparisons Between Model and Laboratory Experiments by Baines and Knapp (R = 2,870)

comparison of the model output to the Baines and Knapp data. The parameters chosen above provided the theoretical N_v solution. Except at the return flow jet near the bottom, the fit is quite good. This behavior is to be expected since the bottom boundary layer is not being modeled. A better fit at the surface can be seen with the "best fit" line in Fig. 9. The only change is that N_s has been lowered to 1×10^{-6} m^2/s. More than one possible explanation for the difference in the theoretical N_s and the "best fit" N_s are apparent. Small errors in u_* could produce discrepancy. The N_s estimates from Csanady (6) are approximate. Finally, the presence of waves at the surface affects N_s. Slight changes in the experimental procedure, such as the addition of detergent by Baines and Knapp, may affect the wave climate in the apparatus and, therefore, N_s.

The fit to the R = 1,900 case in Fig. 10 is similar. From Csanady, we obtain $N_s \simeq 2.0 \times 10^{-6}$ m^2/s and this compares to the best fit case of 1.0×10^{-6}

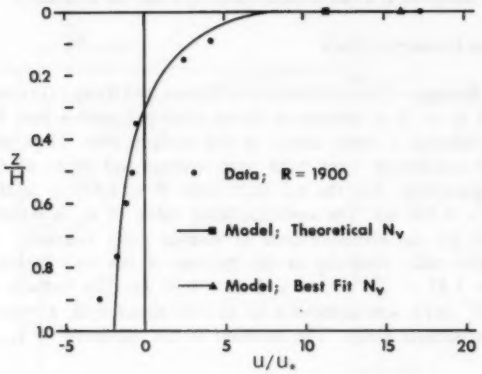

FIG. 10.—Comparisons Between Model and Laboratory Experiments by Baines and Knapp (R = 1900)

m^2/s. The analysis based on the flow Reynolds number provides $N_b = 1.5 \times 10^{-4}$ m^2/s for the interior of the fluid which compares well to the data. A value for c_b of 5×10^{-5} m/s was chosen, which compares to an f value of about 0.03.

Shemdin.—Experiments by Shemdin (23) were performed in a laboratory flume 1 m deep, 45 m long, and 1.83 m wide. The flume was divided into two channels of equal width. One channel of the flume had a wind tunnel over it to induce water motion. The other channel was used to provide a path for return flow. A beach covered with stainless steel shavings was located at the end of the wind tunnel. Three distinct runs were made with wind speeds of 9.1 m/s, 5.4 m/s, and 3.1 m/s. The input for the numerical model was designed so that the surface shear stress agreed with the shear stress measured by Shemdin.

In order to model the situation Shemdin created in his experiments, a boundary condition was established in the model which allowed for a net flux at the

upstream and downstream boundaries. The flux is the amount of water being driven through the stainless steel shavings and along the return channel and was determined from the Shemdin data.

For the 9.1-m/s case shown in Fig. 11, the theoretical N_v model gave $N_s = 6 \times 10^{-6}$ m^2/s, $N_b = 1.05 \times 10^{-3}$ m^2/s, $z_e \simeq 0.19$ meters. The value for c_b

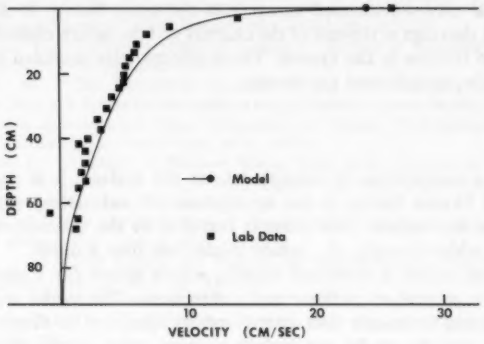

FIG. 11.—Comparisons Between Model and Laboratory Experiments by Shemdin (U = 9.1 m/s)

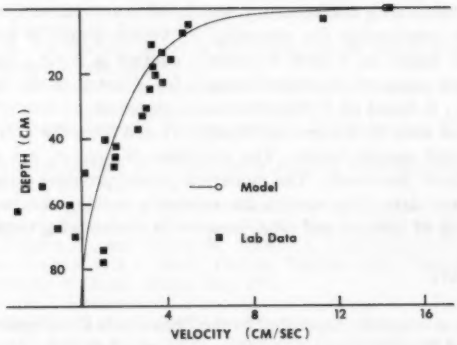

FIG. 12.—Comparison Between Model and Laboratory Experiments by Shemdin (U = 5.4 m/s)

was chosen as 0.02 m/s. The comparison is very good, differing at the surface by about 2 cm/s.

The comparison for the 5.4-m/s case is similar. The theoretical N_v model provides $N_s = 2.5 \times 10^{-6}$ m^2/s, $N_b = 6.3 \times 10^{-4}$ m^2/s, $z_e \simeq 0.19$ m, and c_b = 0.01 m/s. Fig. 12 shows that comparison. The velocity at the surface is matched very closely. The return flow indicated at about 60 cm in Fig. 12 is not modeled. It is difficult to speculate about the apparent three-layered

nature of the laboratory data, although natural thermal statification seems a distinct possibility. A comparison to the case of 3.1 m/s led to comparable results near the surface, but the data indicated an even stronger three-layered nature.

The values chosen for c_b correspond to unreasonably high values of f. Lower values for c_b corresponding to more reasonable values of f were used, but the numerical model continued to oscillate for many hours. It is conjectured that the steel shavings at the end of the channel and the return channel effectively increased the friction in the system. These effects were included by increasing the values of c_b as indicated previously.

Conclusions

Based on a compilation of current data at the surface, it is concluded that the classical Ekman theory is not appropriate for calculating wind generated currents near the surface. The cause is found to be the assumption by Ekman of a vertical eddy viscosity, N_v, which is constant over a depth.

A numerical model is described briefly, which allows for a variation of N_v over depth, z, as well as in the x and y directions. The model was developed using a Galerkin technique first introduced by Heaps (11). Heaps' method is expanded so that the model can include a sharp, wind driven profile near the surface. The method is computationally reasonable, requiring about the same number of computations as a vertically averaged formulation. Simple stability criteria are presented.

In order to test coding and accuracy, the model is compared to several analytic test cases. A relationship for choosing N_v versus depth is presented. That relationship is based on a flow Reynold's number $u_* H/N_v$, from Townsend (31) and a core value of N_v from Csanady (6). Choice of the bottom friction coefficient, c_b, is based on f, from the Darcy equation.

Experimental data by Baines and Knapp (1) and Shemdin (23) are compared to the numerical model results. The variables N_v and c_b are shown by the method described previously. The numerical model provides good comparisons to the measured data. The writers are currently making comparisons to field data in the Gulf of Mexico and other areas with encouraging results.

Acknowledgments

This work was originally supported by the Techniques Development Laboratory of the National Weather Service. Additional support has come from the Instituto Tecnológico Petróleo del Venezolano and from the joint University of Maine-University of New Hampshire Sea Grant program. The writers would also like to thank Gabriel Csanady of the Woods Hole Oceanographic Institution and Keith Stolzenbach and Ole Madsen of the Massachusetts Institute of Technology whose occasional comments aided this development.

Appendix I.—References

1. Baines, W. D., and Knapp, D. J., "Wind Driven Water Currents," *Journal of the Hydraulics Division*, ASCE, Vol. 91, No. HY2, Proc. Paper 4270, Feb., 1965, pp. 205–221.

2. Bowden, K. F., Fairbairn, L. A., and Hughes, P., "The Distribution of Shearing Stresses in a Tidal Current," *Geophysical Journal,* Vol. 2, 1959, pp. 288–305.
3. Carnahan, B., Luther, H. A., Wilkes, J. O., *Applied Numerical Methods,* John Wiley and Sons, Inc., New York, N.Y. 1969, pp. 449–450.
4. Cooper, C. K., and Pearce, B. R., "A Three-Dimensional Numerical Model to Calculate Currents in Coastal Waters Utilizing a Depth Varying Eddy Viscosity," *Technical Report No. 226,* Massachusetts Institute of Technology, Cambridge, Mass., 1977.
5. Courant, R., Friedrichs, K., and Lewy, H., "On the Partial Difference Equations of Mathematical Physics," *IBM Journal,* Mar., 1967, pp. 215–234.
6. Csanady, G. T., "Turbulent Interface Layers," *Journal of Geophysical Research,* Vol. 83, No. C5, 1978, pp. 2329–2342.
7. Davies, A. M., "The Numerical Solution of the 3-Dimensional Hydrodynamics Equations Using a B-Spline Representation of the Vertical Current Profile," *Proceedings of the Eighth International Liege Colloquium on Ocean Hydrodynamics,* Elsevier Scientific Publishing Co., New York, N.Y., 1977.
8. Doebler, H. J., "A Study of Shallow Water Wind Drift Currents at Two Stations Off the East Coast of the U.S.," *USL Report No. 755,* U.S. Navy Underwater Sound Lab., New London, Conn., 1966.
9. Ekman, V. W., "On the Influence of the Earth's Rotation on Ocean Currents," *Ark. Mat. Astron. Fys.,* Vol. 2, 1905, pp. 1–53.
10. Fjeldstad, J. E., "Ein Beitrag zur Theorie der Winderseugten Merresstromungen, *Beitr. Geophys.,* Vol. 23, 1929, pp. 237–247.
11. Heaps, N. S., "On the Numerical Solution of the Three-Dimensional Hydrodynamic Equation for Tides and Storm Surges," *Mem. Soc. R. Sci. Liege,* Vol. 6, No. 2, 1972, pp. 143–180.
12. Heaps, N. S. (1974), "Development of a Three-Dimensional Model of the Irish Sea," *Rapp. P. -v. Réun. Cons. int. Explor. Mer.,* Dec. 167: 147–162.
13. Hughs, P., "A Determination of the Relation Between Wind and Sea Surface Drift," *Quarterly Journal of the Royal Meteorological Society,* Vol. 82, 1956, pp. 494–502.
14. Larnaes, G., "Formation of Wind Waves," Series Paper #10, Technical University of Denmark, Copenhagen, Denmark, 1976.
15. Madsen, O. S., "A Realistic Model of the Wind-Induced Ekman Boundary Layer," *Journal of Physical Oceanography,* 1977.
16. Murray, S. P., "Trajectories and Speeds of Wind-Driven Currents Near The Coast," *Journal of Physical Oceanography,* Vol. 5, Apr., 1975.
17. Neumann, G., *Ocean Currents,* Elsevier Scientific Publishing Co., New York, N.Y., 1968.
18. Neumann, G., and Pierson, W., *Principles of Physical Oceanography,* Prentice-Hall, Inc., Englewood Cliffs, N.J., 1966.
19. Neumann, G., "The Relation Between Wind and Surface Currents Derived from Drift Card Investigations," *Dt. Hydrogr.,* Vol. Z, No. 19, 1966, pp. 253–256.
20. Pearce, B., Cooper, C., and Nelson S., "GAL: A 3-Dimensional Numerical Model to Calculate Currents with a Depth Varying Vertical Eddy Viscosity," *Technical Report,* University of Maine, Orono, Me., 1978.
21. Platzman, G. W., "A Numerical Computation of the Surge of 26 June 1954 on Lake Michigan," *Geophysica,* Vol. 6, 1958, pp. 407–438.
22. Reid, R. O., and Bodine, B. R. (1968), "Numerical Computation of the Storm Surges in Galveston Bay," *Journal of the Waterways and Harbor Division,* ASCE, Vol. 94, No. WW1, Proc. Paper 5805, Feb., 1968, pp. 33–57.
23. Shemdin, O. H., "Wind Generated Current and Phase Speed of Wind Waves," *Journal of Physical Oceanography,* Vol. 2, 1972, pp. 441–459.
24. Shulman, M. D., and Bryson, R. A., "Vertical Variation of Wind Driven Currents in Lake Mendota," *Journal of Limnology and Oceanography,* Vol. 6, No. 3, July, 1961.
25. Smith, J. E., *Torrey Canyon Pollution and Marine Life,* Cambridge University Press, Cambridge, England, 1968.
26. Smith, J. E., and Mac Intryre, W. G., "Investigations of Surface Film—Chesapeake Bay Entrance," *EPA 670/2-73-099,* U.S. Government Printing Office, Washington, D.C., 1974.
27. Stolzenbach, K. D., Madsen, O. S., Adams, E. E., Pollack, A. M., and Cooper,

C. K., "A Review and Evaluation of Basic Techniques for Predicting the Behavior of Surface Oil Slicks," *Technical Report #222*, Massachusetts Institute of Technology, Cambridge, Mass., 1977.
28. Teeson, D., White, F. M., and Schenck, H., "Studies of the Simulation of Drifting Oil by Polyethylene Sheets," *Ocean Engineering*, Vol. 2, Pergamon Press, Inc., New York, N.Y., pp. 1–11.
29. Thomas, J. H., "A Theory of Steady Wind-Driven Currents in Shallow Water and Variable Eddy Viscosity," *Journal of Physical Oceanography*, Vol. 5, 1975, pp. 136–142.
30. Tomczak, G., "Investigations with Drift Cards to Determine the Influence of the Wind on Surface Currents," *Oceanography*, Vol. 10, 1964, pp. 129–239.
31. Townsend, A. A., *The Structure of Turbulent Shear Flow*, Cambridge University Press, Cambridge, England, 1976.
32. Van Dorn, W. G., "Wind Stress on an Artificial Pond," *Journal of Marine Research*, Vol. 12, No. 3, 1963, pp. 219–275.
33. Weare, T. J., "Finite Element or Finite Difference Method for the Two-Dimensional Shallow Water Equations," *Computer Methods in Applied Mechanics and Engineering*, Vol. 7, 1976, pp. 351–357.

Appendix II.—Notation

The following symbols are used in this paper:

c_b = bottom friction coefficient;
c_l, d_l = undetermined coefficients;
f = Darcy's f, also Coriolis parameter;
g = gravity;
H = water depth;
I' = number of functions used in summation;
$N_H N_v$ = horizontal and vertical eddy viscosity;
P_a = atmospheric pressure;
R = Reynolds number;
s, b = subscripts designating at surface, at bottom;
u, v, w = x, y, and z components of water velocity;
u', v', w' = turbulent velocity components;
u_* = $\sqrt{\tau/\rho}$ = friction velocity;
$\bar{u}, \bar{v}$ = x and y flux components;
x, y, z = Cartesian coordinates;
z_e = distance from surface to region of constant N_v;
α, β = coefficients for N_v distribution;
Δt = time step;
η = water depth above datum;
κ = Von Karman's constant;
ρ = water density;
τ, τ_o = shear stress, surface shear stress; and
Ω_l = trial function.

JOURNAL OF THE HYDRAULICS DIVISION

MILLENNIAL CELEBRATION OF KARAJI'S HYDROLOGY

By Hormoz Pazwash,[1] A. M. ASCE and Gus Mavrigian[2]

INTRODUCTION

One thousand years ago, the brilliance of Persian scientific and cultural activity was dominant. While scholarly production was extensive, with many contributors, attention herein is drawn to the writing and transcription of the unique scholar, Mohammed Karaji. To celebrate and acknowledge Karaji is honorable, especially in the light of the recent claim revealing the discovery of his original manuscript in hydrology.

This paper presents a brief account of Karaji's contributions to science, especially to *ground-water hydrology*. The correlation between Karaji's thought and knowledge with later day scientists is brought forth. Response to the question—Was Karaji ahead of his time?—is well-illustrated throughout the article. Because of the discovered manuscript and its assumed original nature, it is the view of the writers that the material should not be neglected or lost among the plethora of technical matter, but should be duly noted and brought to the attention of science historians and hydrologists.

MATHEMATICAL GENIUS OF KARAJI

Mohammed Karaji was a Persian scholar of the late tenth century (12). While identified also by names as Karadji, Karagi, Al-Karaji, Hassen-al-Hasib, . . ., his complete name was Muhammed ibn al-Hasen al-Hasib al-Karaji (16,18). To the mathematical world, Karaji was more often referred to as Al-Karkhi (3,20). Regrettably, much of the production, brilliance, and contribution of Persian scholars during their period of great scientific flourishment, from the ninth century through the twelfth century, has been lost due to language barriers and errors in the etymological description (as in the stresses of inflection within Arabic letters) of translated works (3,20,22).

[1]Prof. of Civ. Engrg., Dept. of Civ. Engrg., Univ. of Teheran, Teheran, Iran.
[2]Prof., Dept. of Mathematical/Computer Sci., Youngstown State Univ., Youngstown, Ohio 44555.

Note.—Discussion open until August 1, 1981. To extend the closing date one month, a written request must be filed with the Manager of Technical and Professional Publications, ASCE. Manuscript was submitted for review for possible publication on May 17, 1979. This paper is part of the Journal of the Hydraulics Division, Proceedings of the American Society of Civil Engineers, ©ASCE, Vol. 107, No. HY3, March, 1981. ISSN 0044-796X/81/0003-0303/$01.00.

Muhammad ibn Musa al-Khwarizmi, called Alkhwarizmi, wrote the first comprehensive book in the field of algebra (c. 825 A.D.). The book, written in the Arabic language, was titled *Hisab al-jabr w-al-muqabala* (and was referred to simply as *Al-Jabr*). In Latinized form, the title reads *Liber algebrae et almucabola*, i.e., *The Science of Reduction and Confrontation*. Note that the Latinization of the Al-Jabr name led to the word *algebra*; also, the Latinization of the Alkhwarizmi name gave the word *algorithm* (3,10,11). Although Alkhwarizmi's work was the first Arabic book on the subject of algebra, it was presented without symbolism. Karaji wrote a superior algebra text (in Arabic, the language of the times), the first with symbolism (5) (c. 1000 A.D.), which provides the basic foundation and principles as known today. Karaji's text was titled *Fakhri* in honor of his patron and protector, the vizir (minister) Fakhr al-Mulk (10,12). This work presents the laws of exponentiation, the operations with surds, e.g., $\sqrt[3]{54} - \sqrt[3]{2} = \sqrt[3]{16}$; an extension of Abu Kamil's algebra on the important addition law of radicals, e.g., $\sqrt{a} \pm \sqrt{b} = \sqrt{a + b \pm 2\sqrt{ab}}$; also a novel method (apparently by a method known today as finite mathematics induction) of summing the cubes of the natural numbers, i.e., showing that $\Sigma_{n=1}^{N}(n^3) = 1^3 + 2^3 + 3^3 + \ldots + N^3 \equiv [(1/2)N(N + 1)]^2$, although the summation formula was known to Nicomachus (c. 100 A.D.); also generalized and solved Diophantine-type problems by ingenious use of parameters (such problems as determine rational numbers x, y, z so that $x^3 + y^3 3\ z^2$), and solved polynomial equations as cubic equations through geometrical means, etc. (20,21).

Transmission of Genius to Engineering

In engineering, Karaji personally invented ingenious and exceptionally exacting instruments that proved useful in the surveying and in the tunneling of ganats (underground channels for conveying water). Perhaps most importantly, Karaji expounded the basic principles of hydrology. Evidently Karaji was familiar with the principal of gravitational attraction, although he did not formally state an analytical formulation [as today's useful Newtonian law (14)]. Further, it appears that Karaji understood the proportionality law between the force of gravity and the mass of a body. Such descriptions, as well as extensive details on surveying and the hydrology of ground water, are found in a recently discovered manuscript of Karaji, entitled (in Arabic) *Inbat al-Miyah al-Khafiya*, which translates as *The Extraction of Hidden Waters to the Surface* (12,18). In 1966, a Persian translation of this manuscript was produced; today, writing projects are underway translating said works into several additional languages (12,16,24).

If authenticated and accepted by historians of science, Karaji's manuscript would serve as the oldest text on the subject of ground-water hydrology. In the search for "hidden water" (ground water), the manuscript delineates Karaji's universality with physical laws, as illustrated by the quotation, ". . . groundwater moves through cracks and cavities from points farther from the earth's center to points closer to it, and that every object has this tendency, with the property becoming stronger for heavier objects . . ." (translated from a transcription of the manuscript) (12).

Recall of Ground-Water History

The origin of ground water has been the subject of speculation from the

earliest days of documented history. During the "Dark Ages," little attention was devoted to the subject. Many scholars followed Biblical thoughts concerning the origin of water. Philosophers such as Aristotle and Seneca believed that springs could not be derived from rainwater alone. In the "Middle Ages" and early years of the Renaissance, scientists such as Kepler, Kircher, Magnus, and Schottus exhibited great interest on the subject and expressed their notions in a form that is essentially different than the basic knowledge of today. Kircher, as an example, with great appetite for imagination, described the earth (in 1619) as a medium which, ". . . drinks water from the sea and digests it like a beast and, as a result of this metabolism, springs originate." Kircher further attributed the mystical whirlpool of the Maelström, on the coast of Norway, as the mouth to underground caverns (1,2,9).

Thus it must appear that explanations offered by early philosophers on the origin of ground water were possibly erroneous. Perhaps it is strange, but explanatory notes for some of these beliefs are attributable to: (1) The desire of God; (2) the theory that the surface of the oceans are higher than the surface of land; and (3) the belief that rock pressure "squeezes" water upward through underground caverns, etc. Leonardo da Vinci, an outstanding figure of the Renaissance and genius of the western world, was one of the earliest to present a true explanation on the origin of rivers. Bernard Palissy, a writer in the sixteenth century, appears as the first to recognize that rain and snowmelt serve as the source of springs and rivers. Later, in 1715, Antonio Vallisnieri emphasized that rivers and springs originate their waters from rain, and also described the mechanism of free-flow operations in artesian wells, presenting extensive graphics of well cross sections (1,7,9).

As Meinzer states, ". . . prior to the latter part of the seventeenth century, it was generally assumed that water discharged from springs could not be derived from rain" (15). It was also generally believed that rain was not adequate in quantity, and that the earth was too impervious to permit the penetration of rainwater far below the surface of earth. Two of the main hypotheses extended by Greek philosophers persisting with confusion through the middle of the seventeenth century were: (1) That sea water was connected to springs via subterranean channels; and (2) that air was condensed into moisture in cold caverns inside the earth. It was not until 1686 that scholars like Mariotte introduced correct ideas regarding the source of springs and the infiltration of rainwater through the ground (7,9). Much later, in 1921, Ototsky, a Russian hydrologist rejected this infiltration concept by reasoning that deep infiltration occurs only in exceptional circumstances within special regions, and he further assumed that condensation serves as an important factor in the origin of ground water (15).

Contributions of Karaji in Ground-Water Science

During the Middle Ages, little recognition was afforded scientific writers from nonwestern nations because of unfamiliarity of language and inaccessability of manuscripts (8,16,17,24). Many physical concepts that have been described as basic fundamental learning of western scholars of the seventeenth century and eighteenth century were apparently known to Persian scholars centuries earlier. Karaji, as cited previously, knew of the origin of "hidden water," i.e.,

ground water, its occurrence, and its relation to rock formations, to aquifers, and to the hydrological cycle. Karaji also recalled that a few dozen deep-rooted plants (phreatophytes) serve as excellent indicators of the occurrence of ground water. Biruni (973 A.D.–1048 A.D.), another masterful and brilliant Persian scientist and philosopher referred to as a "universal scholar," whose contribution amounts to some 180 outstanding publications in various fields (19), was also among the first to give a correct explanation of the mechanism of artesian wells (7,22). Such work, however, remained unnoticed and was repeated seven centuries later by Vallisnieri (9).

Karaji, a contemporary of Biruni, demonstrated interest in the practice of engineering in addition to his promotion of science, and he displayed his talents and knowledge through the subject of "hidden water." The following excerpts from the recently discovered manuscript of Karaji present a brief indication of his contributions to groundwater science (12). These excerpts are translations by the authors, from Persian to English.

Karaji states that

> . . . the source of springs and all water bodies inside the earth, as well as all surface waters, comes from rain and snow and, . . . if the rains and snows cease, then waters are depleted and the earth is gradually wasted.

Also

> Rains and snows percolate the earth with excess waters running off into the seas, and that percolation ceases when hard clays or other solid obstructions are encountered.

Such vivid delineations of the existence of groundwaters point to the description of processes which today defines the *hydrological cycle*.

Further, Karaji states (12)

> . . . I have heard that large springs of fresh water exist on some islands. The source or origin of these is undoubtedly not the water from the seas that surround the islands, because the water surface of the seas is lower than the surface of the islands; rather, this source is located at farthest points and at higher elevations.

On the relation of geological formations to groundwater occurrence, Karaji classifies rock formations by their color—black or dark rock mountains typifying the existence of the richest groundwaters, also, that the abundance of ground water decreases, respectively, for green, yellow, and red rock mountain formations. This subject was totally ignored until a valuable contribution was made in the nineteenth century by Gabriel Daubree, a French geologist, on the relation of geological structures to the occurrence and movement of ground waters (15). Karaji noted that ground waters, analogous to surface waters, can be stagnant; also, that still waters can be located under vast deserts and lowlands. Thus Karaji was illustrating his knowledge of ground-water movement.

Further evidence of the extent of Karaji's knowledge in ground-water movement

is exhibited in the following examples (from his manuscript):

> The water levels of wells in a community near the Diayla River rise whenever there is an increase in river flow, and drop with a decrease in flows such that the water level in the wells is the same as that of the river. With levees (or dikes) constructed along the river, to prevent flooding of adjacent lands, the water levels in the river rise higher and produce corresponding rises in the level of water wells, consequently flooding homes in the community. The water from the river was fresh, though muddy, while clear but saline in the wells.

Karaji thus reasoned that this flow was due to the absence of obstructions or barriers, i.e., impermeable layers of earth, to stop the flow of "hidden water." Further, Karaji wrote

> From a rock, projecting out of a river near the village of Saveh Province, water spouts through vents. The river water is fresh, but the spouted water is so bitter that it induces ill effects to drinkers. The source of this bitter water is certainly not the river, but the percolating waters some distance away which "turned" its taste as it traveled through soils enroute to the rock.

These examples indicate Karaji's knowledge of unconfined and of confined flows, respectively.

Water quality is also considered in Karaji's manuscript. Karaji presents methods to determine such water qualities as hardness, turbidity, taste, color, and odor, also presenting ingenious means by which water quality can be improved (as lowering of hardness and reduction of brine content). To show his "grasp" of the physical laws which relate pressures and volumes of gases, the process of extracting fresh water from the bottom of shallow seas by sailors is detailed. The tools required for such extraction include a heavy lead vase with small holes at the bottom and slim neck at the top connected to a long thin tube of fine waxed leather, a small globe fitted snugly at the bottom of the thin tube, and two long cords—one extending from the sea vessel to the handle of the vase and the other running through the tube and fastened to the inserted globe. To extract fresh water, the entire apparatus is dropped into the sea and allowed to touch the bottom. A pull of the cord attached to the globe results in an increase in the volume of air creating suction (thereby reducing the pressure in the vase) and allowing fresh water from the ground beneath the sea to seep through the small holes at the bottom of the vase. The container is then pulled to the surface and the routine is repeated until a sufficient quantity of fresh water is extracted.

In the subject of qanats, or underground aqueducts, Karaji demonstrated his superior technical talents. While some geohydrologists have referred to the construction of qanats as "the most extraordinary works of ancient man" (23), the methods of qanat construction as described by Karaji are essentially the same as those practiced today (4,6,13)—ten centuries later. The fact that tunneling requires extensive skills in surveying, in the provision of adequate ventilation, and in the prevention of mining disasters shows the extent of technological

advancement of the Persians in qanat construction (6). Indeed, the planning and establishment of many villages, cities, and centers of learning followed such construction technology. Tragically, these centers were sacked and destroyed by invading warriors. Consequently, much of the treasured scientific knowledge was destroyed or lost.

Conclusions

The history of scientific endeavors reveals that Karaji was productive and highly knowledgable in areas of mathematics, ground-water hydrology, surveying, and the engineering of tunneling. Karaji may perhaps have shared many important scientific ideas with his brilliant contemporaries (namely, Biruni and Avicenna). However, errors in ethnography and unfamiliarity with or inaccessibility to other Karaji works other than those on mathematics have caused the omission of Karaji's name as an applied scientist by western writers. The achievements of Persian scholars, which flourished during the ninth century, the tenth century, and the early part of the eleventh century has indeed formed a brilliant era in the history of scientific learning.

Continual political turmoil and religious factionalism precipitously led to periods of inconstant scientific production and a lack of a high degree of uniformity in learning. From the middle of the eleventh century, science efforts by Persians and Arabs were reduced to such a state of decline that it never again rose to the scholarly level attained by Karaji. Overrun by invasions during the twelfth century, centers of learning were sacked and manuscripts were destroyed.

Additionally, western scholars have praised Persian scientists as admirable custodians or preservers of world intellect, which transferred into Europe and the western world. However, western scholars have questioned the originality in Persian writings. Persian scholars made extensive translations of Greek and Roman classical works (such as the works of Apollonius, Diophantus, Euclid, Vitruvius, etc.).

Regardless of the stature assigned to Persian scientific endeavors, Karaji stands alone as a prominent contributor to the hydrological sciences. The recent discovery of Karaji's manuscript on "hidden water" identifies the manuscript as the oldest known text on ground-water hydrology. The reception and authentication of this manuscript by science historians should strengthen the value of this millennium work. Writers of history of science should thus include the significant Persian contributions during the tenth century and eleventh century. It is also very appropriate to call Karaji "the founder of hydrology" in this millennial celebration.

In conclusion, Karaji viewed the subject of ground water with such great importance that the preface in his manuscript reads:

> I do not know of any profession more useful than that of the extraction of ground water to the surface. Because of this profession, land reclaims and the liveliness of man finds organization and plenty of benefits.

Appendix.—References

1. Adams, F. D., "The Origin of Springs and Rivers," *The Birth and Development*

of Geological Sciences, Dover Publications, Inc., New York, N.Y., 1938, pp. 426–460.
2. Baker, M. N., and Horton, R. E., "Historical Development of Ideas Regarding the Origin of Springs and Ground Water," *Transactions of The American Geophysical Union,* Vol. 17, Part II, 1936, pp. 395–400.
3. Boyer, C. B., *A History of Mathematics,* Chapt. 13, John Wiley and Sons, Inc., New York, N.Y., 1968.
4. Bybordi, M., "Ghanats of Iran: Drainage of Sloping Aquifer," *Journal of the Irrigation and Drainage Division,* ASCE, Vol. 100, No. IR3, Proc. Paper 10785, Sept., 1974, pp. 245–253.
5. Cajori, F., *A History of Mathematical Notations,* Vol. 1, Open Court Publishing Co., LaSalle, Ill., 1928.
6. Cressey, G. B., "Qanats, Karez and Foggaras," *Geographical Review,* Vol. 48, No. 1, 1958, pp. 27–44.
7. Davis, S. N., and DeWiest, R. J. M., *Hydrogeology,* John Wiley and Sons, Inc., New York, N.Y., 1966.
8. Davis, S. N., discussion of "Exploration of Hidden Water—The Oldest Textbook on Hydrology," by M. Karaji, *Groundwater,* Vol. 11, No. 4, 1973, p. 45.
9. DeWiest, R. J. M., *Geohydrology,* John Wiley and Sons, Inc., New York, N.Y., 1965.
10. Eves, H., *An Introduction to the History of Mathematics,* 3rd ed., Holt, Rinehart and Winston, New York, N.Y., 1969, pp. 190–205.
11. Gardz, S., "Origin of Term 'Algebra'," *American Mathematical Monthly,* Vol. 33, 1926, pp. 437–440.
12. Karaji, M., *Extraction of Hidden Water,* (c. 1000 A.D.), translated to Persian by H. Khadiv Jam, Bonyad Farhand Iran (Iranian Cultural Foundation) Publications, Tehran, Iran, 1966, 129 pp.
13. Kuros, Gh. R., "The Art of Irrigation and Dam Construction in Ancient Persia," Iranian Cultural Foundation, Tehran, 1966, 127 pp.
14. Lee, R. E., *The Backgrounds and Foundation of Modern Science,* The Williams and Wilkins Co., Baltimore, Md., 1935.
15. Meinzer, O. E., "The History and Development of Groundwater Hydrology," *Journal of the Washington Academy of Sciences,* Vol. 24, 1934, pp. 6–32.
16. Nadji, M. Karadjis, "Erschliesung Verborgener Gewässer," Ein Lehrbuch Der Geowissenschaften ans dem, 11, Jahrhundert, *Zeitschrift der Deutschen Geologischen Gesellschaft,* Vol. 123, 1972, pp. 1–13.
17. Nadji, M., and Voigt, R., "Exploration of Hidden Water—The Oldest Textbook on Hydrology," by Mahammad Karaji, *Groundwater,* Vol. 10, No. 5, 1972, pp. 43–46.
18. Needham, J., *Science and Civilization in China,* Vol. 4, Part III, Cambridge University Press, Cambridge, England, 1971.
19. Neugebauer, O., *A History of Ancient Mathematical Astronomy,* Parts 1, 2, 3, Springer-Verlag, New York, N.Y., 1975.
20. Smith, D. E., *History of Mathematics,* Dover Publications, Inc., New York, N.Y., 1958, Vol. I, pp. 283–287; Vol. II, pp. 380–389, 446–448.
21. Struik, D. J., *Concise History of Mathematics,* Dover Publications, Inc., New York, N.Y., 1967.
22. Taton, R., *History of Science, Ancient and Medieval Science,* Translated by A. J. Pomerans, Basic Books Inc., New York, N.Y., 1963, p. 512.
23. Tolman, C. F., *Groundwater,* 1st ed., McGraw-Hill Book Co., Inc., New York, N.Y., 1937.
24. Zaghi, N. and Finnemore, E. J., discussion of "Exploration of Hidden Water—The Oldest Textbook on Hydrology," by Mohammed Karaji, *Groundwater,* Vol. 11, No. 4, 1973, p. 44.

JOURNAL OF THE HYDRAULICS DIVISION

TURBULENCE MEASUREMENT STUDY

By O. Franklyn Griffith, III[1] and Charles Grimwood,[2] M. ASCE

INTRODUCTION

Increasing concern regarding the environmental effects of changes in flow patterns for bodies of water and streams demands that flow parameters characterizing turbulence be measured and understood. It is necessary, therefore, to determine the significant parameters and to devise measurement methods that utilize instrumentation compatible with field use. Discharge and current are generally used to describe flows, with dissolved oxygen, sediment load, temperature, etc. used to characterize the content or condition of flow. Rapid mixing, sudden pressure changes, and sharp pressure gradients that are associated with turbulent flow have an impact on sediment transport, clustering of soft organisms, and channel stability.

This paper presents the results of tests intended to evaluate the feasibility of using a modified commercially available electromagnetic current meter to measure parameters which would characterize turbulent flows from field measurements in rivers and lake inlets. It is anticipated that the techniques described here will be used in the analysis of the flows in channels connecting Lake Ponchartrain and the Gulf of Mexico.

PROCEDURE

An electromagnetic flow meter, Model 511 manufactured by Marsh-McBirney Inc., Rockville, Md., with a modified time constant circuit was used as a basic sensing instrument in these experiments. Data were recorded on a Gould (Brush 222) two-channel oscillograph recorder and Triplet Model 603 meters were used for voltage measurements. Oscilloscope photographs were also used in laboratory evaluation. Turbulent outflow of the Inner Harbor Navigation Canal (IHNC) Lock, in New Orleans, and tidal flow under the Seabrook Bridge in New Orleans

[1]Engr., United States Corps of Engrs., New Orleans Dist.; also Asst. Prof. of Physics, Univ. of New Orleans, Lake Front, New Orleans, La. 70122.

[2]Environmental Engr., United States Army Corps of Engrs., New Orleans Dist., La.

Note.—Discussion open until August 1, 1981. To extend the closing date one month, a written request must be filed with the Manager of Technical and Professional Publications, ASCE. Manuscript was submitted for review for possible publication on November 14, 1979. This paper is part of the Journal of the Hydraulics Division, Proceedings of the American Society of Civil Engineers, ©ASCE, Vol. 107, No. HY3, March, 1981. ISSN 0044-796X/81/0003-0311/$01.00.

and flow in the Mississippi River at New Orleans were used as field test situations.

The flows are characterized by the following parameters: (1) "Broadband" average root mean square (rms) of the fluctuating velocity $\sqrt{\bar{a}^2}$; (2) time average velocity resultant ($\bar{D}$) as averaged over several seconds; (3) spectral composition from Fourier analysis of strip chart recordings; and (4) the ratio $\sqrt{\bar{a}^2}/\bar{D}$ which is the modified turbulence intensity.

Previous methods of determining the foregoing parameters present problems when attempts are made to apply them in the field where a number of crews must use the instruments from small boats, bridges, and locations where access is difficult. The instrument package described here is relatively light, battery powered and rugged. Techniques described in the literature such as the laser doppler anemometer (1) are not portable and require delicate alignment. The hot film sensors used successfully by McQuivey (3,4) are delicate, etched by abrasives carried in the sediment load and easily contaminated.

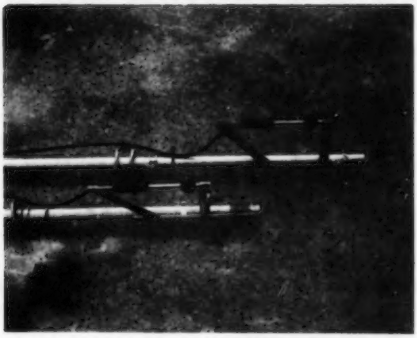

FIG. 1.—Instrument Probe for Model 511 Marsh-McBirney Electromagnetic Current Meter

The Model 511 was evaluated as a potential candidate for yielding turbulence information. The probes for this instrument are shown in Fig. 1. They consist of an electromagnet which is modulated at 30 Hz, two pair of sensing electrodes orthogonally mounted in a 1-1/2 in. (3.8 cm) diam ball. Circuits and physical details are contained in the instrument manual. These systems have been used successfully in field discharge measurements and as fixed flow monitors at remote locations for several years and have proven reliable. The instrument has selectable velocity scales to 10 fps (3.05 m/s) and time constants to 10 sec with the two orthogonal velocity components simultaneously displayed on panel meters. A separate output with 0 V–1 V representing 0-fps–10-fps (0-m/s–3.05-m/s) flow velocity is available. This output was recorded during the experiments described here.

Instrument Evaluation

Modification of the output circuit consisted of reducing the time constant by replacing the 0.47-μf capacitor (C12) with a 0.015-μf capacitor. This increased

the frequency response to approx 10 Hz. The instrument's frequency response shown in Fig. 2 was determined by the use of an oscilloscope to measure

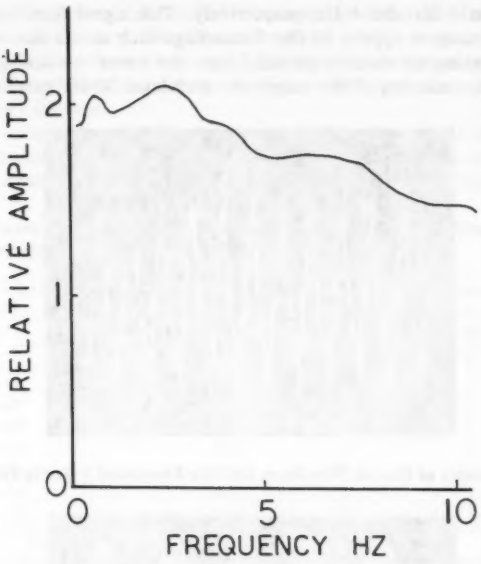

FIG. 2.—Frequency Response of Instrument over Range of Interest

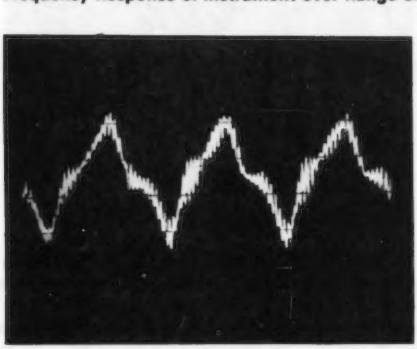

FIG. 3.—Example of Output Waveform for 1-Hz Simulated Velocity Fluctuation

the peak to peak output voltages and also a high impedance a-c voltmeter to indicate rms values. Results from both methods were similar and showed the 3-dB point at 10 Hz. Beats between the modulation and the magnet power

frequency were evident near 14 Hz but were lower in amplitude and did not contribute significantly to the results.

Figs. 3 and 4 show examples of instrument outputs for simulated velocity fluctuations at 1 Hz and 4 Hz, respectively. This signal form was observed for frequencies up to approx 10 Hz. Recordings such as the ones shown were made by inducing an electric potential into the water containing the probe. This potential consisting of the amplitude modulated 30-Hz carrier which was

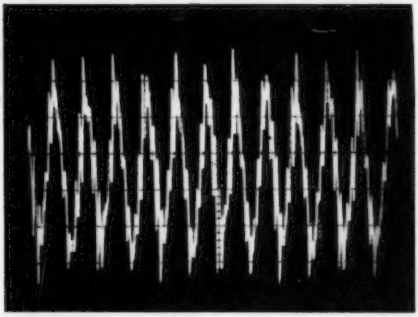

FIG. 4.—Example of Output Waveform for 4-Hz Simulated Velocity Fluctuation

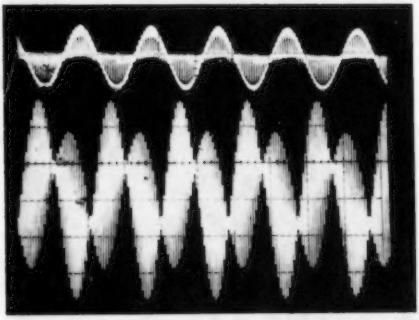

FIG. 5.—Example of Waveform with Ground Loop Noise Shown in Lower Trace; Upper Trace Shows Potential Waveform Used to Simulate Fluctuating Velocity

phase locked to the magnet driver and simulated the signal expected from a sinusoidal velocity fluctuation from turbulent flow. It is necessary to look at the effect of the instrument and the analysis methods on the spectral distribution measurements.

Oscillograph recordings were made in frequency increments from 1 Hz–14 Hz for various noise conditions. A number of these were digitized in 0.03-sec increments and Fourier analyzed to determine the form of output voltage for various frequencies of simulated sinusoidual velocity fluctuations. Two methods

of digitizing these recordings were tested to determine the type of transfer function and noise effect for each. The envelope for a high noise condition is shown in the lower trace of Fig. 5. Use of the short-term averaging of the signal for digitizing removed the 30-Hz component and yielded sharp lines at the modulation frequency. The Fourier analysis of this average for 4 Hz in Table 1 shows a sharp line with no significant spurious components. Information is therefore best obtained by Fourier analysis of the short-term (over a period about 0.05 sec) average.

The noise contribution is difficult to assess since it depends on measurements made in a flowing but nonturbulent medium. There is always uncertainty unless special care is taken to prepare and establish laminar flow. Upper limits, however,

TABLE 1.—Fourier Components of Instrument Output with 4-Hz Simulated Turbulence Fluctuations Induced in Probe Tank

$A(I)$ (1)	$B(I)$ (2)	Frequency, in Hertz (3)
2.74	0.00	0
0.06	0.11	1
0.05	−0.01	2
−0.06	0.01	3
−0.57	−2.33	4
−0.08	0.26	5
0.02	−0.08	7
0.03	−0.13	8

Note: $F(x) = [A(0)/2] + \Sigma_{I=1}^{N} [A(I) \cos (IX) + B(I) \sin (IX)]$.

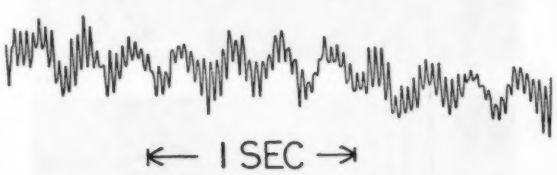

FIG. 6.—Example of Longitudinal Component of Turbulence Recorded in Laboratory Test Tank

can be obtained by using the best steady flow available and comparing with values calculated by methods described in the manufacturer's manual. The wide-band electronic noise is given as $(0.03/t)$ rms fps, in which t = the output time constant, in seconds. The system, as modified, would yield a broad-band noise of 0.1 rms fps (0.03 m/s). This noise in water flow which appeared steady at approx 1 fps (0.305 m/s) was measured to be 0.13 rms fps (0.04 m/s). It is evident from recordings and oscilloscope observations, that the short-term averaging will greatly reduce the noise components near 30 Hz. The noise interference in the digitized data will thus be reduced considerably below the levels indicated which are quoted for broad-band measurements. Since the levels of fluctuating signals in turbulent flow can be as high as five times greater

TABLE 2.—Fourier Components Obtained from Longitudinal Turbulence Component Generated in Test Tank

$A(I)$ (1)	$B(I)$ (2)	Frequency, in Hertz (3)
6.71	0.00	0.0
1.76	1.25	0.5
0.50	0.35	1.0
0.42	−0.83	1.5
0.29	0.49	2.0
0.37	0.42	2.5
0.12	0.94	3.0
−0.28	−0.53	3.5
−0.61	−0.04	4.0
−0.59	0.15	4.5
−0.25	0.21	5.0
0.29	−0.03	5.5
0.02	0.08	6.0
0.12	−0.35	6.5
0.05	−0.30	7.0
0.14	−0.19	7.5

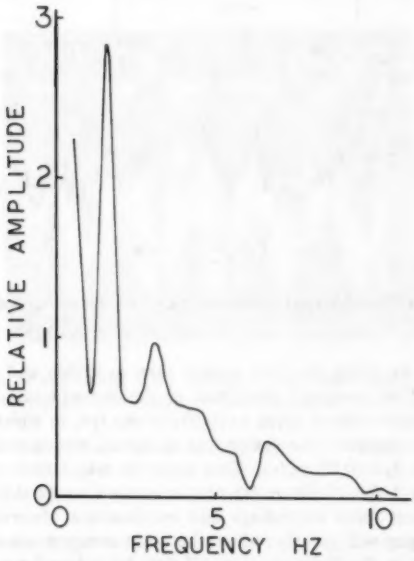

FIG. 7.—Frequency Spectrum of Longitudinal Turbulence Component Observed for Turbulent Mixing in Test Tank

than the broad-band noise, the measurement of turbulence components can usually be made over it even with the rms meter. It should be pointed out that any tests or operation of this type of instrument in a-c fields, tanks, or in any situation where ground loops exist, will result in high periodic noise levels such as shown in Fig. 5. This noise level can usually be eliminated or drastically reduced by changing the grounding configuration.

An example of a strip chart recording from turbulent tank flow is shown in Fig. 6. Attempting to sample every 0.01 sec yielded a noisy result and the very poor fit reconstructed from the series had an average point error of about 40% in the amplitudes. Digitizing the short-term average of a recording like that shown in Fig. 6 yielded the Fourier components shown in Table 2. The

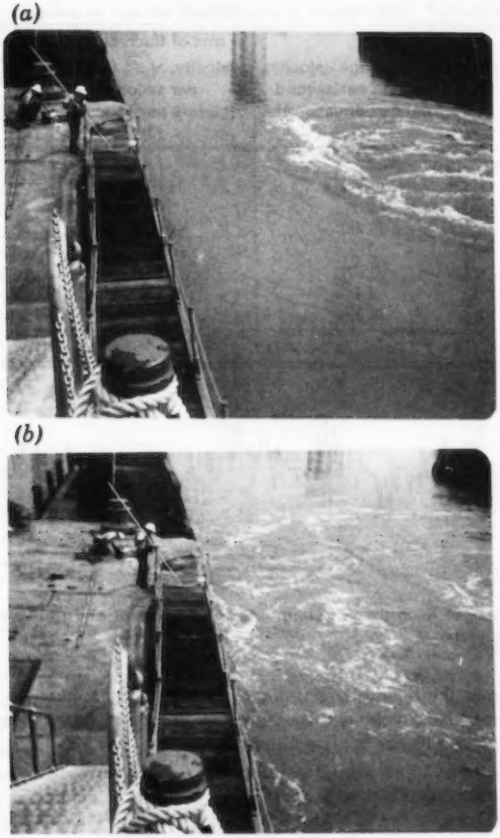

FIG. 8.—Development of Surface Turbulence in IHNC Lock Outflow

fit was considered good showing an average error of 3%. The high amplitude components are seen to be below 3 Hz and almost no energy is contained above 7 Hz. Fig. 7 is a plot of this frequency spectrum.

It can be concluded from the laboratory tests considered, that this instrument is capable of detecting low frequency velocity spectral distributions in natural turbulent water flow. Although the manual analysis methods used here are laborious and would not be practical for large volumes of data, tape recording and automated methods will yield spectral information for a significant number of data stations. Turbulence intensity can be determined by either the use of

TABLE 3.—Examples of Measurements Made at IHNC Lock with rms Voltmeters; $\bar{D}$ Was Determined over 5-sec Time Average

Probe depth, in feet (meters) (1)	Time average velocity, $\bar{D}$, in feet per second (meters per second) (2)	rms of fluctuating velocity, $\sqrt{\overline{d^2}}$, in feet per second (meters per second) (3)	Turbulence intensity, $\sqrt{\overline{d^2}}/\bar{D}$ (4)
near surface	3.2 (0.98)	1.4 (0.43)	0.44
2 (0.61)	2.9 (0.88)	0.3 (0.09)	0.10
4 (1.22)	2.2 (0.67)	1.5 (0.45)	0.68
6 (1.83)	1.8 (0.55)	1.2 (0.37)	0.67

Note: $\bar{D} = \sqrt{\bar{U}^2 + \bar{V}^2}$; $\overline{d^2} = (\overline{u^2} + \overline{v^2})/2$.

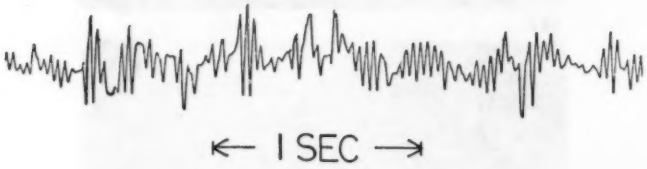

FIG. 9.—Example of Recording of Longitudinal Component of Turbulent Flow from IHNC Lock Outflow

rms values from the digitized recordings or an rms voltmeter. As previously covered, if broad-band voltmeter measurements are used, noise considerations will be an important aspect of data interpretation.

Field Measurements and Tests

The field data collected included broad-band rms measurements as well as the strip chart recordings for the spectral analysis procedures examined. The

sites will be considered separately and, due to the evolution of the methods, the techniques and data are not the same at each site. The differences are reviewed and the methods with results are compared in the conclusion at the end of this section.

IHNC.—The IHNC Lock is the passage between the Mississippi River and the IHNC in New Orleans. The outflow is through a duct and from a head of approx 15 ft (4.57 m). Figs. 8(*a*) and 8(*b*) are photographs spaced approx 30 sec apart as the control gates were opened showing the surface evolution of the turbulent region. This flow can be visually characterized by large eddies with considerable entrained air at the surface. The flow contained extensive apparently random mixing at the center which was characteristic as the radial

TABLE 4.—Tabulation of Fourier Coefficients of Longitudinal Turbulence Data Recorded at IHNC Lock Outflow

$A(I)$ (1)	$B(I)$ (2)	Frequency, in Hertz (3)
5.97	0.00	0.0
2.58	0.74	0.5
−0.62	−0.25	1.0
0.08	0.55	1.5
1.73	−0.08	2.0
−1.61	0.88	2.5
−1.73	0.11	3.0
−0.37	0.27	3.5
−0.85	−0.65	4.0
−0.47	0.52	4.5
−0.70	−1.17	5.0
−0.16	−0.12	5.5
0.72	−0.03	6.0
−0.68	−0.29	6.5
0.06	−0.03	7.0
0.28	−0.40	7.5
0.16	0.38	8.0
0.34	−0.33	8.5
−0.32	0.18	9.0

outward flow developed. Fronts of turbulent water arrived at the probe several seconds apart yielding a very low frequency component in addition to those which appear in the analysis covered. Considerable correlation between the magnitude of the longitudinal and transverse velocities could be observed within the flow as they are indicated by the instrumentation.

Voltmeter measurements were made for several probe depths and the rms velocities were observed over approx 5 sec. Examples of the data are shown in Table 3 in which D is taken as the magnitude of the vector sum of the u transverse channel and v longitudinal channel velocities. The extensive randomness of the flow made the designation of a specific direction as transverse virtually meaningless. The values of turbulence intensity in the last column

indicate high levels of turbulence as compared to maximum values of about 0.43 found by McQuivey (4) in the Columbia River Estuary. The data point at a depth of 2 ft was included to show the approximate lower limit for the rms noise at a relative high flow. This measurement was made during a quiet

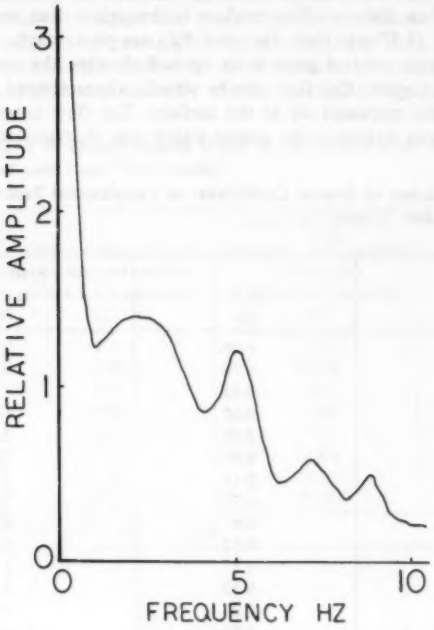

FIG. 10.—Average Relative Amplitude Versus Frequency of Longitudinal Turbulence at IHNC Lock Outflow

FIG. 11.—Recording of Longitudinal Component of Turbulent Flow from Mississippi River at New Orleans

period between turbulent fronts. The flow at this site is in general highly turbulent and may represent an upper standard for comparison with other flows.

Fig. 9 shows an example of a strip chart recording made at this site, and Fourier analysis of the short-term average yielded the components tabulated

TABLE 5.—Example of Fourier Coefficients of Longitudinal Turbulence Data in Mississippi River

$A(I)$ (1)	$(B(I)$ (2)	Frequency, in Hertz (3)
−2.49	0.86	0.33
0.43	−0.28	0.66
3.71	3.11	1.00
−1.20	0.48	1.33
0.04	−1.13	1.66
0.57	0.74	2.0
−0.11	−0.35	2.33
−0.31	0.62	2.66
0.48	0.32	3.00
0.26	0.32	3.33
0.61	−0.15	3.66
0.51	0.27	4.00

Note: Remaining terms are less than 0.50.

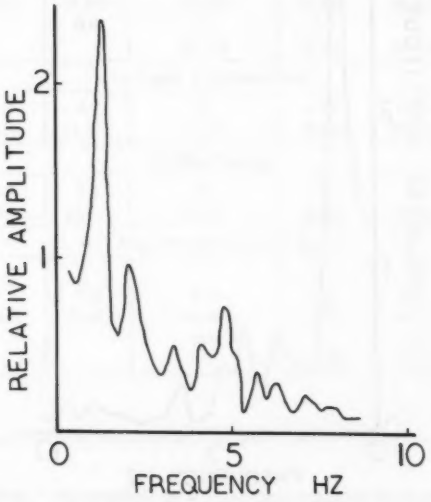

FIG. 12.—Average Relative Amplitude Versus Frequency of Longitudinal Turbulence in the Mississippi River

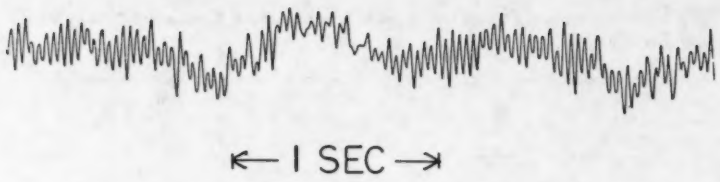

FIG. 13.—Recording of Longitudinal Component of Turbulent Flow in Mississippi River Approx 1,000 ft (304 m) Downstream from Working Tugboat

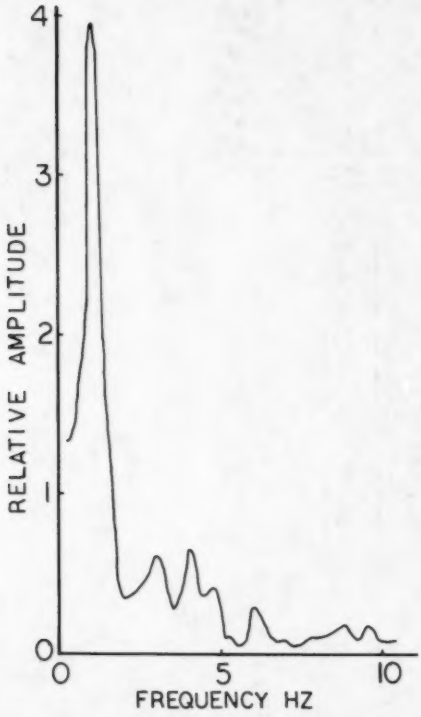

FIG. 14.—Relative Amplitude Versus Frequency of Longitudinal Turbulence Recorded in Mississippi River Downstream from Operating Tug

in Table 4. The most intense component is at 0.5 Hz with more high amplitudes being found below 3.5 Hz. The mean error in the fit of this recording to curves reconstructed from the Fourier components is 3%. A plot of the average of two of these data increments is shown in Fig. 10 indicating the concentration of energy at frequencies below 6 Hz.

TABLE 6.—Measurements and Calculations for Flow Under Seabrook Bridge

Depth, in feet (meters) (1)	Velocity, in feet per second (meters per second)		$D = \sqrt{\bar{U}^2 + \bar{V}^2}$ feet per second (meters per second) (4)	rms Velocity, in feet per second (meters per second)		Intensity, $\sqrt{\overline{d^2}}/\bar{D}$ (7)
	U channel (2)	V channel (3)		U channel (5)	V channel (6)	
			(*a*) Moderate to Light Turbulence			
1.0 (0.30)	4.5 (1.37)	3.8 (1.16)	5.9 (1.80)	0.4[a] (0.12)	0.3[b] (0.09)	0.06
2.5 (0.76)	−3.0 (0.91)	0.8 (0.24)	3.1 (0.94)	0.4 (0.12)	0.4 (0.12)	0.13
4.0 (1.22)		0.0	2.5 (0.76)	1.5 (0.46)	1.5 (0.46)	0.60
			(*b*) Light Turbulent Flow			
1.0 (0.30)	2.4 (0.73)	4.5 (1.37)	5.1 (1.55)	0.25 (0.08)	0.20 (0.06)	0.04
			(*c*) Ship Passage			
4.0 (1.22)	−3.0 (0.91)	0.5 (0.15)	3.1 (0.94)	3.0 (0.91)	3.0 (0.91)	0.97
			(*d*) Apparent Strong Turbulence			
approx 3.0 (0.1)	−1.5 (0.46)	1.5 (0.46)	2.12 (0.65) max	0.7 (0.21) 1.5 (0.46)	0.9 (0.27) 1.5 (0.46)	0.38 0.71

[a] $\sqrt{\overline{u^2}}$
[b] $\sqrt{\overline{v^2}}$

Mississippi River.—An example of a 3-sec data segment from recordings taken in the Mississippi River is seen in Fig. 11. The probe was positioned 8 ft (2.44 m) deep and approx 10 ft (3.05 m) from barges moored near Prytania Street in New Orleans. Visual assessment of the turbulent character of the flow is not usually possible in the river because of the wind ripple on the surface. High noise levels were experienced due to potentials induced in the water around

the barges which are wired with 60-Hz power. Table 5 is a tabulation of the Fourier components. Notice that the energy is again concentrated in the very low frequency region, with the higher amplitude components below 4 Hz. Fig. 12 is a plot of relative amplitude versus frequency resulting from the average of two spectra. The peak at about 1.5 Hz seemed characteristic of data from the river, probably due to boundary patterns generated by the relatively periodic barge assembly which extended up river from the observation site. The steady-state flow during these observations was 1.1 fps (0.33 m/s) and the rms measured by the voltmeter was 0.20 rms fps (0.06 m/s) which yields a value of about 0.18. McQuivey (4) measures values of longitudinal component of turbulence intensity far from the bank in the Mississippi River at Vicksburg as high as 0.206 close to the bottom and as low as 0.055 near the surface. The measurement made during this investigation was very close to a bounding surface, and compares well with McQuivey's data from near the bottom (4).

TABLE 7.—Summary of Turbulence Field Data

Location (1)	Visual indication of turbulence (2)	Average turbulent intensity level (3)	Spectral characteristics (4)
IHNC	High turbulence	0.47	Chaotic with most of the energy below 6 Hz
Mississippi River near a barge	Moderate turbulence	0.18	Energy below 5 Hz with peaks at 1.0 Hz, 1.66 Hz, and 3.66 Hz
Mississippi River downstream from operating tug	Moderate turbulence	0.31	Energy below 5 Hz with high peak at 1.0 Hz
Seabrook Bridge	Light turbulent flow	0.04	Spectrum not recorded
Seabrook Bridge	Light to moderate turbulence	0.26	Spectrum not recorded
Seabrook Bridge	High turbulence	0.55	Spectrum not recorded
Seabrook Bridge	Ship passage	0.97	Spectrum not recorded

Fig. 13 shows a recording made at the same location in the Mississippi River except the wheel wash from a tug boat operating about 1,000 ft (304 m) upstream was propagating across the probe. A comparison of this recording with Fig. 12 shows a considerable increase in the relative amplitudes of the lower frequency content of the turbulence. A plot of the intensity as a function of frequency is shown in Fig. 14. The relative concentration of energy below 2 Hz is significantly higher for turbulence generated by the boat. The average error in the fit of the Fourier analyzed functions was less than 5%.

Seabrook Bridge.—Flows under the Seabrook Bridge can be representative of highly turbulent and nonturbulent conditions depending on wind, tide, and the location of the probe. Voltmeter techniques were used at this location during

a strong flow period. These conditions could not be found again for strip recording and spectral analysis. Table 6 shows data and a calculation of turbulence intensity along with general visual description of the flow for several probe positions as indicated.

The data for moderate turbulence were recorded in flow between a corner of a bounding wall and obstructions consisting of old piles. The analysis as a function of depth is therefore not a useful concept here, but several things can be learned about the instrument from this data. The values of turbulence intensity are within the reasonable limits for slightly turbulent flow and moderate turbulence. The region of least turbulence yielded data labeled "light turbulence" and the intensity is considerably smaller than indicated at the position with moderate turbulence. During the measurements barges under tow passed through the channel resulting in increased turbulent character of the flow. The value of 0.97 for the intensity is quite high and even exceeds that found at the IHNC Lock. This, however, is a transient condition, and these values represent the extreme.

A sequence of measurements was made in the flow where strong turbulence was visible in the form of mixing and eddies. The average lower values of turbulence intensity were found to be about 0.4 and the higher values averaged near 0.7. These values seem to bracket those obtained for the more turbulent flow regions measured by McQuivey (4).

Subsequent data were collected from the low drawbridge across the channel with a flow ranging between 0.4 fps and 1.0 fps (0.12 m/s and 0.30 m/s). The rms measurements indicated between 0.1 fps rms and 0.2 fps rms which is just above the expected noise levels at 1-fps flow.

Conclusions

The summary of turbulence intensity results tabulated in Table 7 shows that the level of turbulence observed at the different field test sites has been quantified and comparisons of turbulent flows can be made. The spectral plots of the turbulence in the river show definite periodic components while a more chaotic spectra were observed at the IHNC Lock. It is concluded that with this instrument a method has been developed to quantitatively compare turbulence intensity and obtain spectral signatures of turbulent flows in the field.

Investigations of the flows between Lake Ponchartrain and its connections to the Gulf of Mexico will be conducted using these methods and results published at a later date. Automated data recording and digitizing will facilitate correlation calculations from which the characteristic or mixing lengths can be obtained. Scaling of these data for comparison to laboratory experiments such as those done by Etheridge and Kemp (2) will also be attempted at a later date.

Appendix I.—References

1. Buchhave, P., George, W. K., Lumley, J. L., "Measurement of Turbulence With the Laser Doppler Anemometer," *Annual Review of Fluid Mechanics*, M. Van Dyke, J. V. Wehausen, J. L. Lumley, eds., Vol. 11, pp. 443–503, 1979.
2. Etheridge, D. W., and Kemp, P. H., "Measurements of Turbulent Flow Downstream of a Rearward Facing Step," *Journal of Fluid Mechanics*, Vol. 86, pp. 545–566.

3. McQuivey, R. S., "Principles and Measuring Techniques of Turbulence Characteristics in Open Channel Flows," *USGS Professional Paper 802-A*, United States Geological Survey, 1973.
4. McQuivey, R. S., "Summary of Turbulence Data From Rivers, Conveyance Channels, and Laboratory Flumes," *USGS Professional Paper 802-B*, United States Geological Survey, 1973.

Appendix II.—Notation

The following symbols are used in this paper:

$A(I)$ = amplitude coefficients for cosine terms in Fourier expansions;
$B(I)$ = amplitude coefficients for sine terms in Fourier expansions;
$\bar{D}$ = time average of resultant velocity $\sqrt{(\bar{U}^2) + (\bar{V})^2}$;
$\sqrt{d^2}$ = average of rms fluctuations for transverse and longitudinal velocity;
$F(x)$ = output function for data set;
I = index numbering terms in Fourier expansion;
t = time, in seconds;
$\bar{U}$ = extended time average of longitudinal velocity;
$\sqrt{u^2}$ = rms value of fluctuating longitudinal velocity;
$\bar{V}$ = extended time average of transverse velocity;
$\sqrt{v^2}$ = rms value of fluctuating transverse velocity;
x = instrument channel (x); and
y = instrument channel (y).

JOURNAL OF THE HYDRAULICS DIVISION

ULTIMATE DIMENSIONS OF LOCAL SCOUR

By Fred W. Blaisdell,[1] F. ASCE, Clayton L. Anderson,[2] and George G. Hebaus,[3] Members, ASCE

INTRODUCTION

The purpose of this paper is to describe an analytical method of estimating the ultimate depth of scour that is based on experimental observations made during the early stage of the scouring process. Because scour approaches its limit asymptotically, current practice is to specify a practical scour limit. This practical scour limit is based on personal judgment and can vary widely among individuals. The method we propose defines a scour limit independent of individual judgment.

Laursen has written (see Ref. 1, pp. 180–181; see also Ref. 4, p. 48): ". . . the following general characteristics which should be basic to any detailed analysis of local scour [are]:

1. The rate of scour will equal the difference between the capacity for transport out of the scoured area and the rate of supply of material to that area.
2. The rate of scour will decrease as the flow section is enlarged.
3. There will be a limiting extent of scour.
4. This limit will be approached asymptotically."

Among the persons concerned with local scour, there seems to be general agreement that Laursen's characteristics describe the scour process. Herein the writers will take a close look at how scour approaches the limit with respect to time, the aforementioned characteristic 4, and suggest a method of analysis

[1]Research Hydr. Engr., United States Dept. of Agr., Sci. and Education Administration, Agricultural Research, St. Anthony Falls Hydr. Lab., Third Avenue Southeast at Mississippi River, Minneapolis, Minn. 55414.

[2]Hydr. Engr., United States Dept. of Agr., Sci. and Education Administration, Agricultural Research, St. Anthony Falls Hydr. Lab., Third Avenue Southeast at Mississippi River, Minneapolis, Minn. 55414.

[3]Research Hydr. Engr., United States Dept. of Agr., Sci. and Education Administration, Agricultural Research, St. Anthony Falls Hydr. Lab., Third Avenue Southeast at Mississippi River, Minneapolis, Minn. 55414.

Note.—Discussion open until August 1, 1981. To extend the closing date one month, a written request must be filed with the Manager of Technical and Professional Publications, ASCE. Manuscript was submitted for review for possible publication on July 8, 1980. This paper is part of the Journal of the Hydraulics Division, Proceedings of the American Society of Civil Engineers, ©ASCE, Vol. 107, No. HY3, March, 1981.

that will permit evaluation of characteristic 2, the rate of scour, and characteristic 3, the limit of local scour. For this examination, we assume the rate of supply to the scoured area to be zero, so that the rate of scour for characteristic 1 will involve only the capacity for transport out of the scoured area.

Linear Semilogarithmic Method

Researchers have found that the shape of local scour is independent of time if suitable normalization parameters are selected to nondimensionalize the units of measurement (see Ref. 1, pp. 183–184; Ref. 2, p. 1197; Ref. 3, pp. 283–287; and Ref. 4, p. 50). However, the progression of the scour with time has not been satisfactorily defined over the entire time range. This is shown Anderson (Ref. 4, p. 52, Fig. 2.17), who has plotted the scour depth against the logarithm of time for the Laursen and Tarapore data. Regarding his Fig. 2.17, Anderson states (Ref. 4, pp. 51–52):

> The curves show that the extent of the scour increases linearly over the range shown with the logarithm of the time. . . . The linear relationship implies that the extent of the scour increased indefinitely, contrary to the . . . hypothesis stated by Laursen. It must be remembered, however, that such a logarithmic function is empirical and is based on fitting the relationship to experimental points. In fitting such a curve, it was often necessary to omit points near the origin in Fig. 2.17, because it is obvious that the logarithmic function cannot hold for small values of time. At the beginning of the experiment, when [the time] is zero, [the relative scour depth] is also equal to zero rather than minus infinity as required by a logarithmic function. . . . For larger values of [the time], it appears that the logarithmic function fits the data better, while for an intermediate range, either a logarithmic or an exponential function might be suitable. . . . Although experiments do not indicate the condition clearly, it is plausible that for large values of time, when the local shear stress is approaching the critical value for the sediment, the scour-time relation may again depart from the logarithmic form. In the absence of an analytical solution that describes the entire range, recourse must be had to empirical descriptions of the various significant parts of the entire curve.
>
> Note that, by virtue of the logarithmic character of the development of the scour region with time, a *practical equilibrium* [emphasis supplied] is reached after a relatively short time, after which the increase in the depth and extent or [sic] scour becomes virtually imperceptible.

The definition of *practical equilibrium* can be interpreted differently by each person. When is *practical equilibrium* reached? When does scour stop, either practically or totally? We agree that there are probably undefined practical limits to the progression of scour, but the random nature of turbulent flow eddy bursts suggests that scour never stops completely. In one experiment, the results of which will be presented later, the writers noted that scour continued even after 14-1/4 months. True, one might have to look for several minutes to detect the movement of a sediment particle, but movement was still continuing. The analytical method we will describe determines the ultimate dimensions of

scour—the asymptotic limit recognized by most researchers—and thus removes the vague limit suggested by the term *practical equilibrium.*

Linear Logarithmic Velocity-of-Scour Method

The writers' ideas originated with and are an extension of the analytical method suggested by Thomas (5,6,7) to forecast the time development of scour, and to extrapolate experimentally-obtained values of scour to considerably longer times than are practical in experiments. Thomas developed a theoretical equation for the velocity of scour—the scour depth divided by the time since the beginning of scour. His theoretical equation, presented in Refs. 6 (Eq. 75), and 7 (Eq. 75), is

$$v_{h,\text{th}} = \frac{h_{\text{th}}}{t} = v_{a,k} + \frac{1}{t} v_{a,k}^2 \frac{\rho_s}{g(\rho_s - \rho)} \times \ln \frac{\cosh \operatorname{arctanh}\left(\frac{v_{\max}}{v_{a,k}} - 1\right)}{\cosh\left[\operatorname{arctanh}\left(\frac{v_{\max}}{v_{a,k}} - 1\right) - \frac{cS\rho v_{a,k}}{2V\rho_s} t\right]} \quad \ldots\ldots\ldots\ldots\ldots\ldots (1)$$

in which $v_{h,\text{th}}$ = the theoretical velocity by which the scour depth increases; h_{th} = the theoretical scour depth; t = the time; $v_{a,k}$ = numerically, the fall velocity of the sediment grain in still fluid; ρ = the density of the fluid; ρ_s = the density of the sediment; g = the acceleration of gravity; $v_{\max}$ = the velocity of the jet at the unscoured bed level; c = a coefficient of hydrodynamic or aerodynamic resistance of the sediment; S = the shaded area of the sediment grain; and V = the volume of the sediment grain.

Thomas has computed theoretical values of $v_{h,\text{th}}$ and has plotted log $v_{h,\text{th}}$ against log t. Fig. 1 is reproduced from Thomas' paper (Ref. 6, Fig. 5). Note that

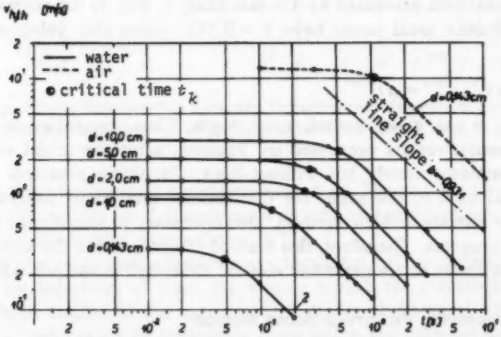

FIG. 1.—Logarithmic Relationship Between Theoretical Velocity of Scour and Time (Ref. 6, Fig. 5)

for short time periods—less than 0.01 sec–0.2 sec for the water data depending on the sand size, and 0.5 sec for the air data—the velocity of scour is, according to Thomas, independent of time. To check Thomas' statement that the velocity of scour is independent of time, the writers differentiated the logarithmic form of Eq. 1 with respect to the logarithm of time for $v_{max} = v_{a,k}$, and evaluated the differential, $d \ln v_{h,th}/d \ln t$, at various times. The evaluation shows that, although the slope is negligible for small values of the time, theoretically the velocity of scour is not independent of time. (Experimental data presented by Thomas show that this time independence may vary with scale, some data suggesting a period as long as 50,000 sec—14 h.) (See Ref. 6, Fig. 8, for full-scale tests of truss piers.)

With increasing time and after a transition, the logarithmic curve for Eq. 1 is, also according to Thomas, a straight line again, but with an average slope of −0.948 for all the lines drawn in Fig. 1. Included are all sand sizes and both air and water. The equation of this line has the form

$$\log v_{h,th} = \log \frac{h_{th}}{t} = \log a - b \log t \quad \ldots\ldots\ldots\ldots\ldots\ldots\ldots\ldots (2)$$

$$\text{or} \quad \log h_{th} - \log t = \log a - b \log t \quad \ldots\ldots\ldots\ldots\ldots\ldots\ldots\ldots (3)$$

$$\text{from which} \quad \log h_{th} = \log a + (1 - b) \log t \quad \ldots\ldots\ldots\ldots\ldots\ldots\ldots\ldots (4)$$

$$\text{and} \quad h_{th} = a t^{(1-b)} \quad \ldots\ldots\ldots\ldots\ldots\ldots\ldots\ldots\ldots\ldots\ldots\ldots (5)$$

in which a and b = coefficients and exponents, respectively.

As noted previously, the average theoretical value of b for the curves in Fig. 1 is given by Thomas as 0.948. However, the writers' evaluation of the differential of the logarithmic form of Eq. 1 gave theoretical values of b = 1.000 for times exceeding 0.1 sec for 0.184-cm material. This value is in close agreement with the Thomas' curves shown in Fig. 1.

If $b = 1$ is substituted in Eq. 5, then $h_{th} = a$ and the theoretical depth of scour is a constant for all times of scour. This constancy is not supported by observations, so Eq. 5 is not valid when $b = 1$.

Experimental data presented by Thomas (Ref. 6, Fig. 8) for several structural forms that induce local scour have $b = 0.931$. Using this value of b, Eq. 5 becomes

$$h_{th} = h_{ex} = a t^{(1-0.931)} = a t^{0.069} \quad \ldots\ldots\ldots\ldots\ldots\ldots\ldots\ldots\ldots\ldots (6)$$

in which h_{ex} = the experimental scour depth. Thus, according to the theory and experimental results presented by Thomas, after the initial scour period the scour increases slowly but without limit. To obtain *practical equilibrium* or a practical limit to the scour for the Thomas method of analysis, it is, as for the linear semilogarithmic method, also necessary to specify the time period of the scour progress. Therefore, this method of analysis has the same limitation as that of the linear semilogarithmic method examined in the preceding section.

Hyperbolic Logarithmic Velocity-of-Scour Method

An inspection of the logarithmic plots of experimental data presented by Thomas—the plot of Fig. 2 (See Ref. 6, Figs. 6 and 7) is typical—shows that

the transition region is much longer than suggested by the theoretical plots. In fact, the experimental data do not exhibit the region where the scour velocity is independent of time. This is not surprising: the region where $v_{h,th}$ is independent of time is very short—this time period is measured in seconds or fractions of seconds. For these extremely short time periods, to obtain meaningful experimental scour data is very difficult or impossible. The writers' experience with the progression of scour at cantilevered pipe or culvert outlets is that satisfactory scour data cannot be obtained for time periods less than about 600 sec (10 min).

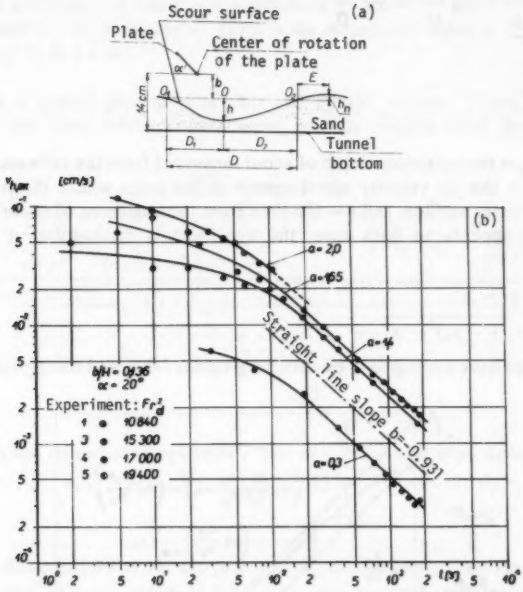

FIG. 2.—Logarithmic Relationship Between Experimental Velocity of Scour and Time: (a) Longitudinal Section; (b) Plot of Experimental Data (Ref. 6, Figs. 6 and 7)

Many of the experimental curves presented by Thomas for the progression of scour resulting from local disturbances caused by baffles, piers, and spillway aprons exhibit the typical shape shown in Fig. 2.

To define the relationship between the logarithm of the average velocity of scour and the logarithm of time, the writers looked for a mathematical curve having a shape similar to the experimental curves of Thomas' plots of log v_h versus log t, and having an asymptote from which the ultimate depth of scour could be computed. Such a curve is a limb of a vertically-oriented hyperbola with the origin of the hyperbola offset on the y-axis. The general form of the equation for the hyperbola shown in Fig. 3 is

$$\frac{(y - y_0)^2}{A^2} - \frac{x^2}{B^2} = 1 \quad (7)$$

in which A = the semitransverse axis; and B = the semiconjugate axis of the hyperbola. We have defined y and x in dimensionless units when applying Eq. 7 to data from our research on scour at cantilevered pipe spillway or culvert outlets. Our definitions of y and x are:

$$y = \log \frac{\frac{Z_m}{D_p}}{\frac{V_p t}{D_p}} = \log \frac{Z_m}{D_p} - \log \frac{V_p t}{D_p} \quad (8)$$

$$x = \log \frac{V_p t}{D_p} \quad (9)$$

in which Z_m = the maximum depth of scour measured from the tailwater surface; V_p and D_p = the jet velocity and diameter at the point where the jet plunges into the tailwater surface; and t = the time from the beginning of scour. Because $\log V_p t/D_p$ appears on both axes, the hyperbola is rectangular, $A = B$, Eq. 7 becomes

$$(y - y_0)^2 - x^2 = A^2 \quad (10)$$

and $$A = \sqrt{(y - y_0)^2 - x^2} \quad (11)$$

The writers have evaluated A by assuming values for y_0 and using experimental

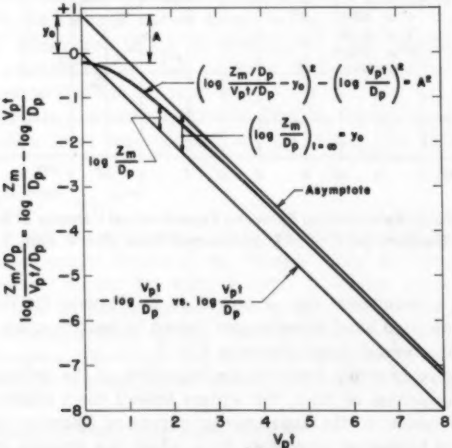

FIG. 3.—General Form of Hyperbola

values y and x to compute A. The best value of A is that value for which the standard error of estimate, σ, is a minimum. The procedure we used is:

1. Plot experimental values of y and x and estimate the asymptote. Extrapolate the asymptote to $x = 0$. The distance on the y-axis between the origin and the asymptote at $x = 0$ is an initial value of y_0.
2. Use the data to compute values of A. (A should be a constant.)
3. Compute the standard error, σ, of A.
4. Assume another value of y_0 and repeat steps 2 and 3.
5. Repeat step 4 until the minimum value of σ is found. (The best fit values of y_0 and A are those for which σ is a minimum.)
6. Compute Z_m/D_p = antilog y_0. (This is the asymptotic value of Z_m/D_p—the value of Z_m/D_p at $t = \infty$.)

Fig. 4 is a typical plot of data obtained by the writers. There it will be noted that the data, which covers scour periods ranging from 600 sec (log

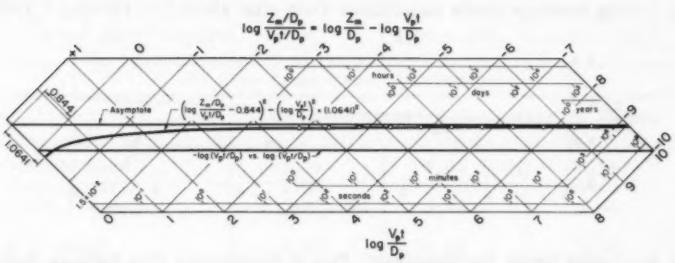

FIG. 4.—Typical Hyperbolic Logarithmic Plot of Cantilevered Pipe Spillway Scour Progression [$Q/\sqrt{gD^5} = 2$, $Z_p/D = +1$, $V_p = 5.04$ fps (154 cm/s); $D_p = 0.07578$ ft (2.31 cm)]

$V_p t/D_p = 4.60$) to 1.90×10^7 sec (log $V_p t/D_p = 9.10$) by 0.5 increments of the logarithm plus a scour period of 3.74×10^7 sec (log $V_p t/D_p = 9.40$), are far to the right of $x = 0$ and approach the asymptote of the hyperbola. The equation of the hyperbola of best fit is

$$(y - 0.844)^2 - x^2 = (1.0641)^2 \quad \ldots\ldots\ldots\ldots\ldots\ldots\ldots\ldots \quad (12)$$

and the ultimate or asymptotic value of the scour depth is

$$\frac{Z_m}{D_p} = \text{antilog}\, y_0 = \text{antilog}\, 0.844 = 6.98 \quad \ldots\ldots\ldots\ldots\ldots\ldots \quad (13)$$

(Experimental data for the 3.74×10^7 sec scour period did not become available until after Eq. 12 had been evaluated. However, this omission affects only the numerical values in Eqs. 12–15. The ommision of the last data point does not affect the sense of the hyperbolic logarithimic velocity-of-scour analytical method or the comparison of methods presented in this paper.)

COMPARISON OF METHODS

Linear Logarithmic Method.—An inspection of Fig. 4 shows that the hyperbolic curve that best fits the data approximates a straight line. The least squares fit straight line has the equation

$$\frac{Z_m}{D_p} = 4.7138 \left(\frac{V_p t}{D_p}\right)^{(1-0.987643)} = 4.7138 \left(\frac{V_p t}{D_p}\right)^{0.012357} \quad \ldots\ldots\ldots\ldots (14)$$

with a correlation coefficient of 0.999,970. This is the form proposed by Thomas (See Eq. 5).

The time predicted by Eq. 14 to reach the ultimate depth computed from the hyperbolic equation can be computed by substituting Z_m/D_p computed from Eq. 13 into Eq. 14. This time turns out to be $V_p t/D_p = 6.43 \times 10^{13}$ or, for the data plotted in Fig. 4 in which $V_p/D_p = 66.5\ s^{-1}$, $t = 30{,}644$ yr.

Linear Semilogarithmic Method.—A similar comparison can be made using the linear semilogarithmic method. The data plotted in Fig. 4 are replotted in Fig. 5 using semilogarithmic coordinates. Only after about 5-1/4 hr (log $V_p t/D_p$

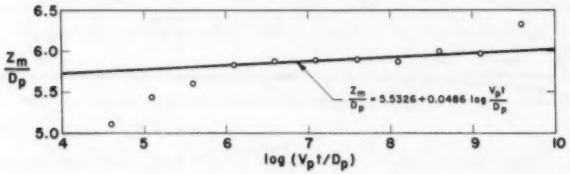

FIG. 5.—Typical Linear Semilogarithmic Plot of Cantilevered Pipe Spillway Scour Progression [$Q/\sqrt{gD^5} = 2$; $Z_p/D = +1$; $V_p = 5.04$ fps (154 cm/s); $D_p = 0.07578$ ft (2.31 cm)]

$\simeq 6.1$) do the data fall on an approximate straight line. This agrees with Anderson's statement that ". . . the logarithmic function cannot hold for small values of time." Therefore, only the data for scour periods greater than log ($V_p t/D_p$) = 6 were used to develop the equation for the relationship between scour depth and time. The least squares fit equation is

$$\frac{Z_m}{D_p} = 5.5326 + 0.0486 \log \frac{V_p t}{D_p} \quad \ldots\ldots\ldots\ldots\ldots\ldots\ldots\ldots (15)$$

with a correlation coefficient of 0.850.

The time predicted by Eq. 15 to reach the ultimate depth computed by the hyperbolic logarithmic equation is $V_p t/D_p = 6.0 \times 10^{29}$ or $t = 2.9 \times 10^{20}$ yr.

Summary Table.—The results obtained using the three computation methods are compared in Table 1(*a*). The slightly higher correlation coefficient for the hyperbolic logarithmic method indicates that the fit of the data to the linear logarithmic curve is slightly inferior to the fit of the data to the hyperbolic logarithmic curve. The correlation coefficient for the linear semilogarithmic curve is relatively low. However, this low correlation coefficient for the linear

semilogarithmic method and the high correlation coefficients for the logarithmic methods may be mathematical and statistical rather than real. Another possible reason for the lower correlation coefficient for the linear logarithmic method is that the actual scour depth was used for the semilogarithmic method, whereas the velocity of scouring was used for the logarithmic methods.

TABLE 1.—Comparison of Methods

Item (1)	Equation: Hyperbolic logarithmic (2)	Linear logarithmic (3)	Linear semilogarithmic (4)
(*a*) Comparison of Equations			
Correlation coefficient	0.999,986	0.999,970	0.850
Time to reach ultimate scour depth[a]--years	∞	3.06×10^4	3.26×10^{20}
(*b*) Time Comparison of Scour Depths			
n	Depth of scour Z_p/D_p after 10^n years		
-3 (8.76 hours)	5.69	5.64	5.84
-2 (3.65 days)	5.85	5.81	5.89
-1 (36.5 days)	5.97	5.97	5.94
0 (1 year)	6.07	6.15	5.99
1 (10 years)	6.16	6.32	6.03
2 (100 years)	6.22	6.50	6.08
3 (1,000 years)	6.28	6.69	6.13
4 (10,000 years)	6.33	6.89	6.18
5 (100,000 years)	6.38	7.08	6.23
6 (1,000,000 years)	6.41	7.29	6.28
∞ (∞ years)	6.98	∞	∞

[a] The ultimate scour depth, 6.98 D_p, is computed by the hyperbolic logarithmic method.

Comparing the depths of scour for the time periods shown in Table 1(b) will permit each person to determine what he feels is a *practical limit*.

Conclusion

The differences in the predicted dimensions of the scour between the various methods may be small. The claim for the hyperbolic method is that: (1) Determination of the ultimate scour dimensions does not depend on deciding what is a *practical* time; and (2) the limiting extent of scour, Laursen's third characteristic, can be determined. On the other hand, if a practical scour dimension

is desired, the hyperbolic method of analysis will provide a prediction equation for any practical time period and also evaluate the difference between the *practical* and *ultimate* dimensions.

The rate of change of the scour velocity, represented by the slope of the hyperbola relative to its asymptote, is maximum at the beginning of scour, decreases rapidly during the early stages of scour, and becomes small as the hyperbola approaches its asymptote. This change in the scour rate with time agrees with Laursen's second and fourth characteristics.

The only scour dimension examined in this paper has been the depth of scour. However, in view of the comments made by others (Ref. 1, pp. 183–184; Ref. 2, p. 1197; Ref. 3, pp. 283–287; Ref. 4, p. 50), and our unreported experiences, the comments made herein apply equally to other dimensions of local scour, i.e., the length and width of the scoured area, and the location of the scour with respect to the pipe exit, pier, or other source of the local scour.

Acknowledgments

This paper is the product of part of the research on the scour that takes place at cantilevered pipe spillway exits. The goal of the research is to determine the location and size of scour holes in various sizes of bed material so that pre-excavated unlined or ripraped plunge pool energy dissipators can be designed. The research is being done at the St. Anthony Falls Hydraulic Laboratory by the Hydraulics of Structures Research Unit, Science and Education Administration-Agricultural Research, United States Department of Agriculture, in cooperation with the Minnesota Agricultural Experiment Station and the St. Anthony Falls Hydraulic Laboratory of the University of Minnesota, at Minneapolis, Minn.

Appendix I.—References

1. Laursen, E. M., "Observations on the Nature of Scour," *Proceedings of the Fifth Hydraulic Conference, Bulletin 34,* University of Iowa, Iowa City, Iowa, June 9–11, 1952, pp. 179–197.
2. Rajaratnam, N., and Beltaos, S., "Erosion by Impinging Circular Turbulent Jets," *Journal of the Hydraulics Division,* ASCE, Vol. 103, No. HY10, Proc. Paper 13287, Oct., 1977, pp. 1191–1205.
3. Rajaratnam, N., and Berry, B., "Erosion by Circular Turbulent Wall Jets," *Journal of Hydraulic Research,* Vol. 15, No. 3, 1977, pp. 277–289.
4. *Sedimentation Engineering, Manual No. 54,* by the ASCE Task Committee for the Preparation of the Manual on Sedimentation of the Sedimentation Committee of the Hydraulics Division, V. A. Vanoni, ed., ASCE, 1975; Chapter II.—Sediment Transportation Mechanics; Section C. Erosion of Sediment—Local Scour, by A. G. Anderson.
5. Thomas, Z., "Time Development of the Deformation of an Alluvial Bottom," *Proceedings, Fourteenth Congress of the International Association for Hydraulic Research,* Paris, France, Vol. 3, Aug. 29–Sept. 3, 1971, pp. 347–354.
6. Thomas, Z., "Time Development of the Dimensions of a Local Scour and Deposit (Časový vývoj Rozměrů Lokálního Výmolu a Nánosu)," *Vodohospodářský Časopis,* Bratislava, Czechslovakia, Vol. 20, No. 1, 1972, pp. 33–65 [Translated for the Agricultural Research Service, United States Department of Agriculture and the National Science Foundation, Washington, D.C., by Franklin Book Programs Inc., 1975 (Translation TT 74-58057 available from Mrs. Audrey Kilgore, United States Department of Agriculture, Science and Education Administration, International Programs Staff, Room 400, Federal Building 1, Hyattsville, Md., 20782)].

7. Thomas, Z., "Hydraulic Construction Scourings, and Erosion of Moving Medium by a Flowing Liquid (A better translation of the title is: Scour at Hydraulic Structures and Erosion of Loose Medium by a Streaming Liquid) (Podemílání vodních staveb a erose sypkého prostředí proudící tekutinou výzkumný ústav vodohospodářský)," *Research Report*, Výzkumný ústav vodohosporářský, Prague, Czechoslovakia, 1972. [Translated for the National Science Foundation and the United States Department of Agriculture, Agricultural Research Service, Washington, D.C., by Lang Faure, Agence Tunisienne de Public-Relations, Tunis, Tunisia, 1975 (Translation TT 75-55040 available from Mrs. Audrey Kilgore, United States Department of Agriculture, Science and Education Administration, International Programs Staff, Room 400, Federal Building 1, Hyattsville, Md., 20782)].
8. Thomas, Z., discussion of "Erosion of Sand Beds Around Spur Dikes," by Mohammad Akram Gill, *Journal of the Hydraulics Division*, ASCE, Vol. 99, No. HY8, Proc. Paper 9895, Aug., 1973, pp. 1272–1274.

Appendix II.—Notation

The following symbols are used in this paper:

A = semitransverse axis of hyperbola;
a = coefficient in exponential equation;
B = semiconjugate axis of hyperbola;
b = exponent in exponential equation; height of plate above original sand bed for Thomas' air tests;
c = coefficient of hydrodynamic or aerodynamic resistance of sediment;
D = pipe diameter;
D_p = jet diameter at point where jet plunges into tailwater surface;
F_d = Froude number of sediment grain for Thomas' air tests;
g = acceleration of gravity;
H = height of approach channel for Thomas' air tests;
h = scour depth for Thomas' air tests;
Q = discharge;
S = shaded area of sediment grain;
t = time;
V = volume of sediment grain;
V_p = jet velocity at point where jet plunges into tailwater surface;
$v_{a,k}$ = numerically equal to fall velocity of sediment grain in still fluid;
v_h = velocity with which scour depth increases;
v_{max} = velocity of jet at unscoured bed level;
x = abscissa;
y = ordinate;
y_0 = offset of origin on y-axis;
Z_m = maximum depth of scour measured from tailwater surface;
Z_p = height of pipe invert above tailwater level;
α = angle of deflector plate with horizontal for Thomas' air tests;
ρ = density of fluid;
ρ_s = density of sediment; and
σ = standard error of estimate.

Subscripts

ex = experimental; and
th = theoretical.

JOURNAL OF THE HYDRAULICS DIVISION

THREE-PARAMETER PROBABILITY DISTRIBUTIONS

By Donthamsetti Veerabhadra Rao,[1] M. ASCE

INTRODUCTION

The United States Water Resources Council, while recommending the Pearson type 3 distribution (P) with log transformation of the data (log Pearson type 3 distribution, LP) as the base method for flood flow frequency analysis, identified a continued study of alternative distributions as a topic for future research (4). The principal consideration in the use of three-parameter probability distributions like P or LP is their flexibility in that three sample statistics (usually the mean, variance, and skewness coefficient, are fitted to the distribution when the method of moments is used for parameter estimation). A comparative study of four well-known three-parameter probability distributions is the subject of this paper. The distributions selected are: Lognormal (LN), Weibull (W), P, and LP.

The three-parameter probability distributions are formed basically by adding a shift or location parameter, c, to their two-parameter counterparts. The location parameter (or a function of it, as in the case of LP) serves as a bound (lower or upper) for the random variable being fitted. Parameter c is not a constant for a given three-parameter probability distribution, but assumes a different value for each combination of the mean, μ, variance, σ^2, and skewness coefficient γ, of the random variable. Moreover, the bound becomes negative in certain instances for LN, W, and P. This parameter has a significant physical interpretation when applied to hydrologic variates such as streamflow, precipitation, etc. These hydrologic variates cannot be negative (unless made negative by some transformation) on one hand, and on the other, imposition of an upper bound implies that there is a "maximum certain value (like flood flow)" which is not physically meaningful. However, probability distributions with negative lower tails like the Gumbel were used for a long time in flood flow frequency analysis. In such cases, since the quantiles in the upper tail of the distribution are of interest, the fact that a portion of the distribution lies in the negative region

[1]Hydro., St. Johns River Water Management Dist., P.O. Box 1429, Palatka, Fla. 32077.

Note.—Discussion open until August 1, 1981. To extend the closing date one month, a written request must be filed with the Manager of Technical and Professional Publications ASCE. Manuscript was submitted for review for possible publication on February 26, 1980. This paper is part of the Journal of the Hydraulics Division, Proceedings of the American Society of Civil Engineers, ©ASCE, Vol. 107, No. HY3, March, 1981. ISSN 0044-796X/81/0003-0339/$01.00.

of the variate will not be readily "perceived" unless a complete investigation of the distribution is made. Nevertheless, the engineer/hydrologist should make sure at least, that the area of distribution in the negative region (henceforth called "negative area" for simplicity) of the variate is insignificant because the statistical parameters (SP) like μ, σ^2, or γ are formed from the population variate values both positive and negative, whereas, the sample values are all positive. For the four three-parameter probability distributions selected, the bounds and the negative areas of the distribution and selected quantiles are presented in a generalized fashion for comparison. Some guidelines are provided for selecting the best applicable three-parameter probability distribution for a given hydrologic sample.

Description of Distributions

For the four distributions selected, the probability density function, $f(x)$, the relations of the distribution parameters, a, b, and c to the SP, i.e., μ_x,

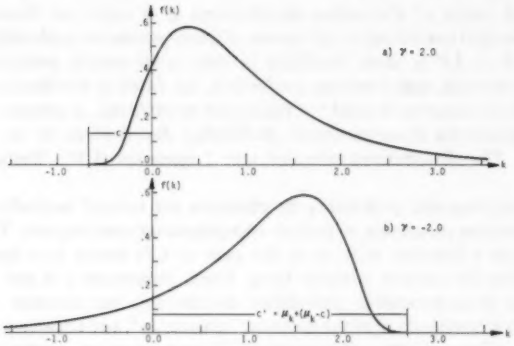

FIG. 1.—Lognormal Densities; $\sigma_k^2 = 1.0$, $c = -0.678$

σ_x^2, and γ_x, and a brief description, are as follows:

1. Lognormal:

$$f(x) = \frac{1}{b(2\pi)^{1/2}(x-c)} \exp\left\{-\frac{1}{2b^2}\left[\ln(x-c)-a\right]^2\right\} \quad \ldots\ldots\ldots (1a)$$

$$\mu_x = c + \exp\left(\frac{b^2}{2} + a\right) \quad \ldots\ldots\ldots (1b)$$

$$\sigma_x^2 = \exp(2a)d^2(d^2+1) \quad \ldots\ldots\ldots (1c)$$

in which $d^2 = \exp(b^2) - 1$ $\ldots\ldots\ldots (1d)$

$$\gamma_x = d^3 + 3d \quad \ldots\ldots\ldots (1e)$$

When γ_x is positive, $c < x \leqq \infty$, and $(x - c)$ is distributed as the two-parameter lognormal (LN2), with its origin shifted by a value, c [see Fig. 1(*a*)]. When γ_x is negative, let c' represent the new location parameter; then, $-\infty \leqq x < c'$ and $(c' - x)$ is distributed as LN2 in the reverse direction (mirror image of the positive skewed distribution), with its origin shifted by c' [see Fig. 1(*b*)]. It can be shown that $c' = \mu_x + (\mu_x - c)$. Eqs. 1*a*–1*e* are applicable when γ_x is negative by replacing $(x - c)$ by $(c' - x)$ in Eq. 1*a*, and replacing c by c' in Eq. 1*b*. The LN is unimodal and bell-shaped (with a skew). Further details may be found in Aitchison and Brown (1).

To solve for the parameters a, b, and c from a given set of μ_x, σ_x^2, and γ_x, the value of d is determined first from Eq. 1*e* by trial. Then, a, b, and c are solved explicitly.

2. Weibull:

$$f(x) = \frac{a}{b}\left[\frac{(x-c)}{b}\right]^{a-1} \exp\left\{-\left[\frac{(x-c)}{b}\right]^{a}\right\}; \quad c \leqq x \leqq \infty \quad \ldots\ldots\ldots (2a)$$

$$\mu_x = c + b\,\Gamma\left(1 + \frac{1}{a}\right) \quad \ldots\ldots\ldots (2b)$$

$$\sigma_x^2 = b^2\left[\Gamma\left(1 + \frac{2}{a}\right) - \Gamma^2\left(1 + \frac{1}{a}\right)\right] \quad \ldots\ldots\ldots (2c)$$

$$\gamma_x = \frac{\left[\Gamma\left(1 + \frac{3}{a}\right) - 3\Gamma\left(1 + \frac{2}{a}\right)\Gamma\left(1 + \frac{1}{a}\right) + 2\Gamma^3\left(1 + \frac{1}{a}\right)\right]}{\left[\Gamma\left(1 + \frac{2}{a}\right) - \Gamma^2\left(1 + \frac{1}{a}\right)\right]^{1.5}} \quad \ldots\ldots (2d)$$

The Weibull distribution, with a modified form of parameter b is equivalent to the Gumbel's Type III asymptotic extreme value distribution of smallest values. Parameter c is the lower bound of the distribution for both positive and negative γ_x.

However, γ_x has a lower limit of -1.1396 (5). The Weibull distribution is unimodal and bell-shaped when $\gamma_x < 2$ or $a > 1$ and has a reverse J-shape when $\gamma_x \geqq 2$ or $a \leqq 1$. Further details may be found in Refs. 5 and 10. For given SP, parameter a is solved first, by trial, from Eq. 2*d*, and then b and c are solved explicitly.

3. Pearson Type 3 (three-parameter gamma)

$$f(x) = \frac{|a|}{\Gamma(b)}\,[a(x-c)]^{b-1} \exp\,[-a(x-c)] \quad \ldots\ldots\ldots (3a)$$

$$\mu_x = c + ba^{-1} \quad \ldots\ldots\ldots (3b)$$

$$\sigma_x^2 = ba^{-2} \quad \ldots\ldots\ldots (3c)$$

$$\gamma_x = \frac{|a|}{a}\,2b^{-1/2} \quad \ldots\ldots\ldots (3d)$$

When γ_x is positive, a is positive and $c \leqq x \leqq +\infty$. When γ_x is negative,

a is negative and $-\infty \leqq x \leqq c$. In P, $(x - c)$ is distributed as the two-parameter gamma (GA2) with its origin shifted by c. As in LN, when γ_x is negative, $(c - x)$ is distributed as GA2 in the reverse direction. The P and W become equivalent when $\gamma_x = 2$. Like W, P is also unimodal and bell-shaped when $\gamma_x < 2$, $(b > 1)$, and reverse J-shaped when $\gamma_x \geqq 2$, $(b \leqq 1)$.

4. Log Pearson Type 3:

$$f(x) = \frac{|a| \exp(ac)}{\Gamma(b)\, x^{1+a}} [a(\ln x - c)]^{b-1} \quad \ldots\ldots\ldots\ldots\ldots\ldots\ldots\ldots\ldots\ldots (4a)$$

$$\mu_x = \frac{\exp(c)}{\left(1 - \frac{1}{a}\right)^b} \quad \ldots\ldots\ldots\ldots\ldots\ldots\ldots\ldots\ldots\ldots\ldots\ldots\ldots\ldots (4b)$$

$$\sigma_x^2 = \exp(2c)\left[\frac{1}{\left(1 - \frac{2}{a}\right)^b} - \frac{1}{\left(1 - \frac{1}{a}\right)^{2b}}\right] \quad \ldots\ldots\ldots\ldots\ldots\ldots\ldots (4c)$$

$$\gamma_x = \exp(3c) \frac{\left\{\frac{1}{\left(1 - \frac{3}{a}\right)^b} - \frac{3}{\left[\left(1 - \frac{2}{a}\right)\left(1 - \frac{1}{a}\right)\right]^b} + \frac{2}{\left(1 - \frac{1}{a}\right)^{3b}}\right\}}{\sigma_x^3} \quad (4d)$$

If a is positive, γ_x is positive and $\exp(c) \leqq x \leqq +\infty$. If a is negative, γ_x is either positive or negative depending on the values of a and b, and $0 < x \leqq \exp(c)$. The many forms taken by LP are analyzed at length by Bobee (2). Solution of LP parameters from given SP is available in Ref. 7.

Generalized Evaluation of Distributions

In the method of moments, parameters of distributions are evaluated by equating population SP, i.e., μ, σ^2, and γ, to the corresponding sample estimates. Thus, it will be more comprehensive if a comparison of different properties of three-parameter probability distributions is made on the basis of SP. In the following sections some properties of the four distributions presented are evaluated in terms of the dimensionless variate $K = X/\mu_x$. Such a transformation of the random variable, X, meaningfully scales data, giving a value of unity for the mean of K i.e., $\mu_k = 1.0$. The transformed data, i.e., $K_i = X_i/\bar{X}$ (in which i = the ith observed value and $\bar{X}$ = sample mean), being ratios to the mean, afford an easy "feel" for the results obtained. The standard deviation of K, σ_k, is equivalent to η_x, the coefficient of variation of X. Skewness coefficient, by definition, is dimensionless; thus $\gamma_x = \gamma_k$. If μ_x is equated to 1.0, the distributions yield different results in terms of K. All results may be classified and compared on the basis of two SP, σ_k^2 and γ_k. The value of σ_k^2 is the variance of K, and represents the squared value of coefficient of variation of data. For floods in real space, Landwehr et al. (6) evaluated the values of mean coefficient of variation ($\overline{CV}$) for the 14 hydrologic regions of the United States for record lengths, n = 10 yr, 20 yr, and 30 yr. Values

of $\overline{CV}$ varied from 0.39–0.99 for the 14 regions and the standard deviations for $\overline{CV}$ are in the range of 0.15–0.43 (the extreme values being applicable to the respective extreme values of $\overline{CV}$). These statistics indicate the general range of σ_k^2 encountered in hydrologic samples.

Ranges of 0.01–5.00 for σ_k^2 and −9.0–9.0 for γ_k were chosen for investigation. However, in the cases of W and LP, γ_k values less than −1.0 were not investigated because W cannot take $\gamma_k < -1.1396$ and LP assumes a U-shape for most negative γ_k values (7). For several combinations of σ^2 and γ_k chosen systematically, the distribution parameters, *a*, *b*, and *c*, whence different results of interest, were evaluated.

Bounds of Distributions

The bound values of different distributions are presented in Tables 1–4. The LN and P are bounded in the lower tail when γ_k is positive (Table 1), and they are bounded in the upper tail when γ_k is negative (Table 2). The W is

TABLE 1.—Lower Bound Values (Expressed as Ratios to Mean) of Lognormal and Pearson Type 3 Distributions

VARIANCE	SKEWNESS COEFFICIENT (γ_k)								
σ_k^2	0.50	1.00	1.50	2.00	3.00	4.00	5.00	7.00	9.00
(1)	(2)	(3)	(4)	(5)	(6)	(7)	(8)	(9)	(10)
				LOGNORMAL DISTRIBUTION					
0.01	0.395	0.690	0.786	0.832	0.878	0.900	0.913	0.929	0.938
0.05	-0.354	0.306	0.520	0.625	0.727	0.776	0.806	0.841	0.861
0.10	-0.915	0.018	0.322	0.469	0.613	0.684	0.726	0.775	0.804
0.20	-1.708	-0.388	0.041	0.250	0.453	0.553	0.613	0.682	0.722
0.30	-2.316	-0.700	-0.175	0.081	0.330	0.452	0.525	0.611	0.660
0.40	-2.829	-0.963	-0.357	-0.061	0.227	0.368	0.452	0.550	0.607
0.50	-3.281	-1.195	-0.517	-0.186	0.135	0.293	0.387	0.497	0.561
0.60	-3.690	-1.404	-0.661	-0.300	0.053	0.225	0.329	0.449	0.519
0.70	-4.066	-1.597	-0.795	-0.404	-0.023	0.163	0.275	0.405	0.480
0.80	-4.415	-1.776	-0.918	-0.501	-0.094	0.106	0.225	0.364	0.444
0.90	-4.744	-1.945	-1.035	-0.592	-0.160	0.051	0.178	0.325	0.411
1.00	-5.055	-2.104	-1.145	-0.678	-0.223	0.000	0.134	0.289	0.379
2.00	-7.562	-3.389	-2.033	-1.373	-0.729	-0.414	-0.225	-0.006	0.121
3.00	-9.487	-4.376	-2.715	-1.906	-1.118	-0.732	-0.501	-0.232	-0.076
4.00	-11.109	-5.208	-3.290	-2.355	-1.446	-1.000	-0.733	-0.422	-0.242
5.00	-12.538	-5.940	-3.796	-2.751	-1.734	-1.236	-0.937	-0.590	-0.389
				PEARSON TYPE 3 DISTRIBUTION					
0.01	0.600	0.800	0.867	0.900	0.933	0.950	0.960	0.971	0.978
0.05	0.106	0.553	0.702	0.776	0.851	0.888	0.911	0.936	0.950
0.10	-0.265	0.368	0.578	0.684	0.789	0.842	0.874	0.910	0.930
0.20	-0.789	0.106	0.404	0.553	0.702	0.776	0.821	0.872	0.901
0.30	-1.191	-0.095	0.270	0.452	0.635	0.726	0.781	0.844	0.878
0.40	-1.530	-0.265	0.157	0.368	0.578	0.684	0.747	0.819	0.859
0.50	-1.828	-0.414	0.057	0.293	0.529	0.646	0.717	0.798	0.843
0.60	-2.098	-0.549	-0.033	0.225	0.484	0.613	0.690	0.779	0.828
0.70	-2.347	-0.673	-0.116	0.163	0.442	0.582	0.665	0.761	0.814
0.80	-2.578	-0.789	-0.193	0.106	0.404	0.553	0.642	0.744	0.801
0.90	-2.795	-0.897	-0.265	0.051	0.368	0.526	0.621	0.729	0.789
1.00	-3.000	-1.000	-0.333	-0.000	0.333	0.500	0.600	0.714	0.778
2.00	-4.657	-1.828	-0.886	-0.414	0.057	0.293	0.434	0.596	0.686
3.00	-5.928	-2.464	-1.309	-0.732	-0.155	0.134	0.307	0.505	0.615
4.00	-7.000	-3.000	-1.667	-1.000	-0.333	0.000	0.200	0.429	0.556
5.00	-7.944	-3.472	-1.981	-1.236	-0.491	-0.118	0.106	0.361	0.503

always bounded in the lower tail (Table 3). The LP is the only distribution of the four with a lower bound $K \geq 0$. The LP has an upper bound when γ_k is negative, and for some combinations of σ_k^2 and γ_k when γ_k is positive (Table 4). The combinations of σ_k^2 and γ_k for which LP has lower and upper bounds are denoted as Class A and Class B, respectively, in Table 4. When the LP has an upper bound, it develops a U-form if σ_k^2 is increased at given γ_k; this occurs because the LP is constrained (from spreading) from both ends

TABLE 2.—Upper Bound Values (Expressed as Ratios to Mean) of Negatively Skewed Lognormal and Pearson Type 3 Distributions

VARIANCE σ_k^2 (1)	SKEWNESS COEFFICIENT (γ_k) -0.50 (2)	-1.00 (3)	-1.50 (4)	-2.00 (5)	-3.00 (6)	-4.00 (7)	-5.00 (8)	-7.00 (9)	-9.00 (10)
				LOGNORMAL DISTRIBUTION					
0.01	1.605	1.310	1.214	1.168	1.122	1.100	1.087	1.071	1.062
0.05	2.354	1.694	1.480	1.375	1.273	1.224	1.194	1.159	1.139
0.10	2.915	1.982	1.678	1.531	1.387	1.316	1.274	1.225	1.196
0.20	3.708	2.388	1.959	1.750	1.547	1.447	1.387	1.318	1.278
0.30	4.316	2.700	2.175	1.919	1.670	1.548	1.475	1.389	1.340
0.40	4.829	2.963	2.357	2.061	1.773	1.632	1.548	1.450	1.393
0.50	5.281	3.195	2.517	2.186	1.865	1.707	1.613	1.503	1.439
0.60	5.690	3.404	2.661	2.300	1.947	1.775	1.671	1.551	1.481
0.70	6.066	3.597	2.795	2.404	2.023	1.837	1.725	1.595	1.520
0.80	6.415	3.776	2.918	2.501	2.094	1.894	1.775	1.636	1.556
0.90	6.744	3.945	3.035	2.592	2.160	1.949	1.822	1.675	1.589
1.00	7.055	4.104	3.145	2.678	2.223	2.000	1.866	1.711	1.621
2.00	9.562	5.389	4.033	3.373	2.729	2.414	2.225	2.006	1.879
3.00	11.487	6.376	4.715	3.906	3.118	2.732	2.501	2.232	2.076
4.00	13.109	7.208	5.290	4.355	3.446	3.000	2.733	2.422	2.242
5.00	14.538	7.940	5.796	4.751	3.734	3.236	2.937	2.590	2.389
				PEARSON TYPE 3 DISTRIBUTION					
0.01	1.400	1.200	1.133	1.100	1.067	1.050	1.040	1.029	1.022
0.05	1.894	1.447	1.298	1.224	1.149	1.112	1.089	1.064	1.050
0.10	2.265	1.632	1.422	1.316	1.211	1.158	1.126	1.090	1.070
0.20	2.789	1.894	1.596	1.447	1.298	1.224	1.179	1.128	1.099
0.30	3.191	2.095	1.730	1.548	1.365	1.274	1.219	1.156	1.122
0.40	3.530	2.265	1.843	1.632	1.422	1.316	1.253	1.181	1.141
0.50	3.828	2.414	1.943	1.707	1.471	1.354	1.283	1.202	1.157
0.60	4.098	2.549	2.033	1.775	1.516	1.387	1.310	1.221	1.172
0.70	4.347	2.673	2.116	1.837	1.558	1.418	1.335	1.239	1.186
0.80	4.578	2.789	2.193	1.894	1.596	1.447	1.358	1.256	1.199
0.90	4.795	2.897	2.265	1.949	1.632	1.474	1.379	1.271	1.211
1.00	5.000	3.000	2.333	2.000	1.667	1.500	1.400	1.286	1.222
2.00	6.657	3.828	2.886	2.414	1.943	1.707	1.566	1.404	1.314
3.00	7.928	4.464	3.309	2.732	2.155	1.866	1.693	1.495	1.385
4.00	9.000	5.000	3.667	3.000	2.333	2.000	1.800	1.571	1.444
5.00	9.944	5.472	3.981	3.236	2.491	2.118	1.894	1.639	1.497

whereas the dispersion of data (variance) about the mean is increased. These combinations of σ_k^2 and γ_k are indicated by the letter U in Table 4. Table 4 also shows, in footnotes, the combinations of σ_k^2 and γ_k at which the LP assumes a J- or reverse J-shape; in all other instances (of Table 4), the LP is unimodal, i.e., it is bell-shaped with a skew.

For hydrologic data, the bounds which may be considered desirable are: a lower bound $\simeq 0$, and an upper bound equal to a very large value like, $K \geq 100$ (which represents a flood value one hundred times the annual mean,

TABLE 3.—Lower Bound Values (Expressed as Ratios to Mean) and Negative Areas of Weibull Distribution

VARIANCE σ_k^2 (1)	SKEWNESS COEFFICIENT (γ_k) -1.00 (2)	-0.50 (3)	0.00 (4)	0.50 (5)	1.00 (6)	1.50 (7)	2.00 (8)	3.00 (9)	4.00 (10)	5.00 (11)	7.00 (12)	9.00 (13)
LOWER BOUND VALUES												
0.01	-3.484	0.368	0.676	0.790	0.847	0.879	0.900	0.924	0.938	0.946	0.957	0.963
0.05	-9.026	-0.413	0.275	0.531	0.658	0.730	0.776	0.830	0.860	0.880	0.904	0.918
0.10	-13.179	-0.998	-0.026	0.337	0.516	0.619	0.684	0.760	0.803	0.830	0.864	0.884
0.20	-19.052	-1.825	-0.451	0.062	0.316	0.461	0.553	0.660	0.721	0.760	0.807	0.836
0.30	-23.559	-2.460	-0.777	-0.149	0.162	0.340	0.452	0.584	0.658	0.706	0.764	0.799
0.40	-27.358	-2.996	-1.051	-0.326	0.032	0.238	0.368	0.520	0.605	0.660	0.727	0.767
0.50	-30.705	-3.467	-1.294	-0.483	-0.082	0.148	0.293	0.463	0.559	0.620	0.695	0.740
0.60	-33.732	-3.894	-1.512	-0.625	-0.185	0.066	0.225	0.412	0.516	0.584	0.666	0.715
0.70	-36.514	-4.286	-1.714	-0.755	-0.280	-0.009	0.163	0.365	0.478	0.550	0.639	0.692
0.80	-39.104	-4.651	-1.901	-0.876	-0.369	-0.078	0.106	0.321	0.442	0.519	0.614	0.671
0.90	-41.537	-4.993	-2.077	-0.990	-0.452	-0.144	0.051	0.280	0.408	0.490	0.591	0.651
1.00	-43.838	-5.318	-2.244	-1.097	-0.530	-0.205	-0.000	0.241	0.376	0.462	0.569	0.632
2.00	-62.411	-7.934	-3.587	-1.966	-1.164	-0.705	-0.414	-0.074	0.117	0.240	0.390	0.480
3.00	-76.662	-9.942	-4.618	-2.633	-1.651	-1.088	-0.732	-0.315	-0.081	0.069	0.253	0.363
4.00	-88.676	-11.635	-5.487	-3.195	-2.061	-1.411	-1.000	-0.519	-0.249	-0.075	0.137	0.265
5.00	-99.261	-13.126	-6.253	-3.690	-2.422	-1.695	-1.236	-0.698	-0.396	-0.202	0.035	0.178
'NEGATIVE AREAS', PERCENT												
0.01	0.000											
0.05	0.147	0.006										
0.10	0.895	0.349	0.000									
0.20	3.080	2.360	1.013									
0.30	5.246	4.765	3.425	0.821								
0.40	7.163	6.996	5.997	3.363								
0.50	8.833	8.965	8.360	6.166	1.490							
0.60	10.292	10.689	10.453	8.781	4.543							
0.70	11.575	12.203	12.295	11.117	7.567	0.286						
0.80	12.715	13.542	13.921	13.182	10.310	3.785						
0.90	13.735	14.736	15.363	15.009	12.745	7.227						
1.00	14.655	15.807	16.650	16.631	14.897	10.292						
2.00	20.642	22.643	24.676	26.453	27.445	27.216	25.390	13.428				
3.00	23.898	26.252	28.764	31.230	33.192	34.324	34.449	31.330	20.527			
4.00	26.031	28.575	31.339	34.159	36.600	38.364	39.347	38.944	35.050	24.742		
5.00	27.572	30.232	33.150	36.183	38.904	41.029	42.466	43.382	41.883	37.530		

TABLE 4.—Upper and Lower Bound Values of Log Pearson Type 3 Distribution

VARIANCE σ_k^2 (1)	SKEWNESS COEFFICIENT (γ_k) -1.00 (2)	-0.50 (3)	0.00 (4)	0.50 (5)	1.00 (6)	1.50 (7)	2.00 (8)	3.00 (9)	4.00 (10)	5.00 (11)	7.00 (12)	9.00 (13)
LOWER BOUND VALUES(CLASS A)												
0.01	1.158	1.277	1.951	0.355	0.739	0.835	0.878	0.918	0.937	0.948	0.960	0.967[1]
0.05	1.275[2]	1.442	1.958	14.260	0.202	0.520	0.653	0.767	0.818	0.846	0.877	0.893[1]
0.10	1.328[2]	1.512	1.967	4.429	##	0.207	0.425	0.616	0.697	0.742	0.789	0.814
0.20	U	1.573[2]	1.983	3.208	15.875	##	0.084	0.355	0.487	0.559	0.635	0.673
0.30	U	U	1.996	2.944	7.030	*	##	0.153	0.309	0.401	0.499	0.550
0.40	U	U	U	2.835	5.408	27.885	*	0.035	0.168	0.268	0.381	0.441
0.50	U	U	U	2.779	4.761	14.172	*	0.001	0.072	0.163	0.281	0.347
0.60	U	U	U	2.748[1]	4.423	10.294	69.920	##	0.020	0.086	0.199	0.267
0.70	U	U	U	U	4.220	8.559	33.070	*	0.002	0.037	0.133	0.200
0.80	U	U	U	U	4.088[1]	7.600	21.972	*	##	0.012	0.083	0.145
0.90	U	U	U	U	3.994[1]	7.000	17.005	*	##	0.002	0.047	0.101
1.00	U	U	U	U	3.930[1]	6.594	14.278	*	###	##	0.024	0.068
2.00	U	U	U	U	U	U	8.293[1]	26.193	*	*	*	##
3.00	U	U	U	U	U	U	U	17.129[1]	49.132	*	*	*
4.00	U	U	U	U	U	U	U	14.706[1]	33.122[1]	86.689	*	*
5.00	U	U	U	U	U	U	U	13.669[1]	27.498[1]	59.603[1]	*	*
UPPER BOUND VALUES(CLASS B)												

NOTES:-

FOR CLASS A THE UPPER BOUND VALUE = ∞
FOR CLASS B THE LOWER BOUND VALUE = 0
* K > 100
** 0 < K < .0005
*** K = 0

1 - THE DISTRIBUTION IS REVERSE J-SHAPED
2 - THE DISTRIBUTION IS J-SHAPED
U - THE DISTRIBUTION IS U-SHAPED

which may never be reached in practice). Tables 1, 3, and 4 show that these desirable bounds lie along a narrow band of σ_k^2 and γ_k values (see the dividing lines in Tables 1, 3, and 4) for LN and P when γ_k is positive, and for W and LP, in general. In fact, the cases in which the lower bound = 0 and the upper bound = ∞ are equivalent to their two-parameter counterparts for LN, W, and P, and LN2 for LP (note, however, that LN2 is not the two-parameter probability distribution but only a special case of LP). In two-parameter probability

TABLE 5.—σ_k^2 and γ_k Relations for Two-Parameter Probability Distributions

VARIANCE	SKEWNESS COEFFICIENT (γ_k)		
σ_k^2 (1)	LOGNORMAL (2)	GAMMA (3)	WEIBULL (4)
0.0100	0.3010	0.2000	-0.7131
0.0500	0.6820	0.4472	-0.2722
0.1000	0.9803	0.6325	0.0245
0.2000	1.4311	0.8944	0.4148
0.3000	1.8075	1.0954	0.7020
0.4000	2.1503	1.2649	0.9410
0.5000	2.4749	1.4142	1.1514
0.6000	2.7885	1.5492	1.3428
0.7000	3.0956	1.6733	1.5204
0.8000	3.3988	1.7889	1.6879
0.9000	3.6999	1.8974	1.8472
1.0000	4.0000	2.0000	2.0000
2.0000	7.0711	2.8284	3.3306
3.0000	10.3923	3.4641	4.4924
4.0000	14.0000	4.0000	5.5781
5.0000	17.8885	4.4721	6.6188

distributions, σ_k^2 and γ_k are related as follows:

LN2: $\gamma_k = \sigma_k^3 + 3\sigma_k$ . . . . . (5)

W2: Parameter a and σ_k^2 are related as: $$\sigma_k^2 = \frac{\Gamma\left(1+\frac{2}{a}\right)}{\Gamma^2\left(1+\frac{1}{a}\right)} - 1 \quad \ldots\ldots (6)$$

GA2: Parameter a and γ_k are related by Eq. 2*d*: $\gamma_k = 2\sigma_k$ . . . . . (7)

The numerical values of σ_k^2 and γ_k for two-parameter probability distributions are presented in Table 5. As may be seen from Tables 1, 3, 4, and 5, the

bounds of the three-parameter probability distributions become less desirable as γ_k value deviates more and more from the two-parameter probability distribution value at given σ_k^2 or as σ_k^2 value deviates more and more from the two-parameter probability distribution value at given γ_k. This suggests that, at least from the bounds point of view, a comparison of sample skewness coefficient (CS) with γ_k of two-parameter probability distributions at the sample variance (S_k^2) will indicate which three-parameter probability distribution is more suitable for application. As an example, assume that S_k^2 and CS were calculated as 0.5 and 1.5, respectively, for a sample. Since CS is close to γ_k of GA2, P will have better acceptable bounds than the other three distributions.

When γ_k is negative, the upper bounds of LN, P and LP appear to be generally low (Tables 2 and 4); their suitability should be determined in conjunction with the type and the largest item of data and the negative area of the distribution.

Negative Areas of Distributions

The LN, W, and P enter the region of negative values for several combinations of σ_k^2 and γ_k. In such cases, their application to analyze hydrologic variables

TABLE 6.—Negative Areas for Positively Skewed Lognormal and Pearson Type 3 Distributions, as a percentage

VARIANCE	SKEWNESS COEFFICIENT (γ_k)								
σ_k^2	0.50	1.00	1.50	2.00	3.00	4.00	5.00	7.00	9.00
(1)	(2)	(3)	(4)	(5)	(6)	(7)	(8)	(9)	(10)
				LOGNORMAL DISTRIBUTION					
0.05	0.000								
0.10	0.001								
0.20	0.319	0.005							
0.30	1.762	0.384	0.002						
0.40	3.896	1.747	0.263	0.000					
0.50	6.184	3.770	1.368	0.103					
0.60	8.383	6.009	3.180	0.852					
0.70	10.412	8.223	5.312	2.359	0.000				
0.80	12.254	10.311	7.506	4.313	0.105				
0.90	13.920	12.238	9.630	6.435	0.798				
1.00	15.426	14.000	11.628	8.560	2.163				
2.00	24.984	25.285	24.821	23.672	19.804	14.488	8.376	0.000	
3.00	29.846	30.932	31.373	31.231	29.631	26.824	23.185	14.067	3.766
4.00	32.875	34.391	35.319	35.715	35.313	33.860	31.735	26.096	18.949
5.00	34.986	36.770	38.000	38.722	39.035	38.372	37.113	33.479	28.771
				PEARSON TYPE 3 DISTRIBUTION					
0.10	0.000								
0.20	0.260								
0.30	1.672	0.047							
0.40	3.837	1.060							
0.50	6.170	3.136							
0.60	8.412	5.578	0.354						
0.70	10.476	8.013	2.670						
0.80	12.347	10.298	5.513						
0.90	14.035	12.390	8.303						
1.00	15.558	14.288	10.882						
2.00	25.177	26.091	26.414	25.390					
3.00	30.041	31.816	33.386	34.469	31.644				
4.00	33.064	35.277	37.424	39.347	41.113				
5.00	35.167	37.641	40.111	42.466	45.978	44.235			

(which are positive) may not be meaningful. However, they may still be applied when the variate values in the upper tail of distribution (like flood flows) are of interest if the area of negative lower tail is insignificant. For the three distributions mentioned, the negative areas are presented as percentages of total area (which is unity) in Tables 3, 6, 7.

The negative areas of distributions may be obtained by evaluating the cumulative distribution function, $F(x)$, between the limits $K = 0$, and the lower (negative)

TABLE 7.—Negative Areas for Negatively Skewed Lognormal and Pearson Type 3 Distributions, as a percentage

VARIANCE σ_K^2	SKEWNESS COEFFICIENT (γ_k)								
	-0.50	-1.00	-1.50	-2.00	-3.00	-4.00	-5.00	-7.00	-9.00
(1)	(2)	(3)	(4)	(5)	(6)	(7)	(8)	(9)	(10)
LOGNORMAL DISTRIBUTION									
0.01	0.000	0.000	0.002	0.007	0.027	0.049	0.067	0.091	0.105
0.05	0.028	0.137	0.287	0.425	0.608	0.699	0.742	0.768	0.763
0.10	0.410	0.837	1.177	1.400	1.608	1.662	1.658	1.598	1.526
0.20	2.286	2.981	3.347	3.499	3.508	3.386	3.242	2.982	2.775
0.30	4.565	5.164	5.366	5.358	5.109	4.806	4.531	4.094	3.772
0.40	6.728	7.115	7.119	6.945	6.457	5.995	5.607	5.021	4.603
0.50	8.666	8.822	8.634	8.310	7.611	7.012	6.528	5.816	5.316
0.60	10.380	10.315	9.954	9.497	8.615	7.898	7.332	6.511	5.941
0.70	11.896	11.629	11.115	10.542	9.500	8.680	8.043	7.128	6.498
0.80	13.244	12.797	12.146	11.471	10.290	9.380	8.681	7.682	6.999
0.90	14.449	13.841	13.070	12.304	11.000	10.012	9.257	8.186	7.455
1.00	15.534	14.782	13.904	13.058	11.645	10.586	9.782	8.646	7.872
2.00	22.503	20.891	19.374	18.048	15.976	14.488	13.381	11.837	10.795
3.00	26.199	24.197	22.386	20.837	18.454	16.760	15.505	13.757	12.578
4.00	28.580	26.356	24.377	22.700	20.135	18.319	16.974	15.103	13.839
5.00	30.278	27.912	25.824	24.063	21.379	19.482	18.079	16.124	14.803
PEARSON TYPE 3 DISTRIBUTION									
0.01	0.000	0.000	0.000	0.002	0.013	0.037	0.069	0.134	0.181
0.05	0.023	0.110	0.253	0.420	0.727	0.937	1.055	1.113	1.060
0.10	0.392	0.814	1.221	1.557	1.984	2.151	2.162	1.985	1.740
0.20	2.285	3.069	3.606	3.932	4.137	4.005	3.733	3.114	2.574
0.30	4.598	5.352	5.764	5.926	5.787	5.350	4.832	3.870	3.118
0.40	6.789	7.369	7.592	7.569	7.097	6.395	5.673	4.437	3.521
0.50	8.747	9.116	9.144	8.944	8.175	7.244	6.352	4.890	3.842
0.60	10.475	10.633	10.477	10.117	9.084	7.957	6.919	5.268	4.107
0.70	12.000	11.961	11.638	11.133	9.869	8.570	7.405	5.590	4.334
0.80	13.354	13.135	12.661	12.027	10.556	9.106	7.830	5.870	4.531
0.90	14.564	14.181	13.571	12.821	11.166	9.581	8.206	6.119	4.705
1.00	15.651	15.120	14.387	13.534	11.713	10.006	8.543	6.341	4.861
2.00	22.616	21.161	19.654	18.139	15.260	12.773	10.737	7.793	5.882
3.00	26.297	24.398	22.505	20.652	17.218	14.313	11.966	8.614	6.462
4.00	28.665	26.503	24.376	22.313	18.527	15.351	12.799	9.175	6.861
5.00	30.353	28.016	25.730	23.522	19.489	16.119	13.419	9.596	7.162

bound. Only W has an equation for $F(x)$ in its closed form, given by

$$F(x) = 1 - \exp\left\{-\left[\frac{(x-c)}{b}\right]^a\right\} \quad \ldots\ldots\ldots\ldots\ldots\ldots\ldots\ldots\ldots\ldots (8)$$

In the cases of LN and P numerical integration methods were used. Note that in LN, ln $(x - c)$ is distributed as normal distribution, and in P, $(x - c)$ is distributed as GA2.

Tables 3, 6, and 7 show that at given γ_k, negative areas of the three distributions increase with σ_k^2, indicating thereby that these distributions spread more and more into the negative region as σ_k^2 is increased. When γ_k is positive they enter the negative region when σ_k^2 is greater than the two-parameter probability distribution value.

Quantiles of Probability Distributions

One of the main uses of probability distributions in hydrology is to predict the magnitude of some hydrologic variate associated with some exceedance/nonexceedance probability. These probabilities are more commonly expressed as recurrence intervals or return periods, T, when the data analyzed are annual events. For the value of variate with nonexceedance probability equal to F, T is given by $1/F$ when data in the lower tail of distribution are of concern, i.e., the annual smallest events (ASE) like low flows, and by $1/(1 - F)$ when data in the upper tail of distribution are of concern, i.e., the annual largest events (ALE) like flood flows.

The LN quantiles may be evaluated from the tables of normal distribution by considering that $\ln (x - c)$ or $\ln (c' - x)$ is distributed as normal with mean = a; and standard deviation = b. The quantiles of W may be evaluated by Eq. 8. The tables available in Ref. 4 may be used to evaluate quantiles of interest for P and LP. These tables provide K' values in the equation

$$X_F = \mu_x + \sigma_x K' \qquad (9)$$

in which X_F = Pearson quantile at nonexceedance probability F; and μ_x and σ_x = the mean and standard deviation of P, respectively. The value of K' depends on γ_x and F. Note that $\ln x$ of LP is distributed as P with parameters a, b, and c being common for both P and LP. After determining parameters a, b, and c for LP, calculate the SP of P by Eqs. 3*b*–3*d*, and proceed to use Eq. 9; the LP quantile, then, is given by $\exp (X_F)$. (In Ref. 4, the K' values of this paper were called K values which may be noted by the reader to avoid confusion.)

The K values at selected frequencies were evaluated for the four distributions and presented in Tables 8 and 9, respectively, for the ASE and the ALE. Some of the ASE are negative for LN, W, and P because these distributions enter the negative range of K. The reciprocal of the negative area (Tables 3, 6, and 7) gives for each of these distributions the limiting T (of ASE); when this is exceeded, the quantiles will be negative.

Tables 8 and 9 show that for some combinations of σ_k^2 and γ_k, the K values for a given T are practically equal for some or all of the four distributions. This indicates that under certain circumstances (shown quantitatively for different ranges of σ_k^2 and γ_k in Tables 8 and 9) it will not really matter which probability distribution is chosen if the method of moments is used for estimating parameters. Further, it is observed that the K values of different distributions for a T differ greatly when these distributions have properties which may not be acceptable in hydrologic analysis. As an example, take the case of a sample for which $S_k^2 = 1.0$ and CS = 1.0 and the data are flood flows. Table 9 shows that, for this case, the K value of LP differs greatly from the other three distributions for $T \geqq 100$ yr; the 500-yr value is less by 29%–35%. The LP

TABLE 8.—K Values for Selected Return Periods: Annual Smallest Events

γ_k	σ_k^2	T = 10 YEARS				T = 25 YEARS				T = 50 YEARS				T = 100 YEARS			
		LN	W	P	LP	LN	W	P	LP	LN	W	P	LP	LN	W	P	LP
(1)	(2)	(3)	(4)	(5)	(6)	(7)	(8)	(9)	(10)	(11)	(12)	(13)	(14)	(15)	(16)	(17)	(18)
-1.0	0.05	0.706	0.706	0.700	0.672	0.549	0.583	0.543	0.519	0.434	0.427	0.432	0.427	0.322	0.311	0.324	0.351
	0.20	0.412	0.412	0.401	0.199	0.098	0.167	0.086	0.040	-0.131	-0.146	-0.137	0.010	-0.356	-0.378	-0.352	0.003
	0.50	0.070	0.071	0.064	U	-0.427	-0.317	-0.351	U	-0.789	-0.812	-0.634	U	-1.145	-1.178	-0.899	U
	1.00	-0.316	-0.314	-0.323	U	-1.018	-0.863	-0.910	U	-1.529	-1.563	-1.311	U	-2.033	-2.080	-1.686	U
-0.5	0.05	0.706	0.701	0.704	0.689	0.574	0.598	0.573	0.566	0.483	0.480	0.483	0.491	0.397	0.400	0.399	0.427
	0.20	0.411	0.402	0.408	0.312	0.147	0.197	0.146	0.145	-0.034	-0.040	-0.033	0.080	-0.205	-0.200	-0.201	0.044
	0.50	0.069	0.054	0.064	U	-0.348	-0.270	-0.351	U	-0.635	-0.645	-0.634	U	-0.906	-0.897	-0.899	U
	1.00	-0.317	-0.338	-0.323	U	-0.907	-0.796	-0.910	U	-1.312	-1.327	-1.311	U	-1.695	-1.683	-1.686	U
0.0	0.05	0.729	0.723	0.728	0.728	0.648	0.656	0.650	0.649	0.600	0.622	0.603	0.602	0.558	0.597	0.563	0.562
	0.20	0.457	0.446	0.456	0.451	0.297	0.312	0.299	0.323	0.200	0.244	0.205	0.255	0.116	0.195	0.126	0.204
	0.50	0.142	0.123	0.140	0.146	-0.112	-0.088	-0.108	0.056	-0.265	-0.195	-0.257	0.028	-0.397	-0.273	-0.382	0.014
	1.00	-0.214	-0.240	-0.216	U	-0.572	-0.538	-0.567	U	-0.698	-0.690	-0.777	U	-0.976	-0.800	-0.955	U
1.0	0.05	0.748	0.748	0.748	0.747	0.687	0.707	0.695	0.685	0.652	0.689	0.666	0.649	0.624	0.678	0.645	0.619
	0.20	0.495	0.496	0.496	0.497	0.374	0.414	0.389	0.387	0.305	0.378	0.333	0.328	0.248	0.356	0.290	0.281
	0.50	0.202	0.203	0.203	0.226	0.010	0.074	0.034	0.123	-0.099	0.017	-0.055	0.080	-0.189	-0.019	-0.123	0.053
	1.00	-0.129	-0.126	-0.128	0.028	-0.400	-0.310	-0.366	0.005	-0.554	-0.390	-0.492	0.001	-0.682	-0.440	-0.588	0.000
2.0	0.05	0.784	0.800	0.800	0.782	0.748	0.786	0.786	0.745	0.729	0.781	0.781	0.726	0.714	0.779	0.779	0.712
	0.20	0.568	0.600	0.600	0.562	0.495	0.571	0.571	0.481	0.457	0.562	0.562	0.437	0.428	0.557	0.557	0.402
	0.50	0.316	0.367	0.367	0.329	0.202	0.322	0.322	0.230	0.142	0.307	0.307	0.182	0.096	0.300	0.300	0.146
	1.00	0.033	0.105	0.105	0.127	-0.129	0.041	0.041	0.061	-0.213	0.020	0.020	0.036	-0.278	0.010	0.010	0.022
3.0	0.05	0.811	0.838	0.852	0.782	0.787	0.832	0.851	0.745	0.775	0.831	0.851	0.726	0.767	0.831	0.851	0.712
	0.20	0.622	0.676	0.705	0.402	0.574	0.665	0.702	0.437	0.550	0.662	0.702	0.481	0.533	0.661	0.702	0.562
	0.50	0.403	0.488	0.533	0.146	0.327	0.470	0.529	0.182	0.289	0.466	0.529	0.230	0.262	0.464	0.529	0.329
	1.00	0.155	0.275	0.340	0.022	0.048	0.251	0.334	0.036	-0.005	0.245	0.334	0.061	-0.044	0.242	0.334	0.127
5.0	0.05	0.845	0.881	0.911	0.853	0.832	0.880	0.911	0.848	0.825	0.880	0.911	0.847	0.821	0.880	0.911	0.847
	0.20	0.691	0.763	0.821	0.659	0.663	0.760	0.821	0.621	0.651	0.760	0.821	0.603	0.642	0.760	0.821	0.591
	0.50	0.511	0.625	0.717	0.457	0.467	0.621	0.717	0.386	0.448	0.620	0.717	0.350	0.435	0.620	0.717	0.323
	1.00	0.308	0.469	0.600	0.276	0.247	0.464	0.600	0.198	0.219	0.463	0.600	0.161	0.200	0.463	0.600	0.134

NOTE: U - THE DISTRIBUTION IS U-SHAPED

TABLE 9.—*K* Values for Selected Return Periods: Annual Largest Events

γ_k	σ_k^2	T = 50 YEARS				T = 100 YEARS				T = 200 YEARS				T = 500 YEARS			
		LN	W	P	LP	LN	W	P	LP	LN	W	P	LP	LN	W	P	LP
(1)	(2)	(3)	(4)	(5)	(6)	(7)	(8)	(9)	(10)	(11)	(12)	(13)	(14)	(15)	(16)	(17)	(18)
-1.0	0.05	1.348	1.346	1.334	1.268	1.376	1.376	1.355	1.272	1.400	1.402	1.372	1.273	1.427	1.431	1.389	1.274
	0.20	1.695	1.693	1.667	1.373	1.752	1.753	1.710	1.373	1.800	1.804	1.744	1.373	1.853	1.863	1.778	1.373
	0.50	2.099	2.095	2.055	U	2.189	2.190	2.123	U	2.265	2.271	2.177	U	2.349	2.364	2.231	U
	1.00	2.554	2.549	2.492	U	2.682	2.683	2.588	U	2.789	2.798	2.664	U	2.908	2.929	2.741	U
	3.00	3.692	3.683	3.584	U	3.913	3.915	3.751	U	4.098	4.114	3.882	U	4.305	4.341	4.015	U
	5.00	4.476	4.464	4.336	U	4.760	4.763	4.552	U	5.000	5.020	4.721	U	5.267	5.314	4.892	U
-0.5	0.05	1.400	1.394	1.397	1.364	1.442	1.434	1.437	1.385	1.478	1.469	1.471	1.400	1.521	1.510	1.511	1.414
	0.20	1.800	1.789	1.795	1.569	1.884	1.869	1.874	1.572	1.957	1.939	1.943	1.573	2.042	2.020	2.021	1.573
	0.50	2.265	2.247	2.257	U	2.397	2.373	2.382	U	2.513	2.484	2.491	U	2.647	2.613	2.614	U
	1.00	2.790	2.764	2.777	U	2.976	2.942	2.955	U	3.140	3.099	3.108	U	3.329	3.280	3.283	U
	3.00	4.100	4.054	4.078	U	4.423	4.364	4.386	U	4.706	4.635	4.652	U	5.034	4.950	4.954	U
	5.00	5.002	4.943	4.974	U	5.419	5.343	5.371	U	5.785	5.693	5.714	U	6.208	6.099	6.105	U
0.5	0.05	1.517	1.511	1.517	1.517	1.603	1.586	1.601	1.601	1.684	1.655	1.680	1.681	1.788	1.739	1.780	1.781
	0.20	2.034	2.022	2.033	2.025	2.205	2.172	2.201	2.160	2.369	2.310	2.360	2.278	2.576	2.478	2.560	2.413
	0.50	2.635	2.616	2.634	2.515	2.906	2.853	2.899	2.609	3.164	3.071	3.150	2.669	3.492	3.341	3.466	2.718
	1.00	3.312	3.286	3.311	U	3.695	3.621	3.686	U	4.061	3.929	4.041	U	4.524	4.304	4.487	U
	3.00	5.005	4.959	5.002	U	5.668	5.539	5.652	U	6.301	6.073	6.267	U	7.104	6.723	7.040	U
	5.00	6.170	6.111	6.167	U	7.026	6.860	7.005	U	7.844	7.549	7.800	U	8.880	8.388	8.798	U
1.0	0.05	1.566	1.569	1.568	1.564	1.678	1.669	1.676	1.678	1.790	1.764	1.780	1.792	1.938	1.883	1.914	1.944
	0.20	2.131	2.138	2.137	2.138	2.356	2.338	2.352	2.355	2.580	2.528	2.560	2.565	2.876	2.765	2.828	2.834
	0.50	2.789	2.799	2.798	2.822	3.145	3.116	3.137	3.094	3.499	3.415	3.467	3.329	3.967	3.791	3.891	3.591
	1.00	3.529	3.544	3.542	3.486	4.033	3.992	4.023	3.657	4.534	4.416	4.489	3.764	5.195	4.947	5.088	3.844
	3.00	5.381	5.406	5.403	U	6.254	6.182	6.235	U	7.121	6.917	7.043	U	8.266	7.837	8.081	U
	5.00	6.656	6.688	6.684	U	7.782	7.690	7.759	U	8.902	8.638	8.801	U	10.381	9.826	10.141	U
2.0	0.05	1.625	1.651	1.651	1.620	1.787	1.806	1.806	1.781	1.958	1.961	1.961	1.953	2.200	2.166	2.166	2.197
	0.20	2.250	2.302	2.302	2.234	2.574	2.612	2.612	2.559	2.917	2.922	2.922	2.905	3.400	3.332	3.332	3.403
	0.50	2.976	3.059	3.059	3.004	3.489	3.549	3.549	3.515	4.031	4.039	4.039	4.046	4.795	4.687	4.687	4.781
	1.00	3.794	3.912	3.912	3.973	4.519	4.605	4.605	4.663	5.284	5.298	5.298	5.329	6.368	6.215	6.215	6.165
	3.00	5.840	6.044	6.044	6.550	7.096	7.244	7.244	6.997	8.423	8.445	8.445	7.227	10.297	10.032	10.032	7.368
	5.00	7.248	7.511	7.511	U	8.870	9.061	9.061	U	10.583	10.611	10.611	U	13.002	12.660	12.660	U
3.0	0.05	1.647	1.688	1.705	1.645	1.845	1.891	1.906	1.839	2.064	2.103	2.111	2.053	2.387	2.397	2.387	2.371
	0.20	2.294	2.376	2.410	2.241	2.690	2.782	2.812	2.645	3.127	3.207	3.222	3.075	3.773	3.794	3.775	3.724
	0.50	3.045	3.176	3.229	3.020	3.472	3.818	3.865	3.439	4.364	4.489	4.514	4.327	5.385	5.418	5.388	5.355
	1.00	3.893	4.078	4.152	3.969	4.779	4.985	5.051	4.875	5.757	5.934	5.970	5.855	7.201	7.248	7.205	7.264
	3.00	6.010	6.331	6.459	6.890	7.546	7.902	8.017	8.472	9.239	9.547	9.608	9.899	11.741	11.821	11.747	11.517
	5.00	7.468	7.882	8.048	9.385	9.451	9.911	10.059	10.981	11.637	12.034	12.112	12.040	14.866	14.970	14.875	12.863
5.0	0.05	1.646	1.690	1.738	1.655	1.885	1.956	2.023	1.888	2.164	2.254	2.323	2.157	2.599	2.695	2.738	2.574
	0.20	2.292	2.380	2.476	2.259	2.771	2.913	3.045	2.700	3.328	3.509	3.646	3.216	4.198	4.390	4.475	4.035
	0.50	3.043	3.182	3.334	2.982	3.800	4.024	4.234	3.684	4.680	4.967	5.184	4.509	6.057	6.360	6.495	5.823
	1.00	3.889	4.085	4.300	3.851	4.959	5.277	5.573	4.890	6.205	6.610	6.916	6.105	8.152	8.580	8.771	8.022
	3.00	6.003	6.344	6.716	6.306	7.858	8.408	8.921	8.395	10.015	10.716	11.248	10.748	13.387	14.129	14.460	14.230
	5.00	7.459	7.899	8.379	8.255	9.853	10.564	11.226	11.240	12.638	13.544	14.229	14.434	16.992	17.950	18.377	18.798

NOTE: U - THE DISTRIBUTION IS U-SHAPED

is bounded upwards, and the bound value is $K = 3.93$ (Table 4). The LN, W, and P enter the negative range of K and the lower bounds are $K = -2.104$, -0.530, and -1.00, respectively, and the negative areas are 14%, 14.9%, and 14.3%, respectively. These properties, in general, may be unacceptable for analyzing hydrologic samples. In the case of ALE, W quantiles are, in general, low compared to LN or P when $\gamma_k < 2$.

The results presented in Tables 1–9 were based on a theoretical evaluation of distributions. Some combinations of σ_k^2 and γ_k presented in these tables, like a low σ_k^2 and a high γ_k or vice versa, may rarely or never be found in practical examples of hydrology. Fortunately, it is for these combinations of σ_k^2 and γ_k that the distribtuions have properties not acceptable in hydrologic frequency.

Practical Applications

Different results presented in the foregoing sections show that the skewness coefficient of the two-parameter counterpart of a three-parameter probability distribution (LN2 in the case of LP) can serve as an index to indicate the behavior of the three-parameter probability distribution at given SP. This CS will be denoted as γ_{2P} henceforth. The value of γ_{2P} is evaluated at sample variance, S_k^2. When CS is positive: (1) The LN and P will enter the negative region of K (or X), if CS $< \gamma_{2P}$; (2) the LP has an upper bound, if CS $< \gamma_{2P}$; and (3) the lower bounds of LN, P, and LP are greater than zero, if CS $> \gamma_{2P}$. The W enters the negative region of K if CS $< \gamma_{2P}$, and the lower bound is greater than zero if CS $> \gamma_{2P}$ for both positive and negative CS. When CS is negative, the LN, P, and LP are bounded upwards. Further, the more the CS deviates from γ_{2P}, the more undesirable the properties of the three-parameter probability distributions become for hydrologic analysis. Thus, in general, for a given hydrologic sample, the three-parameter probability distributions, which has its γ_{2P} closer to CS, will have desirable or more appealing properties than others. However, as mentioned earlier, for certain values of SP, some of the quantiles (for a given T) of different distributions may not differ greatly and the choice of a distribution is only of academic interest. Applications of these concepts are illustrated through the following examples.

Annual flood flow data from two gaging stations (St. Johns River near DeLand, Fla., and Cedar River at Cedar Rapids, Iowa) were selected for analysis. The data were first converted into dimensionless variates, K_i, by the formula $K_i = X_i/\bar{X}$. The unbiased estimates of sample variance and skewness coefficients (S_k^2 and CS_u) are calculated usually by the following formulas:

$$S_k^2 = \frac{1}{(n-1)} \sum_{i=1}^{n} (K_i - \bar{K})^2 \quad \ldots \quad (10)$$

$$CS_u = \frac{n}{S_k^3 (n-1)(n-2)} \sum_{i=1}^{n} (K_i - \bar{K})^3 \quad \ldots \quad (11)$$

in which $\bar{K} = 1.0$; and n = the sample size.

However, Monte Carlo experiments conducted by Wallis, et al. (9) indicated that Eq. 11 does not sufficiently correct for the sample bias in the cases of

LN, W, and P. Based on the results of Ref. 9, Bobee and Robitaille (3) proposed the following formulas for the unbiased estimates of skewness for LN, W, and P distributions:

1. LN Distribution:

$$CS_{LN} = \overline{CS}\left[\left(1.01 + \frac{7.01}{n} + \frac{14.66}{n^2}\right) + \left(\frac{1.69}{n} + \frac{74.66}{n^2}\right)\overline{CS}^2\right] \quad \ldots\ldots (12)$$

2. W Distribution:

$$CS_W = \overline{CS}\left[\left(1.01 + \frac{5.05}{n} + \frac{20.13}{n^2}\right) + \left(\frac{0.69}{n} + \frac{27.15}{n^2}\right)\overline{CS}^2\right] \quad \ldots\ldots (13)$$

3. P Distribution:

$$CS_P = \overline{CS}\left[\left(1 + \frac{6.51}{n} + \frac{20.20}{n^2}\right) + \left(\frac{1.48}{n} + \frac{6.77}{n^2}\right)\overline{CS}^2\right] \quad \ldots\ldots\ldots (14)$$

In the aforementioned, $\overline{CS}$ = mean of the distribution of the skewness coefficient for a sample of size n. Normally only one sample of size n is available and $\overline{CS}$ is substituted by the biased estimate of skewness coefficient given by

$$CS_B = \frac{\frac{1}{n}\sum_{i=1}^{n}(K_i - \bar{K})^3}{\left[\frac{1}{n}\sum_{i=1}^{n}(K_i - \bar{K})^2\right]^{1.5}} \quad \ldots\ldots\ldots\ldots\ldots\ldots\ldots\ldots (15)$$

For the LP also, Eq. 11 is inadequate to correct for the sample bias (8). The writer has evolved the method of mixed moments (MXM1) for LP (8), in which the skewness coefficient of LP (CS_{LP}) is determined on the basis of sample logarithmic mean, $\bar{Y}$, instead of using CS_u. The value of $\bar{Y}$ is calculated by

$$\bar{Y} = \frac{1}{n}\sum_{i=1}^{n} \ln K_i \quad \ldots\ldots\ldots\ldots\ldots\ldots\ldots\ldots\ldots\ldots (16)$$

Since $\bar{Y}$ is an unbiased estimate, CS_{LP} may be regarded as unbiased or less biased than CS_u. The LN, W, P, and LP are fit to the two samples (by the method of moments), first by using the statistics given by Eqs. 10–11, and then by replacing CS_u by the new unbiased estimates, i.e., CS_{LN} in the case of LN, CS_W in the case of W, etc. Table 10 presents the estimates of parameters a, b, and c, and the K values for return periods, T = 50 yr, 100 yr, 200 yr, and 500 yr for the four distributions. For each distribution, the results obtained by using the new unbiased estimate of skewness are shown in parentheses. An analysis of the results is as follows.

Sample No. 1: St. Johns River near DeLand, Fla.—The data are as follows: Sample size = 45 (1934–1978); $\bar{X}$ = 8,126 cfs (230.13 m^3/s); S_k^2 = 0.18133; CS_u = 0.9041; CS_{LN} = 1.0745; CS_W = 1.0083; CS_P = 1.0330; and CS_{LP} = 1.3591. Skewness coefficients γ_{2P}, of LN2, W2, and GA2 (at variance = 0.18133)

are: 1.3547, 0.3526 and 0.8517, respectively (From Eqs. 5–7, substituting $\sigma_K^2 = S_K^2$).

Case 1.—Results obtained by using CS_u for all distributions: In this case, $CS < \gamma_{2P}$ for LN and LP and $CS > \gamma_{2P}$ for W and P. Therefore, LN will enter the negative range of K, LP will be bounded upwards, and W and P will have a lower bound greater than zero. However, since CS is close to γ_{2P} in the case of P, P will have better acceptable bounds. The LP has an upper bound, $K = \exp(c) = 11.450$. The LN, W, and P have lower bounds, $K = -0.453$, 0.313, and 0.058, respectively. The negative area of LN is 0.0045%, which is very negligible. For $T = 50$ yr–500 yr, the quantiles of P and LP are practically equal, and LN values differ from P and LP by 0.3%–1.7% (Table 10). Thus, although P has better attributes, LP also gives equivalent results.

TABLE 10.—Results of Illustrative Examples

Distribution (1)	Estimates of Parameters			K Values for Return Period			
	a (2)	b (3)	c (4)	50 yr (5)	100 yr (6)	200 yr (7)	500 yr (8)
(*a*) St. Johns River near Deland, Fla.							
Lognormal	0.333	0.287	−0.453	2.061	2.266	2.468	2.732
	(0.156)	(0.335)	(−0.236)	(2.089)	(2.311)	(2.533)	(2.828)
Weibull	1.658	0.769	0.313	2.063	2.244	2.415	2.627
	(1.556)	(0.722)	(0.351)	(2.085)	(2.277)	(2.458)	(2.685)
Pearson	5.195	4.893	0.058	2.065	2.260	2.450	2.692
	(4.547)	(3.749)	(0.176)	(2.088)	(2.296)	(2.498)	(2.757)
Log Pearson	−13.141	33.240	2.438	2.067	2.262	2.449	2.687
	(1620.)	(4.37×10^5)	(−269.7)	(2.128)	(2.379)	(2.634)	(2.981)
(*b*) Cedar River at Cedar Rapids, Iowa							
Lognormal	0.837	0.262	−1.389	2.563	2.855	3.142	3.515
	(0.662)	(0.303)	(−1.030)	(2.581)	(2.892)	(3.200)	(3.605)
Weibull	1.753	1.214	−0.081	2.561	2.819	3.060	3.359
	(1.639)	(1.123)	(−0.005)	(2.577)	(2.847)	(3.102)	(3.419)
Pearson	3.844	5.982	−0.556	2.566	2.847	3.118	3.463
	(3.397)	(4.565)	(−0.344)	(2.581)	(2.875)	(3.159)	(3.524)
Log Pearson	−2.923	4.963	1.460	2.570	2.798	2.795	3.217
	(−4.519)	(9.988)	(1.997)	(2.655)	(2.958)	(3.241)	(3.588)

Case 2.—Results obtained by using the new unbiased estimates of skewness for each distribution: In this case, $CS_{LN} < \gamma_{2P}$ but CS_W, CS_P, and CS_{LP} are greater than γ_{2P}. Therefore, LN will enter the negative range of K and W, P, and LP will have a lower bound greater than zero. However, CS_{LP} is practically equal to γ_{2P} and thus LP is clearly the "best" choice in this case. With use of the new unbiased estimates of skewness, the statistical attributes of LN and LP improved, but those of W and P became less attractive. The LN, W, and P have lower bounds, $K = -0.236$, 0.351 and 0.176, respectively, and LP has a lower bound, $K = \exp(c) \simeq 0$. The negative area of LN = 0.0001%.

Sample No. 2: Cedar River at Cedar Rapids, Iowa.—The data are as follows: Sample size = 70 (1903–1972). The writer had an opportunity to work on this

sample in a different context in the past, but did not get a chance to update data for the present study. $\bar{X}$ = 27,558 cfs (771.62 m^3/s); S_k^2 = 0.3957; CS = 0.8595; CS_{LN} = 0.9595; CS_W = 0.9227; CS_P = 0.9360; and CS_{LP} = 1.1405. Skewness coefficients, γ_{2P}, of LN2, W2, and GA2 (at variance = 0.3957) are: 2.166, 0.952, and 1.273, respectively.

Case 1.—Results obtained by using CS_u for all distributions: In this case $CS < \gamma_{2P}$ for the four distributions. As a result, LN, W, and P will enter the negative range of K, and LP will be bounded upwards. Since CS is closer to γ_{2P} in the case of W, W will have better acceptable bounds. The lower bounds of LN, W, and P are $K = -1.387$, -0.081, and -0.556, respectively. The upper bound of LP is $K = \exp(c) = 4.306$. The effect of relatively lower upper bound of LP is reflected by its low K values compared to the other three distributions when $T \geq 100$ yr (Table 10). The negative areas of LN, W, and P are 2.62%, 0.86%, and 2.25%, respectively. Although W has better bounds and a lower negative area, its quantiles for ALE are inherently low compared to LN and P. In this case, the choice of a distribution makes a difference in the final results for $T \geq 100$ yr. The LP quantiles differ from LN by 2%–8.5% as T is increased from 100 yr–500 yr. However, if LP, because of its low upper bound, and W, owing to its inherently low quantiles are considered unsuitable in this particular instance, the next best choice is P, but LN also gives comparative results.

Case 2.—Results obtained by using the new unbiased estimates of skewness for each distribution: In this case also, the estimates of skewness are less than γ_{2P} for the four distributions, but are greater than CS_u. As a result, the attributes of the distributions are improved compared to Case 1. The lower bounds of LN, W, and P are $K = -1.030$, -0.005, and -0.344, respectively. The upper bound of LP is $K = \exp(c) = 7.367$. The negative areas of LN, W, and P are 1.83%, 0.014%, and 1.26%, respectively. Again, W will have the best attributes, but its quantiles are inherently low (Table 10). The next best choice is P, but LN and LP also give comparative results (maximum error is 3% for T = 50 yr–500 yr).

The foregoing examples show that use of the new unbiased estimates of skewness may not always improve the statistical attributes of a distribution. This may be because such distributions are not suitable for analyzing a particular hydrologic sample. Nevertheless, in view of the new knowledge regarding the behavior of sample skewness, use of the new unbiased estimates of skewness is preferable in place of the conventional CS_u.

In two instances (Case 1 of Sample 1 and Case 2 of Sample 2), the LP has seemingly low upper bounds (K = 11.450 and 7.367, respectively), but its upper quantiles compare well with the best distribution identified by the criteria of this paper. This suggests an area for further investigation, i.e., whether LP can emerge as the single most practical distribution for application, which may always give results comparable to the best alternative distribution (especially when the MXM1 method is used for parameter estimation). Note that when LP has an upper bound, its lower tail starts at the zero value which is a condition most suitable for analyzing the ASE.

A computer program is available to fit data to the four distributions. The program evaluates different results presented in the foregoing examples including quantiles for F = 0.005–0.999.

Summary and Conclusions

The lognormal, Weibull, Pearson type 3, and log Pearson type 3, each a three-parameter distribution, were evaluated in a generalized fashion in terms of the dimensionless variate K ($K = X/\mu_x$) which has a population mean of unity. The bounds of the distributions, areas of the portion of distributions in the negative region of variate when they enter such regions, and the differences in important quantiles among the four distributions are presented on the basis of σ_k^2 and γ_k. Since $\sigma_k^2 = \eta_x^2$ and $\gamma_k = \gamma_x$, this study allows an understanding of the differences existing among distributions and their properties on the basis of statistical parameters (mean, variance, and skewness coefficient) of a data sample. The conclusions from this study are as follows:

1. The four distributions studied become less applicable for hydrologic frequency analysis as they deviate more and more from their two-parameter counterparts (LN2 in the case of LP).
   a. At given σ_k^2 the lower bound is negative when γ_k is less than the two-parameter probability distribution value and positive when γ_k is greater than the two-parameter probability distribution value for LN and P when γ_k is positive, and for W in general. The magnitudes of the lower bound (positive or negative), and the negative area of the three distributions increase with the deviation of γ_k from the two-parameter probability distribution value.
   b. At given γ_k, the lower bound is negative when σ_k^2 is greater than the two-parameter probability distribution value and positive when σ_k^2 is less than the two-parameter probability distribution value for LN and P when γ_k is positive, and for W in general. The magnitudes of the lower bound (positive or negative) and the negative area of the three distributions increase with the deviation of σ_k^2 from the two-parameter probability distribution value.
   c. At given σ_k^2, the LP is bounded upwards when γ_k is less than that of LN2 and the bound value decreases with γ_k. When γ_k is greater than that of LN2, LP is bounded in the lower tail and the bound value increases with γ_k.
   d. At given positive γ_k, LP is bounded upwards when σ_k^2 is greater than that of LN2 and the bound value decreases with the increase of σ_k^2. When σ_k^2 is less than that of LN2, LP is bounded in the lower tail and the bound value increases with the decrease of σ_k^2.
   e. When γ_k is negative, LN, P, and LP are bounded upwards and the bound values appear generally low.
2. A comparison of CS with γ_k of two-parameter probability distributions at S_k^2 will serve as a rule of thumb to determine which three-parameter probability distribution has better properties for application in hydrology; in general, the three-parameter probability distribution whose two-parameter counterpart (LN2 in case LP) has its γ_k close to CS will have better applicable properties.
3. For some combinations of σ_k^2 and γ_k the upper quantiles of some or all of the four distributions are practically equal for a given T. Thus, the choice of a distribution is not critical under those conditions for flood flow frequency analysis.
4. For some samples, the LP may have a seemingly low upper bound, but its upper quantiles may compare well with the best alternative distribution identifiable by the criteria of this paper.

Acknowledgment

This study was conducted as a part of a wider investigation of frequency distributions for use in different projects of the St. Johns River Water Management District, Fla. Permission to offer this paper for publication was granted by the Governing Board of the District.

Appendix I.—References

1. Aitchison, J., and Brown, J. A. C., *The Log Normal Distribution*, Cambridge University Press, London, England, 1957.
2. Bobee, B., "The Log Pearson Type 3 Distribution and Its Application in Hydrology," *Water Resources Research*, Vol. 11, No. 5, Oct., 1975, pp. 681–689.
3. Bobee, B., and Robitaille, R., "Correction of Bias in the Estimation of the Coefficient of Skewness," *Water Resources Research*, Vol. 11, No. 6, Dec., 1975, pp. 851–854.
4. "Guidelines for Determining Flood Flow Frequency," *Bulletin No. 17A*, Water Resources Council, Washington, D.C., 1977.
5. Gumbel, E. J., *Statistics of Extremes*, Columbia University Press, New York, N.Y., 1958, pp. 272–302.
6. Landwehr, J. M., Matalas, N. C., and Wallis, J. R., "Some Comparison of Flood Statistics in Real and Log Space," *Water Resources Research*, Vol. 14, No. 5, Oct., 1978, pp. 902–920.
7. Rao, D. V., "Log Pearson Type 3 Distribution: A Generalized Evaluation," *Journal of the Hydraulics Division*, ASCE, Vol. 106, No. HY5, Proc. Paper 15391, May, 1980, pp. 853–872.
8. Rao, D. V., "Log Pearson Type 3 Distribution: Method of Mixed Moments," *Journal of the Hydraulics Division*, ASCE, Vol. 106, No. HY6, Proc. Paper 15477, June, 1980, pp. 999–1019.
9. Wallis, J. R., Matalas, N. C., and Slack, J. R., "Just a Moment!," *Water Resources Research*, Vol. 10, No. 2, Apr., 1974, pp. 211–219.
10. Weibull, W., "Statistical Distribution Function of Wide Application," *Journal of Applied Mechanics*, ASME, Vol. 18, 1951, p. 293.

Appendix II.—Notation

The following symbols are used in this paper:

a, b, c, c' = parameters of distributions;
CS = sample skewness coefficient;
CV = sample coefficient of variation;
F = nonexceedance probability;
$F(x)$ = cumulative distribution function;
$f(x)$ = probability density function;
GA2 = two-parameter gamma distribution;
K, k = dimensionless variate;
$\bar{K}$ = sample mean of K;
K' = constant;
LN = three-parameter lognormal distribution;
LN2 = two-parameter lognormal distribution;
LP = log Pearson type 3 distribution;
MXM1 = method of mixed moments—*I*;
n = sample size;
P = Pearson type 3 distribution;

S^2 = sample variance;
T = return period;
W = three-parameter Weibull distribution;
W2 = two-parameter Weibull distribution;
X, x = random variable;
$\bar{X}$ = sample mean of X;
Γ = gamma function;
γ = population skewness coefficient;
η = population coefficient of variation;
μ = population mean;
σ = population standard deviation; and
σ^2 = population variance.

Subscripts

B = biased estimate;
i = ith value (for variates);
2P = two-parameter probability distribution; and
u = unbiased estimate (conventional).

JOURNAL OF THE
HYDRAULICS DIVISION

TECHNICAL NOTES

Note.—Discussion open until August 1, 1981. To extend the closing date one month, a written request must be filed with the Manager of Technical and Professional Publications, ASCE. This paper is part of the Journal of the Hydraulics Division, Proceedings of the American Society of Civil Engineers, ©ASCE, Vol. 107, No. HY3, March, 1981.

Technical Notes

To provide a place within ASCE for publication of technical ideas that have not advanced, as yet, to the point where they warrant publication as a Proceedings paper in a *Journal*, the publication of Technical Notes was authorized by the Board of Direction on October 16–18, 1967, under the following guidelines:

1. An original manuscript and two copies are to be submitted to the Manager of Technical and Professional Publications, ASCE, 345 East 47th Street, New York, N.Y., 10017, along with a request by the author that it be considered as a Technical Note.
2. The two copies will be sent to an appropriate Technical Division or Council for review.
3. If the Division or Council approves the contribution for publication, it shall be returned to Society Headquarters with appropriate comments.
4. The technical publications staff will prepare the material for use in the earliest possible issue of the *Journal*, after proper coordination with the author.
5. Each Technical Note is not to exceed 4 pages in the *Journal*. As an approximation, each full manuscript page of text, tables, or figures is the equivalent of one-half a *Journal* page.
6. The Technical Notes will be grouped in a special section of each *Journal*.
7. Information retrieval abstracts and key words will be unnecessary for Technical Notes.
8. The final date on which a Discussion should reach the Society is given as a footnote with each Technical Note.
9. Technical Notes will not be included in *Transactions*.
10. Technical Notes will be included in ASCE's annual and cumulative subject and author indexes.

The manuscripts for Technical Notes must meet the following requirements:

1. Titles must have a length not exceeding 50 characters and spaces.
2. The author's full name, Society membership grade, and a footnote reference stating present employment must appear on the first page of the manuscript. Authors need not be Society members.
3. The manuscript is to be submitted as an original copy (with two duplicates) that is typed double-spaced on one side of 8-1/2-in. (220-mm) by 11-in. (280-mm) white bond paper.
4. All mathematics must be typewritten and special symbols must be properly identified. The letter symbols used must be defined where they first appear, in figures or text, and arranged alphabetically in an Appendix.—Notation.
5. Standard definitions and symbols must be used. Reference must be made to the lists published by the American National Standards Institute and to the *Authors' Guide to the Publications of ASCE*.
6. Tables must be typed double-spaced (an original ribbon copy and two duplicate copies) on one side of 8-1/2-in. (220-mm) by 11-in. (280-mm) paper. An explanation of each table must appear in the text.
7. Figures must be drawn in black ink on one side of 8-1/2-in. (220-mm) by 11-in. (280-mm) paper. Because figures will be reproduced with a width of between 3 in. (76 mm) to 4-1/2 in. (110 mm), the lettering must be large enough to be legible at this width. Photographs must be submitted as glossy prints. Explanations and descriptions must be made within the text for each figure.
8. References cited in text must be typed at the end of the Technical Note in alphabetical order in an Appendix.—References.
9. Dual units, i.e., U.S. Customary followed by SI (International System) units in parentheses, should be used throughout the paper.

Comparison of Two Surface Heat Exchange Models

By Richard D. Noble[1]

Introduction

Mathematical modeling of water temperature has received considerable attention over the years (1,2,3,5,9,11,12,13). It has been observed that it is not possible to develop an analytic solution for the water temperature in many cases due to the nonlinearity of some terms in the expression for the net heat flux at the air-water interface. One example is the T^4 dependence shown by the back radiation term. Also, the incoming short-wave radiation term is subject to rapid and unpredictable changes due to cloud cover and other atmospheric changes. Therefore, methods have been developed to linearize the net heat flux expression to simplify the calculations.

The concept of the equilibrium temperature was developed to linearize the net heat flux expression. The equilibrium temperature was defined as the temperature which the water surface would attain when the net heat flux became zero. The net heat flux was then expressed as the product of a surface exchange coefficient and the difference between the actual water surface temperature and the equilibrium temperature. Gameson, Gibbs, and Barrett (7) used this concept to model the temperature in a heated river. They used a simplified analysis with an empirical expression relating air temperature and equilibrium temperature. Velz and Gannon (14) applied this method to a heat balance for ponds and streams. Edinger, Duttweiler, and Geyer (5) used the concept of equilibrium temperature in a detailed linearization of the net heat flux term. Dingman (4) developed a simplified method for computing the equilibrium temperature by developing curves of heat exchange rate (excluding shortwave radiation) versus the difference between the water surface temperature and the air temperature. The slope and intercept of these curves could then be used to predict the equilibrium temperature.

The equilibrium temperature method has been applied to predictive models for water temperature. Edinger (6) used this concept to model vertical temperature structure in static systems. Brocard and Harleman (1) developed a one-dimensional model for water temperatures in rivers in unsteady flow.

[1]Asst. Prof., Chemical Engrg. Dept., Box 3295, Univ. Station, Univ. of Wyoming, Laramie, Wyo. 82071.

Note.—Discussion open until August 1, 1981. To extend the closing date one month, a written request must be filed with the Manager of Technical and Professional Publications, ASCE. Manuscript was submitted for review for possible publication on May 8, 1980. This paper is part of the Journal of the Hydraulics Division, Proceedings of the American Society of Civil Engineers, ©ASCE, Vol. 107, No. HY3, March, 1981. ISSN 0044-796X/81/0003-0361/$01.00.

Yotsukura, Jackman, and Faust (15) developed a linearization method for the net heat flux term by expanding each term in a Taylor series about an undefined base temperature and neglecting higher than first-order terms. This allows one to write the net heat flux as the sum of a zero order and first order term with respect to the water surface temperature.

Paily, Macagno, and Kennedy (12) used the aforementioned linearization method to develop an analytical solution to the dissipation of excess heat from rivers under subfreezing conditions. The writer (10) developed an analytic solution to river water temperature based on the aforementioned linear approximation of the net heat flux.

The objective of this paper is to show that a relationship can be developed which relates the parameters in the equilibrium temperature model to the parameters in the Taylor Series expansion model. This allows one to use either method for any model considered by interchanging the parameters as shown. It will be further shown that the equilibrium temperature model is a special case of the Taylor Series expansion model.

It should be noted that either linearization scheme mentioned is an approximation and strictly valid only during steady meteorological conditions.

Description of Net Heat Flux

The net heat exchange at an air-water interface H can be expressed as

$$H = H_r - H_s - H_L - H_c - H_{ac} \quad \ldots\ldots (1)$$

in which H_r = sum of the short-wave and long-wave atmospheric radiation absorbed by the water; H_s = radiation from the water surface; H_L = heat transfer due to the latent heat of vaporization (evaporation); H_c = heat transfer due to conduction at the air-water interface; and H_{ac} = sensible heat transfer due to the advection of water through the air-water interface.

The parameter H_{ac} is normally very small and is neglected in practice. The expression for H then becomes

$$H = H_r - H_s - H_L - H_c \quad \ldots\ldots (2)$$

$$H_s = \epsilon\sigma(T + \Delta)^4 \quad \ldots\ldots (3)$$

$$H_L = \rho u \lambda (e_T - e_a) \quad \ldots\ldots (4)$$

$$H_c = C_1 \rho u \lambda (T - T_{\text{air}}) \quad \ldots\ldots (5)$$

Substituting Eqs. 3, 4, and 5 into Eq. 2, one obtains

$$H = H_r - \epsilon\sigma(T + \Delta)^4 - \rho u \lambda (e_T - e_a) - C_1 \rho u \lambda (T - T_{\text{air}}) \quad \ldots\ldots (6)$$

Description of Taylor Series Expansion

Applying the method of Yotsukura, Jackman, and Faust (15) to Eq. 6, one expands H in a Taylor series about an undefined temperature T_b and neglects higher than first order terms:

$$H \approx H_b + \left(\frac{\partial H}{\partial T}\right)_b (T - T_b) \quad \ldots\ldots (7)$$

in which H_b = net heat exchange term evaluated at T_b and

$$H \approx H_r - \epsilon\sigma(T_b + \Delta)^3 - \rho u\lambda(e_{T_b} - e_a) - C_1\rho u\lambda(T_b - T_{air})$$
$$- \left[4\epsilon\sigma(T_b + \Delta)^3 + \rho u\lambda\left(\left(\frac{\partial e_T}{\partial T}\right)_b + C_1\right)\right](T - T_b) \quad \ldots\ldots\ldots\ldots (8)$$

$$\text{Let} \quad \beta_b = \left\{H_r - \epsilon\sigma(T_b + \Delta)^4 - \rho u\lambda\left[(e_{T_b} - e_a) + C_1(T_b - T_{air})\right]\right.$$
$$\left. + 4\epsilon\sigma T_b(T_b + \Delta)^3 + \rho u\lambda T_b\left(\left(\frac{\partial e_T}{\partial T}\right)_b + C_1\right)\right\} \quad \ldots\ldots\ldots\ldots (9)$$

$$\alpha_b = \left[4\epsilon\sigma(T_b + \Delta)^3 + \rho u\lambda\left(\left(\frac{\partial e_T}{\partial T}\right)_b + C_1\right)\right] \quad \ldots\ldots\ldots\ldots (10)$$

Substituting Eqs. 9 and 10 into Eq. 8

$$H \approx \beta_b - \alpha_b T \quad \ldots\ldots\ldots\ldots (11)$$

note that the values of β_b and α_b depend on the value of T_b chosen.

Description of Equilibrium Temperature Model

Edinger, Duttweiler, and Geyer (5) developed a linearization of Eq. 6 using the concept of equilibrium temperature. Initially, a binomial expansion of H_b was calculated. All terms higher than second order were neglected:

$$H_b = \epsilon\sigma(T + \Delta)^4 \approx \epsilon\sigma\Delta^4\left[1 + 4\left(\frac{T}{\Delta}\right) + 6\left(\frac{T}{\Delta}\right)^2\right] \quad \ldots\ldots\ldots\ldots (12)$$

Next, the rate of change of saturation water vapor pressure with respect to water temperature is approximated as

$$\frac{de_T}{dT} \approx \frac{e_T - e_a}{T - T_d} = \gamma \quad \ldots\ldots\ldots\ldots (13)$$

It should be noted that this is not a good assumption. Equation 13 can be rearranged to yield

$$(e_T - e_a) = \gamma(T - T_d) \quad \ldots\ldots\ldots\ldots (14)$$

Substituting Eqs. 12 and 14 into Eq. 6

$$H \approx H_r - \epsilon\sigma\Delta^4 - 4\epsilon\sigma\Delta^3 T - 6\epsilon\sigma\Delta^2 T^2 - \rho u\lambda\left[\gamma(T - T_d) + C_1(T - T_{air})\right] \quad (15)$$

The equilibrium temperature T_e is defined as the surface water temperature which would be attained when $H = 0$:

$$0 \approx H_r - \epsilon\sigma\Delta^4 - 4\epsilon\sigma\Delta^3 T_e - 6\epsilon\sigma\Delta^2 T_e^2 - \rho u\lambda\left[\gamma(T_e - T_d) + C_1(T_e - T_{air})\right] \quad (16)$$

Subtracting Eq. 16 from Eq. 15

$$H = 4\epsilon\sigma\Delta^3(T_e - T) + 6\epsilon\sigma\Delta^2(T_e^2 - T^2) + \rho u\lambda(\gamma + C_1)(T_e - T) \quad \ldots\ldots (17)$$

Neglecting the nonlinear terms

$$H = [4\epsilon\sigma\Delta^3 + \rho u\lambda(\gamma + C_1)](T_e - T) \quad (18)$$

Let $K = [4\epsilon\sigma\Delta^3 + \rho u\lambda(\gamma + C_1)]$ (19)

$$H = K(T_e - T) \quad (20)$$

Neglecting the second order term in Eq. 16, one can solve for T_e:

$$T_e = \frac{H_r - \epsilon\sigma\Delta^4 + \rho u\lambda(\gamma T_d + C_1 T_{air})}{4\epsilon\sigma\Delta^3 + \rho u\lambda(\gamma + C_1)} \quad (21)$$

Comparison of Two Models

First, note from Eq. 13 that it is assumed that

$$\gamma \approx \left(\frac{\partial e_T}{\partial_T}\right)_b$$

so they can be used interchangeably. Next, calculate α_b and β_b using Eqs. 9 and 10 and setting $T_b = 0$:

$$\beta_o = \{H_r - \epsilon\sigma\Delta^4 - \rho u\lambda[(e_o - e_a) - C_1 T_{air}]\} \quad (22)$$

$$\alpha_o = [4\epsilon\sigma\Delta^3 + \rho u\lambda(\gamma + C_1)] \quad (23)$$

Returning to Eq. 14 evaluated at $T_b = 0$

$$(e_o - e_a) = -\gamma T_d$$

Substituting the aforementioned into Eq. 22

$$\beta_o = [H_r - \epsilon\sigma\Delta^4 + \rho u\lambda(\gamma T_d + C_1 T_{air})] \quad (24)$$

Comparing Eqs. 20 and 23

$$K = \alpha_o \quad (25)$$

Comparing Eqs. 21 and 24:

$$T_e = \frac{\beta_o}{\alpha_o} \quad (26)$$

Therefore, the parameters in the equilibrium temperature model can be evaluated in terms of the Taylor Series expansion model by setting $T_b = 0$.

Therefore, the choice of $T_b = 0$ is usually not an optimum one. Use of the Taylor Series expansion model with a better choice of T_b, e.g., the natural temperature of the water unaffected by artificial heat, as suggested by Yotsukura et al. (15) should yield better results.

As an example for comparison, let us use the following situation, $H_r = 279$ (W/m^2); $T_{air} = 10°$ C; wet-bulb air temperature = 5° C; $\lambda = 2.448$ kJ/g; $\rho = 998.23$ kg/m^3; $P = 1$ atm; $u = 7.157 \times 10^{-9}$ m/s·mb (corresponding to a wind speed of 15 km/h); water surface temperature = $T_b = 20°$ C; $C_1 = 0.61$ mb/K; and $\gamma = 1.456$ mb/K. Using Eq. 6, $H = -549$ W/m^2. From Eqs. 10 and 11, $\beta_b = 285$ W/m^2 and $\alpha_b = 41.7$ W/m^2 in the Taylor Series expansion method. In addition, $K = 40.6$ W/m^2·K and $T_e = 5.09°$ C when using Eqs. 20 and 23 for the equilibrium temperature method. As expected,

the Taylor Series expansion model (Eq. 11) predicts that $H = -549$ W/m^2 at $T = 20°$ C. The equilibrium temperature model (Eq. 20) predicts $H = -605$ W/m^2, an error of 9.3%.

It should be noted that Eqs. 11 and 20 can be equated and a general relationship developed between the parameters in the two models.

Conclusions

Two methods for linearizing the net heat flux at an air-water interface were considered. The derivation of the linearized heat flux was developed for each method and compared. It was determined that the parameters in each method could be simply related when T_b was set to zero in the Taylor Series expansion method.

Since setting T_b equal to zero is normally too low a value, it is recommended that the Taylor Series expansion method be used with a better choice of T_b, such as the natural water temperature.

Appendix.—References

1. Brocard, D. N., and Harleman, D. F., "One-Dimensional Temperature Predictions in Unsteady Flows," *Journal of the Hydraulics Division,* ASCE, Vol. 102, No. HY3, Proc. Paper 11982, Mar., 1976, pp. 227–240.
2. Brown, G. W., "Predicting Temperatures of Small Streams," *Water Resources Research,* Vol. 5, No. 1, Feb., 1969, pp. 68–75.
3. Chen, C., "Fate of Thermally Polluted Surface Water in Rivers," *Journal of the Sanitary Engineering Division,* ASCE, Vol. 97, No. SA3, Proc. Paper 8197, June, 1971, pp. 311–331.
4. Dingman, S. L., "Equilibrium Temperatures of Water Surfaces as Related to Air Temperature and Solar Radiation," *Water Resources Research,* Vol. 8, No. 1, Feb., 1972, pp. 42–49.
5. Edinger, J. E., Duttweiler, D. W., and Geyer, J. C., "The Response of Water Temperatures to Meteorological Conditions," *Water Resources Research,* Vol. 4, No. 5, Oct., 1968, pp. 1137–1143.
6. Edinger, J. C., "Vertical Temperature Structure and Water Surface Heat Exchange," *Water Resources Research,* Vol. 6, No. 5, Oct., 1970, pp. 1392–1395.
7. Gameson, A. L. H., Gibbs, J. W., and Barrett, M. J., "A Preliminary Temperature Survey of a Heated River," *Water and Water Engineering,* Jan., 1959, pp. 14–17.
8. Jobson, H. E., "The Dissipation of Excess Heat From Water Systems," *Journal of the Power Division,* ASCE, Vol. 99, No. PO1, Proc. Paper 9702, May, 1973, pp. 89–103.
9. Morse, W. L., "Stream Temperature Prediction Under Reduced Flow," *Journal of the Hydraulics Division,* ASCE, Vol. 98, No. HY6, Proc. Paper 8962, June, 1972, pp. 1031–1047.
10. Noble, R. D., "Analytical Prediction of Natural Temperatures in Rivers," *Journal of the Environmental Engineering Division,* ASCE, Vol. 105, No. EE5, Proc. Paper 14870, Oct., 1979, pp. 1014–1018.
11. Noble, R. D., and Jackman, A. P., "Predicting the Natural Temperature Profile Throughout a River Basin," *Journal of Environmental Systems,* Vol. 9, No. 4, 1980, pp. 361–381.
12. Paily, P. P., Macgano, E. O., and Kennedy, J. F., "Winter-Regime Thermal Response of Heated Streams," *Journal of the Hydraulics Division,* ASCE, Vol. 100, No. HY4, Proc. Paper 10479, Apr., 1974, pp. 531–551.
13. Raphael, J. M., "Prediction of Temperature in Rivers and Reservoirs," *Journal of the Power Division,* ASCE, Vol. 88, No. PO2, Proc. Paper 3200, July, 1962, pp. 157–181.

14. Velz, C. J., and Gannon, J. J., "Forecasting Heat Loss in Ponds and Streams," *Journal of the Water Pollution Control Federation*, Vol. 32, 1960, pp. 393–417.
15. Yotsukura, N., Jackman, A. P., and Faust, C. R., "Approximation of Heat Exchange at the Air-Water Interface," *Water Resources Research*, Vol. 9., No. 1, Feb., 1973, pp. 118–128.

Return Period for Mean Annual Hydrologic Event

By Donthamsetti V. Rao,[1] M. ASCE

Introduction

Engineering hydrologists sometimes wish to assign a return period (T) to the mean annual hydrologic event. The value of the mean annual event is usually the arithmetic average ($\bar{X}$) of annual series of data, such as annual flood flows, annual low flows, etc. The value of T is not a constant for this event ($\bar{X}$), but depends upon the probability distribution (PD) assumed for the data sample. If F represents the nonexceedance probability for $\bar{X}$ based on the assumed PD, T for $\bar{X}$ ($T_{\bar{X}}$) is given by $1/(1 - F)$ if data are annual largest events (ALE), such as flood flows and by $1/F$ if data are annual smallest events (ASE), such as low flows. For the normal and Gumbel distributions which have a constant skewness coefficient (γ), $T_{\bar{X}}$ is also a constant; for the normal distribution $T_{\bar{X}} = 2$ yr for both ALE and ASE, and for the Gumbel $T_{\bar{X}} = 2.33$ yr when it is applied to ALE. For other PDs, the value of $T_{\bar{X}}$ depends on the statistical parameters of the random variable. This paper presents $T_{\bar{X}}$ values for some commonly used PDs in a generalized fashion.

Method of Evaluation

Given data can be made dimensionless by the transform $K_i = X_i/\bar{X}$ in which K_i represents a dimensionless variate corresponding to the ith data item X_i. The mean of dimensionless data is $\bar{K} = 1.0$. Different PDs can be evaluated in terms of K by assuming the population mean of the random variable as unity. The variance of K, σ_k^2, is equivalent to η_x^2, in which η_x = population

[1]Hydro., Engrg. Div., Water Resources Dept., St. Johns River Water Management Dist., P.O. Box 1429, Palatka, Fla. 32077.

Note.—Discussion open until August 1, 1981. To extend the closing date one month, a written request must be filed with the Manager of Technical and Professional Publications, ASCE. Manuscript was submitted for review for possible publication on April 2, 1980. This paper is part of the Journal of the Hydraulics Division, Proceedings of the American Society of Civil Engineers, ©ASCE, Vol. 107, No. HY3, March, 1981. ISSN 0044-796X/81/0003-0366/$01.00.

coefficient of variation of X. The coefficient of skewness (γ) being dimensionless, is common for X and K. The two- and three-parameter lognormal (LN), gamma (GA), and Weibull (WB) distributions and log Pearson Type 3 (LP) distribution were evaluated for a wide range of σ_k^2 and γ. The value of F was determined at $K = 1.0$ and values of $T_{\hat{x}}$ were then calculated for ALE and ASE. Note

TABLE 1.—Values of $T_{\hat{x}}$ for Two Parameter Probability Distributions

	Annual Largest Events			Annual Smallest Events		
σ_k^2 or η_x^2 (1)	Lognormal (2)	Gamma (3)	Weibull (4)	Lognormal (5)	Gamma (6)	Weibull (7)
0.05	2.19	2.13	1.92	1.84	1.89	2.09
0.10	2.28	2.18	2.00	1.78	1.84	2.00
0.20	2.41	2.27	2.12	1.71	1.79	1.89
0.30	2.51	2.34	2.22	1.66	1.75	1.82
0.40	2.59	2.40	2.31	1.63	1.71	1.76
0.50	2.67	2.46	2.39	1.60	1.68	1.72
0.60	2.73	2.52	2.46	1.58	1.66	1.68
0.70	2.79	2.57	2.53	1.56	1.64	1.65
0.80	2.85	2.62	2.60	1.54	1.62	1.63
0.90	2.90	2.67	2.66	1.53	1.60	1.60
1.00	2.95	2.72	2.72	1.51	1.58	1.58
2.00	3.33	3.15	3.20	1.43	1.46	1.46
3.00	3.60	3.54	3.56	1.39	1.39	1.39
4.00	3.80	3.90	3.86	1.36	1.34	1.35
5.00	3.97	4.25	4.11	1.34	1.31	1.32

TABLE 2.—Values of $T_{\hat{x}}$ for Three Parameter Probability Distributions

Skewness coefficient	Annual Largest Events			Annual Smallest Events		
γ (1)	Lognormal (2)	Gamma (3)	Weibull (4)	Lognormal (5)	Gamma (6)	Weibull (7)
0.50	2.14	2.14	2.15	1.88	1.88	1.87
1.00	2.29	2.31	2.33	1.78	1.77	1.75
1.50	2.43	2.50	2.52	1.70	1.67	1.66
2.00	2.55	2.72	2.72	1.64	1.58	1.58
3.00	2.78	3.25	3.08	1.56	1.44	1.48
4.00	2.95	3.90	3.41	1.51	1.34	1.41
5.00	3.10	4.66	3.70	1.48	1.27	1.37
7.00	3.33	6.44	4.20	1.43	1.18	1.31
9.00	3.50	8.54	4.62	1.40	1.13	1.28

that the three-parameter GA is equivalent to the Pearson Type 3 distribution. For brevity, no equations of PDs are presented herein. Different relations for the four distributions are available in Ref. 1. (For LN, GA, and WB, the equations of three-parameter distributions can be converted into the equations of two-parameter distributions by setting the location parameter, $c = 0$.)

Results

For two-parameter LN, GA, and WB, values of $T_{\hat{x}}$ are tabulated as a function of σ_k^2 or η_x^2 (Table 1). For the three-parameter versions of the preceding three PDs, $T_{\hat{x}}$ is a function of γ only (Table 2). For LP, $T_{\hat{x}}$ depends on both σ_k^2

TABLE 3.—Values of $T_{\hat{x}}$ for Log Pearson Type 3 Distribution

σ_k^2 or η_x^2 (1)	Skewness Coefficient (γ) 0.50 (2)	1.00 (3)	1.50 (4)	2.00 (5)	3.00 (6)	5.00 (7)	9.00 (8)
			(*a*) Annual Largest Events				
0.05	2.14	2.28	2.41	2.54	2.78	3.19	3.78
0.10	2.15	2.28	2.41	2.52	2.71	3.01	3.39
0.20	2.17	2.31	2.42	2.52	2.68	2.90	3.14
0.30	2.19	2.33	2.45	2.54	2.68	2.87	3.06
0.40	2.21	2.36	2.48	2.57	2.70	2.87	3.03
0.50	2.23	2.39	2.51	2.60	2.73	2.88	3.03
0.60	2.26	2.43	2.55	2.63	2.75	2.90	3.03
0.70	U	2.46	2.58	2.67	2.79	2.92	3.04
0.80	U	2.50	2.62	2.70	2.82	2.95	3.06
0.90	U	2.53	2.66	2.74	2.85	2.97	3.08
1.00	U	2.57	2.70	2.78	2.89	3.00	3.10
2.00	U	U	U	3.21	3.26	3.31	3.35
3.00	U	U	U	U	3.67	3.62	3.60
4.00	U	U	U	U	4.14	3.95	3.85
5.00	U	U	U	U	4.69	4.29	4.09
			(*b*) Annual Smallest Events				
0.05	1.88	1.78	1.71	1.65	1.56	1.46	1.36
0.10	1.87	1.78	1.71	1.66	1.58	1.50	1.42
0.20	1.86	1.77	1.70	1.66	1.60	1.53	1.47
0.30	1.84	1.75	1.69	1.65	1.59	1.54	1.49
0.40	1.83	1.73	1.68	1.64	1.59	1.54	1.49
0.50	1.81	1.72	1.66	1.63	1.58	1.53	1.49
0.60	1.80	1.70	1.65	1.61	1.57	1.53	1.49
0.70	U	1.68	1.63	1.60	1.56	1.52	1.49
0.80	U	1.67	1.62	1.59	1.55	1.51	1.48
0.90	U	1.65	1.60	1.57	1.54	1.51	1.48
1.00	U	1.64	1.59	1.56	1.53	1.50	1.48
2.00	U	U	U	1.45	1.44	1.43	1.43
3.00	U	U	U	U	1.37	1.38	1.38
4.00	U	U	U	U	1.32	1.34	1.35
5.00	U	U	U	U	1.27	1.30	1.32

Note: U = U-shaped distribution.

(or η_x^2) and γ (Table 3). For ALE, $T_{\hat{x}}$ increases with σ_k^2 or η_x^2 and γ, or both, but for ASE it decreases as the latter are increased (with some exceptions in the case of LP). For practical application of Tables 1–3 one may first determine the sample statistics mean ($\bar{X}$), variance (S_x^2), and the skewness coefficient

(CS). Then, the sample coefficient of variation is given by, $CV = S_x/\bar{X}$. With $\eta_x^2 = CV^2$ and $\gamma = CS$ one may enter Tables 1–3 and obtain an approximate value for $T_{\hat{x}}$. When γ is negative, $T_{\hat{x}}$ values of ALE and ASE in Table 1 represent the $T_{\hat{x}}$ values of ASE and ALE, respectively, for LN and GA.

In the case of LP, for some combinations of σ_k^2 and γ the parameter values do not permit evaluation of F values, and for some combinations the form of LP is U shaped. In both instances $T_{\hat{x}}$ values are not shown in Table 3.

An application of the results presented in this paper is as follows: Different regulatory agencies apply certain criteria in allowing development within the riverine floodplains. Assume that one of such agencies does not permit any development activity within the mean annual floodplain of rivers in its jurisdiction. The structures built before the enactment of such regulations escape the law. Suppose a river within the jurisdiction of the agency has $CV^2 = 1.0$ and $CS = 2.0$ for its floods. Property located within the mean annual floodplain will be inundated, on the average, once in 2.95 yr if floods are distributed as the two-parameter LN, but once in 2.55 yr if distributed as the three-parameter LN. An insurance agency accepting flood insurance may charge more to insure such property if it assumes the three-parameter LN in determining its premium rates.

Appendix.—Reference

1. Rao, D. V., "Three-Parameter Probability Distributions," *Journal of the Hydraulics Division*, ASCE, Vol. 107, No. HY3, Proc. Paper 16124, Mar., 1981, pp. 339–358.

JOURNAL OF THE
HYDRAULICS DIVISION

DISCUSSION

Note.—This paper is part of the Journal of the Hydraulics Division, Proceedings of the American Society of Civil Engineers, ©ASCE, Vol. 107, No. HY3, March, 1981. ISSN 0044-796X/81/0003-0373/$01.00.

Discussions

Discussions may be submitted on any Proceedings paper or technical note published in any *Journal* or on any paper presented at any Specialty Conference or other meeting, the *Proceedings* of which have been published by ASCE. Discussion of a paper/technical note is open to anyone who has significant comments or questions regarding the content of the paper/technical note. Discussions are accepted for a period of 4 months following the date of publication of a paper/technical note and they should be sent to the Manager of Technical and Professional Publications, ASCE, 345 East 47th Street, New York, N.Y. 10017. The discussion period may be extended by a written request from a discusser.

The original and three copies of the Discussion should be submitted on 8-1/2-in. (220-mm) by 11-in. (280-mm) white bond paper, typed double-spaced with wide margins. The length of a Discussion is restricted to two *Journal* pages (about four typewritten double-spaced pages of manuscript including figures and tables); the editors will delete matter extraneous to the subject under discussion. If a Discussion is over two pages long it will be returned for shortening. All Discussions will be reviewed by the editors and the Division's or Council's Publications Committees. In some cases, Discussions will be returned to discussers for rewriting, or they may be encouraged to submit a paper or technical note rather than a Discussion.

Standards for Discussions are the same as those for Proceedings Papers. A Discussion is subject to rejection if it contains matter readily found elsewhere, advocates special interests, is carelessly prepared, controverts established fact, is purely speculative, introduces personalities, or is foreign to the purposes of the Society. All Discussions should be written in the third person, and the discusser should use the term "the writer" when referring to himself. The author of the original paper/technical note is referred to as "the author."

Discussions have a specific format. The title of the original paper/technical note appears at the top of the first page with a superscript that corresponds to a footnote indicating the month, year, author(s), and number of the original paper/technical note. The discusser's full name should be indicated below the title (see Discussions herein as an example) together with his ASCE membership grade (if applicable).

The discusser's title, company affiliation, and business address should appear on the first page of the manuscript, along with the *Proceedings* paper number of the original paper/technical note, the date and name of the *Journal* in which it appeared, and the original author's name.

Note that the discusser's identification footnote should follow consecutively from the original paper/technical note. If the paper/technical note under discussion contained footnote numbers 1 and 2, the first Discussion would begin with footnote 3, and subsequent Discussions would continue in sequence.

Figures supplied by the discusser should be designated by letters, starting with A. This also applies separately to tables and references. In referring to a figure, table, or reference that appeared in the original paper/technical note use the same number used in the original.

It is suggested that potential discussers request a copy of the *ASCE Authors' Guide to the Publications of ASCE* for more detailed information on preparation and submission of manuscripts.

Experiments in Longitudinal Dispersion With Dead Zones[a]

Closure by Eric M. Valentine,[5] A. M. ASCE and Ian R. Wood,[6] M. ASCE

The writers wish to thank Almquist and Holley for their interests in the paper and for their comments.

It was recognised by the writers that the transverse distribution of velocity always plays an important role in the differential advection in natural rivers. However, in the rectangular flume in which the reported experiments were performed, where two-dimensional dead zones were present in the form of strips across the flow, the following points are noted: (1) The vertical velocity distribution varied very little across the flow; and (2) tests carried out in this flume with six probes mounted across the flow at equal intervals demonstrated little difference in the statistical parameters calculated for these different locations.

The writers were therefore satisfied that the flow closely approximated a two-dimensional situation, and, for this case, that a comparison between physical measurements made at one point in flow with cross-sectionally averaged computations of the numerical model was justified. It had also been found that there was very little difference in the values of parameters calculated from higher moments (i.e., varience and skew): (1) Where these were computed by employing only the moments from the flow zone elements comparable in "sensing area" to the probe; and (2) where the figures represented the whole cross section.

The foregoing situation applied only to the two-dimensional experiment with dead zones. In the case where a "smooth bed" was examined, the velocity gradient across the flow was greater as shown in Fig. 13. Similar transverse variation of concentrations was then found to those reported by the discussers in Fig. 12. The writers' observation of this transverse variation led to a more refined consideration of the physical relationship of the probe positions and dimensions to the three-dimensional model elements as discussed in Ref. 27.

It was never intended that results from the two-dimensional (vertical) model should be compared directly to natural streams as they were produced to demonstrate the importance of the dead zone concept and to provide a physical understanding of the mechanism related to the delay of the Taylor period caused by dead zones.

Following velocity measurements made in a water race (27) the writers calculated the value of $\bar{U}$ in Eq. 5 for the side dead zones as the average of the values in those flow elements horizontally adjacent and corresponding as closely as possible in width to the flow depth. Physical observation suggested this was appropriate. While the writers agree with the discussers' observation

[a]August, 1979, by Eric M. Valentine and Ian R. Wood (Proc. Paper 14790).

[5]Sr. Engr., Central Labs., Ministry of Works and Development, Wellington, New Zealand.
[6]Prof. of Civ. Engrg., Univ. of Canterbury, Christchurch 1, New Zealand.

that in transverse models the dead zone mass exchange is controlled by more parts of the velocity distribution, the lower side dead zone exchange velocity led to longer side dead zone retention times. This emphasizes the importance of the mechanism in the dispersion process in streams.

The short comings of the "frozen cloud" assumption are apparent but in progressing to the three-dimensional case including side dead zones a practical method of comparing experimental with numerical computations was required.

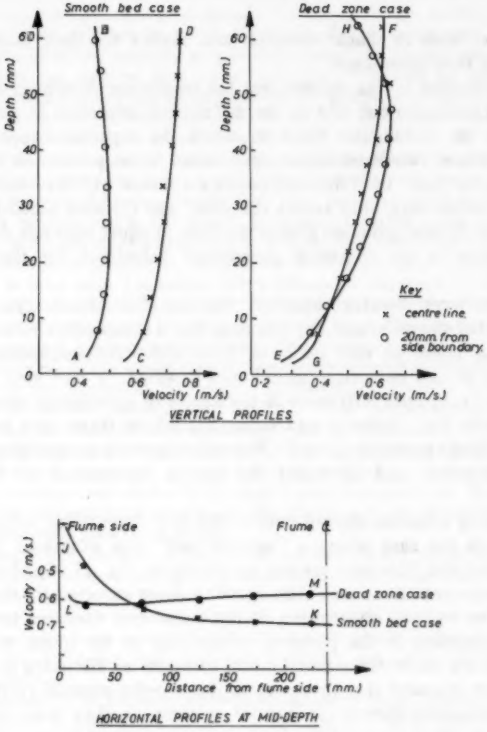

FIG. 13.—Smooth Bed: Velocity Gradient Across Flow

It is agreed that the "frozen cloud" assumption appears to be met in the two-dimensional experiments only for the higher values of $\bar{U}$. The spatial domain experiments were performed as an investigation of the errors inherent in employing the "frozen cloud" conversion where dead zones are present. The errors were small and were considered to justify its use until the experimental and numerical results could be compared directly in the same domain.

To answer the final points raised by the discussers:

1. The difficulties in making accurate depth measurements where y_n is very small prompted the comparison of experimental data with numerical runs employing $y = y_n \pm 2$ mm. Some small standing waves increased this problem especially for the smallest depths. The velocity distribution in the laboratory flume was thoroughly measured for those depths where a miniature flow meter could be accommodated. Values of ϵ_y were then computed.

2. The increase in the values of ξ_L (Table 1) with decreasing y_n/d are due to the use of the depth (y_n) as the nondimensionalising length scale. This reverses the progression of values which ranged from 4.65 m (y_n = 10 mm)–17.42 m (y_n = 67 mm). The duration for these extreme cases were approximated 24 sec and 33 sec, respectively. This would appear to be in agreement with the discussers' observations in a transverse model of a slight decrease in the duration of the initial period for decreasing $y_{n/d}(\theta y)$.

Appendix.—Reference

27. Valentine, E. M., "Dispersion in Rough Rectangular Channels," *Journal of Hydraulics Division*, ASCE, Vol. 105, No. HY12, Proc. Paper 15088, Dec., 1979, pp. 1537–1553.

Errata.—The following correction should be made to the original paper:

Page 1010, Table 1, Col. 2 heading: Should read "y_n, in millimeters" instead of "Y_n, in millimeters"

Modeling in Design of Pumping Pits[a]

Closure by J. Paul Tullis,[4] A. M. ASCE

The writer expresses his appreciation to the two discussers for their interest in the paper and their thoughtful comments and questions. One question raised by Talukder was; "Is it imperative to make a model study for evey pumping pit?" As the discusser pointed out, even when a pumping pit is built which appears to be identical to one that was modeled and operated successfully, one may still encounter operational problems. Also a model cannot guarantee a problem-free prototype. The decision of whether or not to conduct a model study for each installation is a complex one. However, the final decision appears to the writer to depend primarily on the level of peace of mind the owners wish to have. It is somewhat like buying an insurance policy. A thorough model study minimizes the chances of difficulties. Then if difficulties are encountered

[a]September, 1979, by J. Paul Tullis (Proc. Paper 14812).

[4]Prof. of Civ. Engrg., Dept. of Civ. Engrg., Utah Research Lab., UMC 82, Utah State Univ., Logan, Utah 84322, and Colorado State Univ., Ft. Collins, Colorado.

the designers and owners know that they took all normal precautions. As a more direct answer to the question, the writer recommends that with present technology and the lack of correlation and generalization of model study data, a model study be performed on each major pumping pit installation. This will only be changed when the results of the many model studies are correlated and additional research is funded to provide more fundamental information on the problem.

Talukder's second question related to who should initiate the model study. The discusser answered his own question quite well. The two parties who are expected to provide expert advice to the owners are the consulting/design engineer and the pump manufacturer. Either are in a position to recommend a model study. However, the involvement of the pump manufacturer may come too late. He may not enter the picture until after the civil works are completely designed. It is, therefore, suggested that the major responsibility for considering the modeling need rests on the consulting/design engineer.

The third comment by Talukder was on how to reduce the need for so many models. The writer and discusser again agree on a general solution. Funds must be made available to allow an indepth comparison of many recent studies. Basic research is also needed on the physics of the problem and a look at a scale effects problem. The writer has attempted to obtain Federal funding for such a study without success. Unless the government or a cooperative effort of pump companies and engineering firms provide such funding, the need of modeling each installation will continue.

The second discusser, Spurr, emphasized the importance of vorticity and the influence of turbulence. Vorticity is a particularly nasty problem to deal with in the model since there is not satisfactory means of direct measurement. Intrusive devices upset an individual vortex and since the vortex is not stationary, nonintrusive devices cannot be used. A qualitative estimate from visual observations is still the accepted means of classifying individual vortices.

Proper modeling of the turbulence level is definitely important in evaluating the susceptibility of a design to generate and sustain vortices. The largest single problem, as viewed by the writer, is that most model studies are performed before the prototype is built and operated. Consequently, it is not possible to obtain prototype turbulence measurements to guide the operation of the model. There is also the problem of quantifying the dependence of the vorticity on turbulence and how to scale this relationship down to the model. It would be helpful to have more model-prototype studies to evaluate the influence of turbulence.

Mississippi River Shoaling: A Diagnostic Study[a]

Closure by Tatsuaki Nakato,[5] A. M. ASCE, Richard M. Baker,[6] and John F. Kennedy,[7] M. ASCE

The writers concur with Glover's view that physical models have been an invaluable tool in river-engineering practice for many years, and that they will continue to play a central role. Nevertheless, the writers still are of the opinion that there is no substitute for good prototype observations and data, and under optimal conditions prototype and model investigations will proceed in consort. To be sure, many riverine problems cannot be solved with field data alone, although some can. By the same token, model data produced without calibration and verification using prototype results must be viewed with a high degree of circumspect.

Glover properly questions the reliability of the bed-load-transport data obtained with the Helley-Smith sampler. At the time the reported field data were obtained, relatively little work had been done to establish the accuracy of results obtained with this device. In the intervening years to the present, however, data have been published which largely remedy this deficiency. In his detailed field calibration of the Helley-Smith sampler in the East Fork River, Wyo., Emmett (17) found that the sampler has a near-perfect sediment trapping efficiency for the sediment particle sizes between 0.50 mm and 16 mm. Most of the bed-load sediment sizes in the writers' study areas fall in this range. A field study similar to the writers' was conducted in 1978 in the same Pool 20 reaches, to calibrate several one-dimensional numerical sediment models (18). The bed-load data obtained in 1978 are plotted in Fig. 12 against the mean flow velocity, U, together with the 1976 data included in the writers' paper. Note that the measured bed-load discharge is given in units of tons/ft/day. As seen in the figure, the bed-load-discharge data vary over nearly two log cycles. The correlation between two variables seems to be astonishingly good, considering the wide variations in lateral distributions of the bed-load discharge in natural rivers, and the two sets of data are in good agreement. While this agreement does not conform the accuracy of the Helley-Smith data, it does lend credibility to them. It should be added that elaborate laboratory testing of the Helley-Smith samplers has also been undertaken at the St. Anthony Falls Hydraulic Laboratory, University of Minnesota.

Physical model, numerical, and prototype investigations will all continue to

[a]November, 1979, by Tatsuaki Nakato, Richard M. Baker, and John F. Kennedy (Proc. Paper 14978).

[5]Research Scientist, Inst. of Hydr. Res., and Adjunct Asst. Prof., Energy Engrg., Univ. of Iowa, Iowa City, Iowa 52242.

[6]Civ. Engrg. Tech., Rock Island Dist., Army Corps of Engrs., Rock Island, Ill.

[7]Dir., Inst. of Hydr. Res., and Prof., Div. of Energy Engrg., Univ. of Iowa, Iowa City, Iowa 52242.

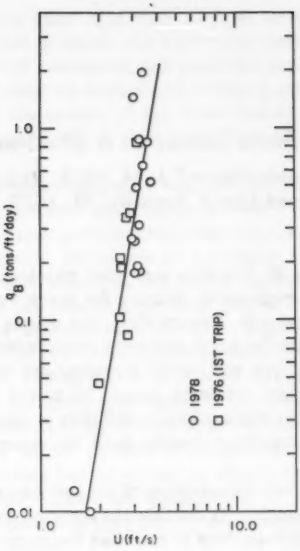

FIG. 12.—Relationship between U and q_B

be essential river-engineering tools, and many problems will require application of all three. Nevertheless, the writers believe that well-known limitations in physical and numerical modeling techniques and the results they produce will make prototype study the preferred approach in some instances, especially those involving complex, three-dimensional, bed-load-transporting flows.

APPENDIX.—REFERENCES

17. Emmett, W. W., "A Field Calibration of the Sediment-Trapping Characteristics of the Helley-Smith Bedload Sampler," *Open-File Report 79-411*, United States Geological Survey, 1979.
18. Vadnal, J. L., "Field Study of Sediment Transport Characteristics of the Mississippi River Near Buzzard Island," thesis presented to The University of Iowa, at Iowa City, Iowa, in 1979, in partial fulfillment of the requirements for the degree of Master of Science.

Errata.—The following correction should be made to the original paper:

Page 1379, Table 1 heading: Should read "Summary of Principal Quantities Obtained from Field Data" instead of "Summary of Principal Quantities Obtained from Field Data (1st Trip)"

Flood Frequency Estimates on Alluvial Fans[a]

Closure by David R. Dawdy,[3] M. ASCE

The writer fears that the discusser did not read the paper carefully, and the discusser's conclusions are therefore somewhat too harsh. The paper was not meant to be a treatise on the development of alluvial fans. The excellent references by W. B. Bull are not germane to the problem of the determination of flood hazards on alluvial fans. "The discharge usually passes through the fan apex and the uppermost segments of the fan in a well-defined, perhaps entrenched, channel" is not felt by the writer to be correct or helpful unless "usually" and "well-defined, perhaps entrenched" are more quantitatively defined.

Many (most) fans are not entrenched, and how well a channel is defined on an alluvial fan normally is in the eye of the beholder. Where fans are entrenched the flood frequency distribution at the apex can be considered to apply through the entrenched portion, and the method described by the writer applied to that portion below the lower point of entrenchment.

The discusser makes four major points: They shall be answered in order.

1. A 100-yr flood, calculated for the fan apex cannot have a recurrence interval of significantly less than 100 yr at the intersection point. For the 100-yr flood at the apex to be, say, the 50-yr flood at a lower point on the fan requires that two floods of that magnitude or greater must pass that point. Those two floods must pass the apex. Therefore, the 100-yr flood at the apex is in fact, a 50-yr flood, quod erat demonstrandum.

2. The development of alluvial fans is a random process. Regularity in the mean value function of a process does not require a deterministic process. The discusser is referred to the work of Price (16) for an excellent discussion of the theories of the formation of alluvial fans. The writer does not see how this multitude of contrasting and conflicting theories "absolutely refute any assumption pertaining to a random development model for alluvial fans." The writer does concede that the various geomorphologists attempt to refute each other. Perhaps the discusser does not understand that "random," "erratic," and "somewhat unpredictable" are almost synonymous. The name random variable derives from the fact that its value cannot generally be predicted exactly in advance (15). A valid question might be whether, in fact, it should be "assumed that a channel caused by a given flood has an equal probability to cross at any point on a contour." This assumption of a uniform distribution is somewhat arbitrary, and quantitative evidence to the contrary would be appreciated.

3. The assumption of a log-Pearson III distribution at the apex is an operational

[a]November, 1979, by David R. Dawdy (Proc. Paper 15001).

[3]Sr. Hydro., Suite 700, Dames & Moore, 7101 Wisconsin Ave., Washington, D.C. 20014.

assumption, as stated by the writer. That distribution, however, is used only for convenience of interpolation. The choice of a distribution (a nonparametric distribution could be used) is not inconsistent with either of the statements quoted by the discusser.

4. In the conclusions section, the writer states the three assumptions underlying the method. Each of those assumptions may be counterargued against. However, it is rather unfair of the discusser to quote out of context so as to accuse the writer of "brushing aside" the problems which he concedes and with which he ends his paper. Suggestions for improvement would be appreciated, particularly if quantitative, and if based on field evidence germane to the problem of determination of flood frequency distributions at an arbitrary point on an alluvial fan.

Appendix.—References

15. Cramer, H., and Leadbetter, M. R., *Stationary and Related Stochastic Processes*, John Wiley and Sons, Inc., New York, N.Y., 1967, page 2.
16. Price, W. E., Jr., "A Random-Walk Simulation Model of Alluvial Fan Deposition," *Technical Report No. 7*, University of Arizona, 1972.

Two-Dimensional Buoyant Jets in Stratified Fluid[a]

Errata

The following corrections should be made to the original paper:

Page 1395, Eq. 4: Should read $\frac{Z_m}{l'_b} = \text{constant } (C_1)$

instead of $\frac{Z_m}{l'_m} = \text{constant } (C_1)$

Page 1395, Eq. 5: Should read $\frac{Z_m}{l'_m} = \text{constant } (C_2)$

instead of $\frac{Z_m}{l'_b} = \text{constant } (C_2)$

Page 1400, Fig. 2: Should be Eq. 23 and Eq. 26 instead of Eq. 8 and Eq. 9, respectively.

[a]November, 1979, by Steven J. Wright and Roger B. Wallace (Proc. Paper 15003).

Finite Element Method for Direct Runoff Flow[a]

Discussion by Raymond J. Dever, Jr.,[3] A. M. ASCE

The authors have presented an application of the Galerkin finite element method to an important problem in applied hydrology, namely, the simulation of time-dependent rainfall-runoff. However, the authors' model as presently formulated includes a deficiency serious enough to render the model unacceptable for practical applications.

The authors have solved the time-dependent, two-dimensional equations of momentum and continuity for rainfall-runoff. For the hypothetical problem shown in Fig. 1, rainfall-runoff from an impervious plane, these equations appear to be properly stated and solved. However, for practical problems such as the Ina Basin example given in the paper, the equation of continuity is stated incorrectly.

The equation of continuity, Eq. 2, accounts for three terms: (1) Rainfall on the watershed; (2) discharge from the watershed; and (3) the rate of change of flow depth on the watershed. What the authors have failed to take into account here are the significant rainfall losses that occur on all watersheds. These losses can include infiltration, surface depression storage, and interception by vegetal cover. Quantifications of these losses are routinely included in the most widely-used rainfall-runoff models, such as the United States Environmental Protection Agency's Storm Water Management Model (16). For the authors' model to properly represent rainfall-runoff, the equation of continuity must be modified to include a loss term.

The example problems which the authors presented avoided the issue of rainfall losses. Their model reproduced the results of Schreiber and Bender (11) well, but these data were obtained in a laboratory experiment using a small impervious plane as a model watershed. The authors also applied their model to the Ina Basin of the Tenryu River, but no rainfall-runoff data from this site were available for purposes of comparison.

In summary, the authors have developed a finite element model of rainfall-runoff that is flawed because it does not account for significant rainfall losses such as infiltration and depression storage. However, what is more important here is that the authors' results are an example of a disturbing trend in water resources modeling in which increasingly sophisticated mathematical solutions become an end in themselves. Although advances in applied mathematics have enabled us to solve some problems in hydraulics and hydrology that we could not solve before, the importance of the mathematics must be kept in proper perspective. It is not true that the more mathematically sophisticated a model is, the better a model is. In this paper, the authors have presented an impressive example

[a]April, 1980, by Mutsuto Kawahara and Teruyuki Yokoyama (Proc. Paper 15341).

[3]Engr., Camp Dresser and McKee Inc., 7620 Little River Turnpike, Annandale, Va. 22003.

of the numerical solution of differential equations, but have failed to properly state the most basic principle in all hydraulic and hydrologic models, the principle of continuity.

APPENDIX.—REFERENCE

16. Huber, W. C., et al., "Storm Water Management Model: User's Manual, Version II," *Report No. EPA-670/2-75-017*, U.S. Environmental Protection Agency, Cincinnati, Ohio, Mar., 1975.

TURBULENCE PREDICTION IN OPEN CHANNEL FLOW[a]

Discussion by Rema Devi[5] and Arun Kumar[6]

The authors are to be commended for their effort to predict analytically the turbulent fluctuations in uniform flow in a channel. The writers, however, feel that this study mainly reiterates what is already known about turbulence characteristics and on the formulation of the prediction model.

A major part of the paper is devoted towards deriving a working model for predicting turbulent intensities of velocity for the streamwise and crosswise directions in open channel uniform flow. The basic assumptions, the subsequent derivation, the model and the concluding observations about the values of the model parameters r and c are exactly similar to the one already published by the first author along with Shen (3).

The suggested model relates the turbulent intensity u', with $E(U_i V_i)$. Taking the product of r and c equal to -0.4 (Table 1) for smooth boundaries, the relationship given in Eq. 16 can be reduced to :

$$\frac{u_i'}{u_*} < 1.58 \left(\frac{1 - y_i}{h}\right)^{1/2} \quad \ldots \ldots \ldots \ldots \ldots \ldots \ldots \ldots \ldots \ldots \ldots \ldots \quad (23)$$

In other words, the maximum value of streamwise turbulent velocity $u' < 1.58\, u_*$, whereas, in Laufer's (2) experiments, the maximum value of u' ranged from $1.8\, u_*$–$2.4\, u_*$. Similarly, Blinco and Partheniades (11) observed the range of maximum value of u' to be 2.6–$3.0\, u_*$. This shows that the model perhaps, underestimates the maximum turbulent intensity u'. Moreover, this model which is expressed as a decreasing function of the relative distance y/h cannot estimate u' near the boundary where it increases with y/h. The variation in u' with depth warrants two different relationships as suggested by Nelluri and Novak (12).

---

[a]April, 1980, by Ruh-Ming Li, James D. Schall, and Daryl B. Simons (Proc. Paper 15347).

[5]Asst. Prof. in Civ. Engrg., Delhi Coll. of Engrg., Kashmere Gate, Delhi-6, India.
[6]Asst. Prof. in Civ. Engrg., Delhi Coll. of Engrg., Kashmere Gate, Delhi-6, India.

The authors have estimated u_* taking the hydraulic radius, R, equal to the depth of flow, h. This is equivalent to assuming that the laboratory flumes whose data are studied act hydraulically as infinitely wide. For example, the measurements taken by the authors for a discharge of 0.0056 m^3/s on a 0.003 bed slope with an approximate average velocity of 50 cm/s (Table 2) on a 20-cm wide, 1:1 trapezoidal flume results in significantly different u_* at the bed. Approximating R equal to h gives u_* as 3.66 cm/s whereas, by using R directly, u_* is 3.16 cm/s. Since the turbulent intensities u' and v' are directly related to u_*, it is important to know the reasons for using depth of flow as the hydraulic radius even when the channel is not wide.

The author's observation that at $y/h > 0.15$, u'/u_* is a function of y/h only ($\nu\, u_*/\kappa\, y$ being negligible) is at variance with the observation of Blinco and Partheniades (11) who concluded that u'/u_* is apparently a universal function of $u_*\, y/\nu$ rather than y/h.

From Table 1, it is obvious that the product of r and c is approximately constant but it does not imply that either r or c is individually constant throughout the depth of the channel. Taking the value of c as 0.55 tends to overestimate transverse fluctuating velocity v' near the bed and to underestimate near the free surface (Table 2). Moreover, Smutek (13) has shown that c is not only a function of y/h but also of the Reynolds number. Both these factors could have been accounted for if a simple functional relationship between v'/u_* and u_*y/ν had been derived.

Appendix.—References

11. Blinco, P. H., and Partheniades, E., "Turbulent Characteristics in Free Surface Flows over Smooth and Rough Boundaries," *International Association of Hydraulic Research*, Vol. 9, No. 1, 1971, pp. 43–72.
12. Nalluri, C., and Novak, P., "Turbulence Characteristics in a Smooth Open Channel of Circular Cross Section," *International Association of Hydraulic Research*, Vol. 11, No. 4, 1973, pp. 343–368.
13. Smutek, R., Discussion on "Measurement of Turbulence in Water," *Journal of Hydraulics Division*, ASCE, Vol. 95, No. HY1, Proc. Paper 6323, Jan., 1969, pp. 519–523.

Force Fluctuations on Sill of Hydraulic Jump[a]

Errata

The following corrections should be made to the original paper:

Page 584, Fig. 7, the ordinate: should read in "Variation of C'_{DM}" instead of "Variation of C'_D"

Page 599, Appendix II, line 10: Should read "l = distance from sill to sluice;" instead of "y_1 = distance from the sill to sluice;"

[a]April, 1980, by Rangaswami Narayanan and Loizos S. Schizas (Proc. Paper 15368).

Linear Theory Methods for Pipe Network Analysis[a]

Discussion by Don J. Wood,[3] M. ASCE

The authors present a method to solve the pipe network head equations simultaneously. They have failed to cite several important references which also develop procedures for solving the head equations simultaneously. Martin and Peters (15) in 1963 presented a technique which utilized Newton's method of gradient approximation to linearize the nonlinear head equations. In 1966 Marlow, et al. (14) formulated the head equations using approximation which appears to be very similar to the method described in this paper. Shamir and Howard (16), Lui (13) and Lemieux (12) all presented similar methods based on the simultaneous solution of the head equations. It appears that, considering the similarities in the approach to pipe network analysis, these references should have been cited. Certainly this approach has been widely advocated, and only the method utilized to linearize the nonlinear head equations seems different. It also appears that the simplified method proposed by the authors is inferior to the use of gradient methods. This is certainly true of the method developed by this writer and cited in the paper where the flow equations were linearized in a similar manner [Wood, Charles (10)]. We subsequently found that linearization of the flow equations using gradient methods has convergence characteristics superior to those obtained by the method proposed in Ref. 10. It is likely that the same is true of the head equations and the method proposed by the authors has inferior convergence properties.

The authors also state that convergence problems occur with this method, and that no method can be guaranteed. While it is true that no method is guaranteed, several methods based on the flow equations have excellent convergence characteristics which consistently produce reliable results. Studies at the University of Kentucky consisted of analyzing over 100 pipe networks ranging in size to over 500 pipes. The correct solution was obtained for every case in an average of under seven trials using a method based on the simultaneous solution of the flow equations. Using a method based on the simultaneous solution of the head equations, convergence difficulties were encountered frequently, and a failure rate of nearly 20% occured. As pointed out by the authors, lines carrying low flows caused particular difficulty. This can be generalized to state that lines with small head changes may cause convergence difficulties for this method. Unfortunately, this does not mean that these lines can be ignored in the analysis. Often lines connecting storage tanks have very small head changes but carry significant flow and have a great effect on the system. An accurate steady state analysis of the pipe system requires an accurate flow calculation for these pipes. It appears that algorithms using the head equations are unable

[a]July, 1980, by Lewis T. Issacs and Kevin G. Mills (Proc. Paper 15559).

[3]Prof. of Civ. Engrg., Coll. of Engrg., Dept. of Civ. Engrg., Univ. of Kentucky, Lexington, Ky. 40506.

to do this consistently. Others have reported convergence problems associated with these methods. Shamir and Howard (16) noted oscillations and reported that a solution may not be obtained. Lui (13) noted that divergence was possible and Collins and Kennington (11) presented some data which documented convergence problems. This writer has concluded that algorithms are available for pipe network analysis which are reliable, but these are based on solving the flow equations (or flow correction equations). The method presented by the authors, which is based on head equations, will be unreliable in certain cases.

The authors' method 2 for computing flow rates is an innovation which apparently improves convergence. This may be a significant improvement if it can be shown to do so generally and eliminate a significant number of convergence problems. The authors also noted that accelerator factors were applied and different numerical values were used. It was not clear how the accelerator was applied, but it has been the experience of this writer that accelerators are of limited value, because a factor which improves convergence in one situation may adversely affect it in another. A great deal of testing would be required to select an appropriate accelerator.

Appendix.—References

11. Collins, M. A., and Kennington, J. L., discussion of "Extended Period Simulation of Water Systems—Part B," by H. S. Rao, L. C. Markel, and D. W. Brue, Jr., *Journal of the Hydraulics Division*, ASCE, Vol. 103, No. HY12, Proc. Paper 13378, Dec., 1977, pp. 1496–1500.
12. Lemieux, P. F., "Efficient Algorithm for Distribution Networks," *Journal of the Hydraulics Division*, ASCE, Vol. 98, No. HY11, Proc. Paper 9336, Nov., 1972, pp. 1911–1920.
13. Liu, K. T. H., "The Numerical Analysis of Water Supply Networks by Digital Computer," *Proceedings*, 13th Congress of the International Association for Hydraulic Research, Vol. 1, Subject A, Sept., 1969, pp. 35–42.
14. Marlow, T. A., Hardison, R. L., Jacobson, H., and Biggs, G. E., "Improved Design of Fluid Networks with Computers," *Journal of the Hydraulics Division*, ASCE, Vol. 92, No. HY4, Proc. Paper 4866, July, 1966, pp. 43–61.
15. Martin, D. W., and Peters, G., "The Application of Newton's Method to Network Analysis by Digital Computer," *Journal of the Institute of Water Engineers*, Vol. 17, 1963, pp. 115–129.
16. Shamir, U., and Howard, C. D. D., "Water Distribution Systems Analysis," *Journal of the Hydraulics Division*, ASCE, Vol. 94, No. HY1, Proc. Paper 5758, Jan., 1968, pp. 219–234.

VISUALIZATION OF SEPARATION OVER SAND WAVES[a]

Discussion by Peter Engel[3] and Y. Lam Lau[4]

The authors are to be commended for demonstrating the use of a simple and relatively inexpensive technique to measure flow separation lengths over dunes. Such a method is a step forward in providing information for the development of semi-analytical models for determining dune length such as that proposed by Fredsøe (14). However, the writers feel that the analysis of the data is not entirely correct. In addition, the results obtained by the authors differ from those obtained from recent experiments (paper in preparation) by the writers.

In general for a fixed bed, the flow separation length must be expressed as a function of the following independent variables (using the author's notation)

$$L = f(\Delta, \Lambda, D_{50}, U, H, \rho, \mu, g) \quad \ldots\ldots\ldots\ldots\ldots\ldots\ldots\ldots\ldots\ldots \quad (10)$$

in which L = separation zone length; f denotes a function, Δ = height of the dunes; Λ = length of the dunes; D_{50} = median grain size roughness on the dunes (for uniform grain size distribution); U = average velocity of the flow; H = average depth of the fluid; ρ = density of the fluid; μ = viscosity of the fluid; and g = acceleration due to gravity. Eq. 10 can be written in dimensionless form as

$$\frac{L}{\Lambda} = f_1\left(\frac{\Delta}{\Lambda}, \frac{\Lambda}{H}, \frac{D_{50}}{\Delta}, \frac{U H \rho}{\mu}, \frac{U}{\sqrt{gH}}\right) \quad \ldots\ldots\ldots\ldots\ldots\ldots\ldots\ldots\ldots\ldots \quad (11)$$

Yalin (13) has shown that for the boundary Reynolds number $v_* D_{50}\rho/\mu > 25$ (v_* = shear velocity), the sand waves are dunes and under these conditions the dune length is given by $\Lambda/H = 2\pi$. Accepting the fact that Λ/H will be more or less constant, the term can be eliminated from Eq. 11. In general Δ/Λ and D_{50}/Δ both have an effect on L/Λ. However, in this case, the authors have held Δ/Λ constant at 0.06. The writers have found that in this range of steepness D_{50}/Δ has no effect but is significant for smaller values of Δ/Λ. Therefore, for the authors' data

$$\frac{L}{\Lambda} = f_2(\mathsf{R}, \mathsf{F}) \quad \ldots\ldots\ldots\ldots\ldots\ldots\ldots\ldots\ldots\ldots\ldots\ldots\ldots\ldots \quad (12)$$

in which R = the Reynolds number as given by $\mathsf{R} = U H\rho/\mu$; and F = the Froud number given as $U/\sqrt{gH}$.

---

[a]August, 1980, by M. Emin Karahan and Allan W. Peterson (Proc. Paper 15652).

[3]Research Engr., Environmental Hydr. Section, Hydr. Div., National Water Research Inst., Canada Centre for Inland Waters, P.O. Box 5050, Burlington, Ontario, L7R 4A6 Canada.

[4]Head, Environmental Hydr. Section, Hydr. Div., National Water Research Inst., Canada Centre for Inland Waters, P.O. Box 5050, Burlington, Ontario, L7R 4A6 Canada.

For small values of Froude number, properties of the dunes and flow over the dunes should be independent of the Froude number. The authors have plotted L/Λ versus F (without keeping R constant) and suggested that L/Λ increases with decreasing F when $F < 0.2$. They also plotted the same data as L/Λ versus R showing L/Λ increasing with decreasing R. The writers wish

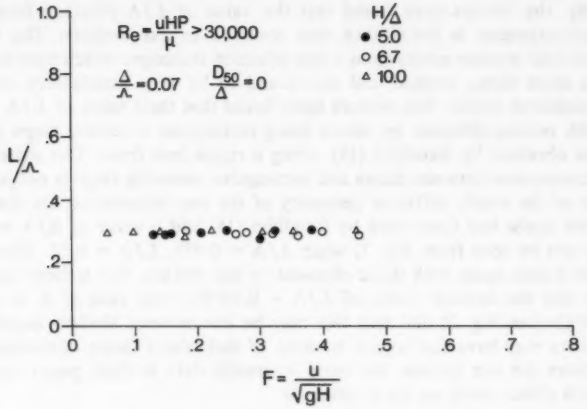

FIG. 6.—Variation of Dimensionless Separation Zone Length, L/Λ, with Average Flow Froude Number F

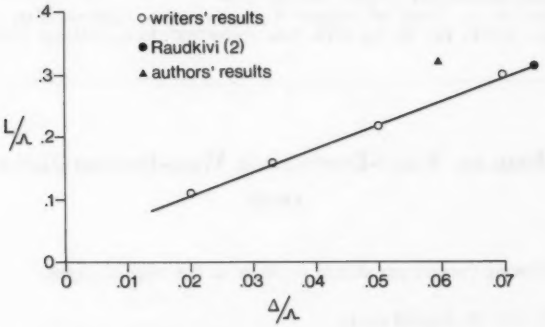

FIG. 7.—Variation of Dimensionless Separation Zone Length, L/Λ, with Dune Steepness Δ/Λ

to emphasize that what is shown in Fig. 3 is actually the effect of R and not any Froude number effect. This can be substantiated by the writers recent data in Fig. 6. For constant Δ/Λ and D_{50}/Δ and with $R > 30{,}000$, a constant L/Λ was obtained for values of F between 0.05 and 0.45. Therefore the writers are of the opinion that L/Λ is independent of F and that if the authors had

used R as a parameter in Fig. 3, they might have arrived at the same conclusion.

The effect of Δ/Λ can be seen in Fig. 7 in which the writer's data are plotted for values of $\Delta/\Lambda = 0.02$, 0.033, 0.05 and 0.07, keeping D_{50}/Δ constant and having again $R > 30{,}000$. The results show a clearly defined relationship between L/Λ and Δ/Λ. This shows that, for a given D_{50}/Δ, L/Λ is a function of Δ/Λ only.

Finally, the writers have found that the value of L/Λ obtained from their own measurements is lower than that obtained by the authors. The writers obtained their measurements using a dye injection technique which they consider to be a more direct method and was found to be very satisfactory over the flow conditions tested. The authors have found that their value of L/Λ agreed well with results obtained by others using rectangular reversing steps as well as those obtained by Raudkivi (15), using a ripple bed form. The writers feel that a comparison between dunes and rectangular reversing steps is not justified because of the totally different geometry of the two boundaries. On the other hand, the ripple bed form used by Raudkivi (15) had a value of $\Delta/\Lambda \approx 0.075$ and, as can be seen from Fig. 7, when $\Delta/\Lambda \approx 0.075$, $L/\Lambda \approx 0.32$. Therefore, Raudkivi's data agree with those obtained by the writers. The writers therefore suggest that the authors' value of $L/\Lambda \approx 0.32$ for their case of $\Delta/\Lambda = 0.06$ is too high (see Fig. 7) and that this may be due to very shallow depths that the authors may have had to use because of their small flume. Unfortunately, the authors did not include the basic hydraulic data in their paper and thus this depth effect could not be determined.

Appendix.—References

14. Fredsøe, J., "Dimensions of Stationary Dunes," *Progress Report No. 49*, Technical University of Denmark, August, 1979, pp. 3–10.
15. Raudkivi, A. Y., "Study of Sediment Ripple Formation," *Journal of the Hydraulics Division*, ASCE, Vol. 89, No. HY6, Proc. Paper 3692, Nov., 1963, pp. 15–33.

Modeling Three-Dimensional Wind-Induced Flows[a]

Errata

The following corrections should be made to the original paper:

Page 1848, Eq. 34: Should read

$$\xi_{i,j}^{n+1/2} = \xi_{i,j}^{n-1/2} - Dt\, H_{ij}\left\{\frac{[U_{i+1,j}^{n} - U_{i,j}^{n}]}{Dx} + \frac{[V_{i,j+1}^{n} - V_{i,j}^{n}]}{Dy}\right\}$$

instead of

$$\xi_{i,j}^{n+1/2} = \xi_{i,j}^{n-1/2} - Dt\, H_{ij}\left\{\frac{[U_{i+1,j}^{n+1} - U_{i,j}^{n+1}]}{Dx} + \frac{[V_{i,j+1}^{n+1} - V_{i,j}^{n+1}]}{Dy}\right\}$$

[a]November, 1980, by Christopher Koutitas and Brian O'Connor (Proc. Paper 15836).

Technical Papers

Original papers should be submitted in triplicate to the Manager of Technical and Professional Publications, ASCE, 345 East 47th Street, New York, N.Y. 10017. Authors must indicate the Technical Division or Council, Technical Committee, Subcommittee, and Task Committee (if any) to which the paper should be referred. Those who are planning to submit material will expedite the review and publication procedures by complying with the following basic requirements:

1. Titles must have a length not exceeding 50 characters and spaces.

2. The manuscript (an original ribbon copy and two duplicate copies) should be double-spaced on one side of 8-1/2-in. (220-mm) by 11-in. (280-mm) paper. Three copies of all figures and tables must be included.

3. Generally, the maximum length of a paper is 10,000 word-equivalents. As an *approximation*, each full manuscript page of text, tables or figures is the equivalent of 300 words. If a particular subject cannot be adequately presented within the 10,000-word limit, the paper should be accompanied by a rationale for the overlength. This will permit rapid review and approval by the Division or Council Publications and Executive Committees and the Society's Committee on Publications. Valuable contributions to the Society's publications are not intended to be discouraged by this procedure.

4. The author's full name, Society membership grade, and a footnote stating present employment must appear on the first page of the paper. Authors need not be Society members.

5. All mathematics must be typewritten and special symbols must be identified properly. The letter symbols used should be defined where they first appear, in figures, tables, or text, and arranged alphabetically in an appendix at the end of the paper titled Appendix.—Notation.

6. Standard definitions and symbols should be used. Reference should be made to the lists published by the American National Standards Institute and to the *Authors' Guide to the Publications of ASCE*.

7. Figures should be drawn in black ink, at a size that, with a 50% reduction, would have a published width in the *Journals* of from 3 in. (76 mm) to 4-1/2 in. (110 mm). The lettering must be legible at the reduced size. Photographs should be submitted as glossy prints. Explanations and descriptions must be placed in text rather than within the figure.

8. Tables should be typed (an original ribbon copy and two duplicates) on one side of 8-1/2-in. (220-mm) by 11-in. (280-mm) paper. An explanation of each table must appear in the text.

9. References cited in text should be arranged in alphabetical order in an appendix at the end of the paper, or preceding the Appendix.—Notation, as an Appendix.—References.

10. A list of key words and an information retrieval abstract of 175 words should be provided with each paper.

11. A summary of approximately 40 words must accompany the paper.

12. A set of conclusions must end the paper.

13. Dual units, i.e., U.S. Customary followed by SI (International System) units in parentheses, should be used throughout the paper.

14. A practical applications section should be included also, if appropriate.